2022-12-01

Nano-Engineered Soft Magnets: Potential Application In Water Treatment, Hyperthermia And Molecular (organic) Magnets

Yohannes Weldemariam Getahun
University of Texas at El Paso

NANO-ENGINEERED SOFT MAGNETS: POTENTIAL APPLICATION IN WATER TREATMENT, HYPERTHERMIA AND MOLECULAR (ORGANIC) MAGNETS

by

YOHANNES GETAHUN

Doctoral Program in Environmental Science and Engineering

APPROVED:

_____
Ahmed El-Gendy, Ph.D., Chair

_____
Jorge Gardea-Torresdey, Ph.D.

_____
Mark Pederson, Ph.D.

_____
Craig Tweedie, Ph.D.

_____
Stephen Crites, Ph.D.
Dean of the Graduate School

DEDICATION

First, I would like to dedicate this to the almighty for the blessings bestowed on me and my family. I would like to thank my mother for raising me to the best of her capability and unique effort on the path of my education despite life rigors. To my wife and my partner in life and my children whose pure love have been a source of my courage and perseverance. To my friends who believed in me and joined the struggles and joys we had. To my professors, advisors who offered compassionate support, encouragement and direction and shared their experience which I used them as tools in the challenging times. To my people, the people of Tigray for the culture of democracy, integrity, perseverance, and freedom which my principles and contributions to humanity is based up on.

NANO-ENGINEERED SOFT MAGNETS: POTENTIAL APPLICATION IN WATER TREATMENT, HYPERTHERMIA AND MOLECULAR (ORGANIC) MAGNETS

by

YOHANNES GETAHUN, MSc.

DISSERTATION

Presented to the Faculty of the Graduate School of

The University of Texas at El Paso

in Partial Fulfillment

of the Requirements

for the Degree of

DOCTOR OF PHILOSOPHY

Environmental Science and Engineering Doctoral Program

THE UNIVERSITY OF TEXAS AT EL PASO

December 2022

ACKNOWLEDGEMENTS

I am indebted to all the people whom I use their support at any time of my study that brought me to this stage of my career. I would like to thank my advisor Dr. Ahmed El-Gendy for his unsubstituted supervision, support, and guidance. The opportunity I got to work in your lab with full access your resources has helped me develop skills necessary for my future career.

My sincere gratitude to members of my dissertation committee, Jorge Gardea-Torresdey, P.h.D., Mark Pederson, P.h.D. Craig Tweedie, PhD for accepting being member in my committee, your collective guidance, feedback has helped me polish my skills and work on my professional stand.

Special thanks to the scientists who collaborated on this project: Dr. Mark Pederson, Dr. Felicia Manciu, Dr. XiuJun (James) Li, Dr. Chintalapalle Ramana and Dr. Debabrata Das through resources, knowledge sharing and professional feedback.

I want to acknowledge Dr Alejandro Metta and Dr. Michael Lyubchenko from the instrumental rooms for your assistance and knowledge sharing during sample characterization and Mr. Guillermo Campos from chemical store for your dedicated help with materials and equipment.

To my best friends Cletus Ogbodo, Arturo Andujo, Bryant Lopez and Marcos Gracia , for the memorable time we had at work and in our leisure times.

To Dr. Zebib Yenus for your valuable input in my path to doctoral study.

I want to thank all my lab mates who were my right hand during my experiments and sincere friends outside the laboratory. You will always be remembered for your support, jokes and generous invitations and gifts.

To Nodjimbadem family, me and my family wants to appreciate you and how glad we are to have you as family.

Lastly and with great importance, I owe special thanks to Dr. Criag Tweedie and Mrs. Lina Hamdan for your guidance, advice and unsubstituted support which are important elements of my study.

ABSTRACT

Scrutinizing the remarkable and tunable properties of magnetic materials at a nanoscale size *" There's Plenty of Room at the Bottom…"* Richard Feynman, this study attempts to find sustainable solutions to some of the deteriorating environmental, health, and energy problems the world is encountering. Due to their simple preparation, surface adaptability, tunable magnetic and optical properties, magnetic nanoparticles have been extensively investigated in water treatment, cancer therapy, data storage, and more. However, relying on non-reusable and chemical-based treatment agents in water, complex and costly cancer treatment procedures and molecular magnets that operate far below room temperature limited those attempts from feasibility. Thus, green, and sustainable materials and methods have long been in high demand. Here in we developed novel and optimized in organic and organic soft magnets suitable for water treatment, tumor cell obliteration, and room-temperature molecular magnets as energy-efficient data storage and spintronic devices. Green synthesized nanoparticles removed MB and 4-NA above 80% efficiency under a wide range of conditions and 94% under optimum conditions in 2 – 160 minutes. Moreover, nanoparticles were successfully grown on PVA surfaces as alternative recyclability for weakly magnetic materials. We introduced secondary metabolites as novel platform in magnetic hyperthermia for the first time that showed a temperature in the therapeutic limit, Tmax=45^{o}C, high dT/dt and SAR = 230.61 W/g, and improved dispersion. Different sizes (Ave. D_{SEM} = 64 nm) and magnetic properties (106 emu/g – 241emu/g) were tuned at various reaction temperatures and concentrations. Ultra-high magnetic saturation (241 emu/g) observed in response to low reaction temperature. We also discovered graphene-based, stable, and room-temperature molecular magnets (2.9 emu/g at 300K) with magnetocrystalline anisotropy of 8 x10^{5} and 3x 10^{7} J/m^{3} in aminoferrocene and graphene-based aminoferrocene respectively. These

values are comparable and even two orders of magnetiude larger than the pure iron metal under normal conditions.

TABLE OF CONTENTS

LIST OF TABLES

LIST OF FIGURES

CHAPTER 1

INTRODUCTION

1.1. Motivation and Approach

Nanotechnology is coined as promising advancement to bring novel solutions to many of the problems seen in some of the large sectors: water, health and energy worldwide (Aghebati-Maleki et al., 2020; Pasinszki & Krebsz, 2020; Sekoai et al., 2019; X. Sun et al., 2017). As a result, the use of nanomaterials in general and particularly magnetic nanoparticles has been a heated source of research interest due to tunable and remarkable properties that the particles show relevant to the desired applications (A. Ali et al., 2021; Kianfar, 2021). Till today, nanoparticles have proven practical uses in industry, manufacturing, agriculture, environment, technology, medicine, electronics, and energy (A. Ali et al., 2021). Nanoparticles encompass wide range classes of materials that differ in physical and chemical properties. It is generally agreed that the nanoscale size is a parameter used to identify these particles. Up to around 250nm size, nanoparticles has used for many applications (Meng & Li, 2018). Researchers have used the advantage of reduced surface area due to size differences, shape and structural variations, distinct optical and electronic and mechanical features, thermal conductivities and modifiable surfaces properties and applied in chemical and photocatalytic reactions as catalysts, in water treatment as adsorbents and other biomedical applications. Moreover, magnetic properties of nanoparticles added novel advantages making them suitable agents in drug delivery and magnetic hyperthermia (A. Ali et al., 2021; Joudeh & Linke, 2022; I. Khan et al., 2019).

Undoubtedly, the potential application nanoparticles further open solutions to the deteriorating environmental, health and energy problems across the globe. However, there are also shortcomings with respect to chemical and physical nature of the materials, their sustainable use in water treatment and biomedical applications. For instance, inadequate distribution of particles in water hinders efficacies and selectivity among pollutants despite large group of contaminants, long-term health impacts from toxic compounds leached from the particles surface and limited performance after the instant interaction with pathogens to mention some (Gehrke et al., 2015). Similarly, there is significant issue with transport of nanoparticles through biological environment and extended localized heating in magnetic hyperthermia(Rytov et al., 2022; Włodarczyk et al., 2022). In this project, we attempt to establish novel solutions to several of drawbacks associated with rigid properties of nanoparticles particles from preparation to application. We placed our emphasis on monitoring surface, textural and magnetic properties.

1.2. Multiple Contaminants in Drinking Water and Water Treatment Process

Fresh water gets its contaminants from municipal, industrial and agricultural waste, animal manures, sewage sludge, pesticides, and nutrient run-off, power generation, heavy industry, automobiles, mine tailings, disposal of high metal wastes, leaded gasoline and paints, land application of fertilizers, coal combustion residues, spillage of petrochemicals, and atmospheric deposition wastewater and other anthropogenic activists (Garcia-Ordiales et al., 2017; I. Khan et al., 2019; Wuana & Okieimen, 2014; Zhou et al., 2020). According to UNEP 2017, 2 billion tonnes of human waste pollute water on a regular basis. The contamination level of organic pollutants has already reached extreme that in Africa, Asia, and Latin America it about 14.28 percent of all the rivers are rich in organic pollutants and this trend has been steadily increasing for years. In organic pollutants are other major classes of pollutants abundant in water

constituting most of hazardous heavy metal. They have extended toxic effect due to their inability to side reaction that led to further degradation to less harmful biproducts same as organic pollutants. It is believed, many fresh water sources all over the world has elevated number of heavy metals as well. The concentrations of these contaminates is much higher in the rivers of the continents mentioned above. The type and number of metal pollutants has also been progressively growing (Garcia-Ordiales et al., 2017; Qa & Ms, 2016; Zhou et al., 2020). Water used for drinking purposes is also host for many photogenic organisms. Reports indicate that 4,000 children die every day from diseases associated with polluted water and inadequate sanitation. Diarrhoea is one of the most popular water borne diseases responsible for 1.8 million deaths each year. Recently, Wolf-Baca & Piekarska, (2020) detected four pathogenic bacterias namely *Actinobacteria*, *Bacteroidetes*, *Firmicutes,* and *Proteobacteria*. Moreover, alarge number of pathogenic microorganisms that exist in water has been summarized elsewhere (Pandey et al., 2014). List of those organisms abundant in freshwater systems can be seen in Figure SA 14. The resulting economic shock is considerable and demands attention UNEP, 2017. Furthermore, all of these pollutant groups has substantial health and environmental impacts on humans and on the ecosystem (Chen et al., 2019; Haseena, 2017; Jayaswal et al., 2018; Shakoor et al., 2017).

1.2.1. Water treatment processes and some advancements

In a typical water treatment process contaminated water passes five major steps after heavier dirt is removed, Figure 2. The steps include coagulation, flocculation, sedimentation, filtration, and disinfection. In coagulation chemicals with charges are added to contaminated water. As a result, negatively or positively charged pollutant particles will interact with the chemicals to form bigger neutral particles that settles down Figure 1. The purpose of the is step along with flocculation and sedimentation is to minimize particles from reaching the filtration process and

hence blocks the filter. However, it also leaves large volume of hazardous sludge that still pose health and environmental treat but also the disposal process is expensive making the entire technique unsustainable solution. Some substances from both treatment agents and pollutants will remain suspended in the water.

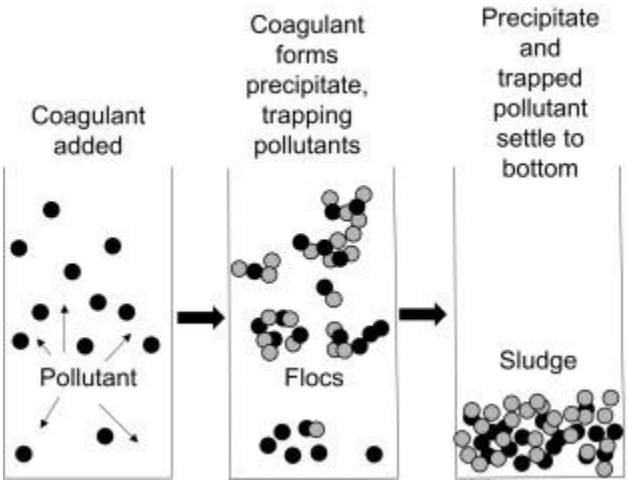

Figure 1: Coagulation process in water treatment. Reproduced from (Barrera-Díaz et al., 2018).

In the filtration process, the water with dissolved solids is allowed to pass through the filter to remove remaining particles and germs(Pai et al., 2020; Qian et al., 2014; CDC, 2022).

Some of the recent water treatment plants are using various membrane purification techniques including microfiltration, ultrafiltration, nanofiltration and reverse osmosis. Advanced membrane techniques such as nanofiltration and reverse osmosis have small pores and are believed to remove smaller particles and microorganism such as and parasites, bacteria, and viruses. However, slow flow rate hinders its efficiency for large scale purification. Moreover, membrane fouling has been a permanent problem in filtration. It endangers the membrane and worsens the slow rate. Consequently, it has been requiring installation of pressure feed equipment and several filters before the final membrane to supplement the filtration process.

This has increased the cost of operation as well as threaten long term use of the technique (Archismita et al., 2020; Belli et al., 2021; Yuan & He, 2015) .

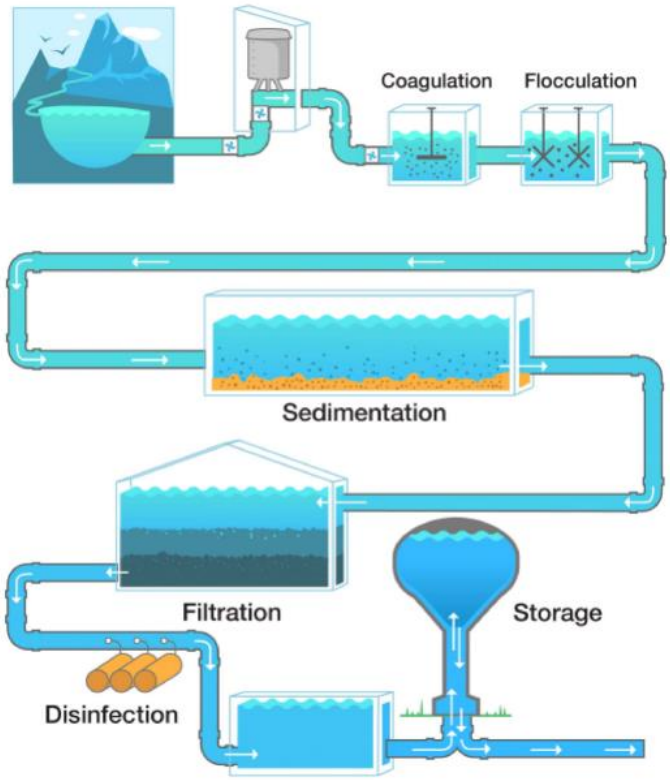

Figure 2: Drinking water treatment process. Adpated from CDC.gov/drinkingwater

1.2.2. Chemicals used in water treatment process

Aluminum sulfate, aluminum chloride, and sodium aluminate are aluminum-based coagulants and ferric sulfate, ferrous sulfate, ferric chloride, and ferric chloride sulfate are iron based inorganic coagulants. Additionally, Polyamines, Polydiallyldimethylammonium chloride (Poly DADMACs) and Polytannate are organic coagulants used in typical water treatment (MCS, 2022). To produce the sludge appropriate amount of these chemicals should added proportional to the particles and in terms of the affluent effluent quantity, this amount, with even excluding acids and bases added to adjust solution pH and coagulant aid chemicals, is huge. Additionally,

all effluents are not neutralized by a specific chemical at the same time. Thus, it requires additional chemicals and supplementary techniques. The fate of all added chemicals is to be discarded along with the sludge and those that do not settle will float in water. Figure 3 below lists some of the common chemicals used in water treatment process.

a. "Online" chemicals

Group	Chemical
Coagulants and Flocculants	Aluminium and iron salts Cationic, anionic and non-ionic polyelectrolytes
Disinfectants and Oxidizers	Chlorine, Chlorine dioxide, Chloramines, Ozone, Hypochlorite,
Precipitation and softening	Calcium oxide, Hydrated lime, Sodium hydroxide, Carbon dioxide, Soda ash, Calcium carbonate
Algaecides	Copper sulphate, iron salts, rosin amine salts and benzalkonium chloride
Corrosion inhibitors	Chromates, nitrites and nitrates; Phosphates and molybdates; Compounds of arsenic and antimony; Silicates and phosphates
Biocides	Acrolein, Amines, Chlorinated phenolics, Copper salts, Organo-sulphur compounds, Quaternary ammonium salts
Antifoam blends	Oils combined with small amounts of silica
Antiscalants	Organic polymeric acids

b. "Offline" chemicals

Group	Chemical
Chelating agents	Citric acid, EDTA, Phosphates
Resin cleaners	Sodium chloride, potassium chloride, citric acid and chlorine dioxide
Fouling cleaners	Inorganic acids and bases, oxidizers

Figure 3: Chemicals used in water treatment in 2016. Reproduced from (Gitis & Hankins, 2018; Rehwoldt, 1982)

Contaminated water is rich in pathogenic microorganisms as shown Figure SA14. Worldwide, chlorine is major disinfectant in drinking water systems. Other chlorine-based treatment agents,

such as chloramine, or chlorine dioxide are also added to inhibit parasites, bacteria, or viruses. Chlorine was argued by many because of its reduced efficiency in turbid waters and incapability to inhibit protozoa. Customers has complained test and odor issues with chlorinated waters. Consequently, chlorine-based treatment agents were launched. Chloring and all other substances in water can reside as well as undergo side reaction in water creating long term health impacts (Clayton et al., 2019; How et al., 2017). The fact that all these chemicals including chlorine are not recyclable, it poses health impacts long term, even though some water treatment plants employed UV or Ozone to disinfect water. (CDC, 2022). Moreover, the side reaction of this chemicals with organic matter would lead to different bi products that could result in direct health impacts.

Therefore, despite the advancement of water treatment techniques, the amount of chemicals used in water has also been increased throughout the period. Figure 4 (a -e) shows the increasing treatment trend in different groups of water treatment chemicals, their market value, and the water treatment technology in relation to chemical consumption. This urges a search for alternative materials with sustainable use in water treatment. Especially those produce safe water, with high reusability and efficient recovery (Hadi et al., 2019; Ang, et.al., 2015; Neoh et al., 2016; Werber et al., 2016).

a

Chemicals	Percentage (%)	
	2009	2019
Corrosion and Scale inhibitors	33%	34.5%
Coagulants and flocculants	30%	31.5%
Biocides and disinfectants	13%	9.7%
Chelating agents	9%	9.4 %
Foam control	2%	2.4%
Others	13%	12.5%

b

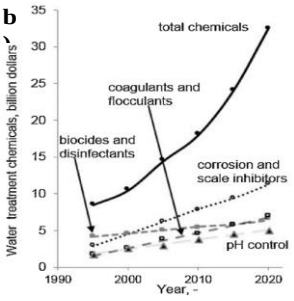

c

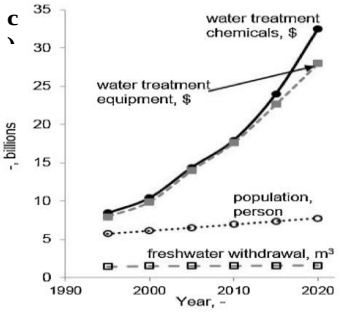

d

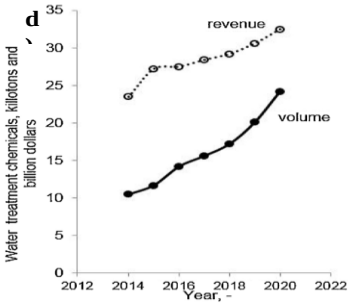

e

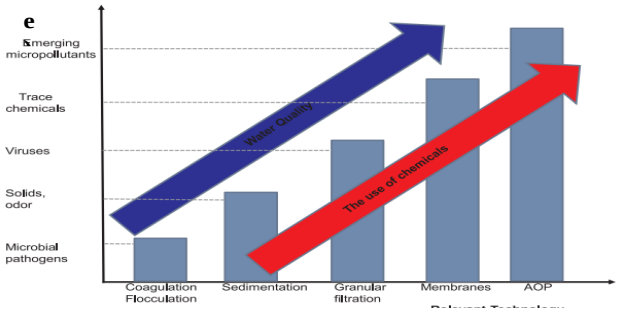

Figure 4: Groups of chemicals in water treatment chemical market 2009 and 2019 where 2019 projection is by Zion Research Analysis (a), production of water treatment chemicals worldwide (b) changes in freshwater consumption (billion m^3), population growth (billion capita), water treatment equipment (billion $) and water treatment chemicals market (billion $) from 1990 to 2020(c), Water treatment chemicals market from 2014 to 2020 by volume and revenue (d) and The progress in technology and water quality over the years(e) (Gitis & Hankins, 2018; Rehwoldt, 1982).

1.2.3. Magnetic nanoparticles in water treatment

Adjustable surface property at appeal to pollutant nature and magnetic property for easily recycling of particles after treatment are two novel advantages that attract mass research on application of magnetic nanomaterials for purification of contaminated water following the growing limitations in the conventional water treatment process including the alarming issue of membrane fouling. (Archismita et al., 2020; Sharma et al., 2018) So far, 75–99 mol% removal efficiency of several organic and in organic pollutants and microorganisms has been reported by polyoxometalate-supported ionic liquid phases (magPOM-SILPs) nanoparticles, 60- 100% efficiency for adsorption of Pb(II) and methylene blue using cellulose@ultrasmall iron oxide nanoparticles (Xiong et al., 2014), above 95% removal of erythrosine from tab, karoon and maroon water by iron oxide nanoparticles coated with methyl trioctyl ammonium chloride (Aliquat 336)Pourreza et al. (2016) and removal of cadmium and lead by EDTA functionalized iron oxide nanoparticles Chin et al. (2011) to mention some. However, surface coated substances on magnetic particles are often vulnerable to leaching. Hence, chemical-based surfactants

detaching into the water has similar health impacts to conventional materials used in water treatment. Thus, green synthesized nanoparticles has been rapidly growing. Yet, incapability of natural products to fully reduce particles into their high magnetic states turned researchers to use chemical based and complex synthesis process (Chin et al., 2011; Xiong et al., 2014; Pourreza et al., 2016).

1.3. Magnetic Nanoparticles in Biomedical Applications

1.3.1. Magnetic hyperthermia

Magnetic nanoparticles have many possible uses in biomedical and other applications(Biehl et al., 2018; Frey et al., 2009; Gul et al., 2019; Pinto et al., 2020). Magnetic hyperthermia is an experimental technique for cancer treatment through magneto thermal heat originated from magnetic particles (X. Liu et al., 2020; Mahmoudi et al., 2018;Blazar et al., 2021 Thiesen & Jordan, 2008). Pertaining to benefits from the technique, an intensive research has been conducted for several tens of years (Mahmoudi et al., 2018; X. Liu et al., 2020; Thiesen & Jordan, 2008). Heating efficiency of particles is determined by their magnetic saturation and other morphological properties. While their ability to accumulate cancerous cells depends on their surface affinity towards the biological medium usually hydrophilic (Fatima et al., 2021; X. Liu et al., 2020; Rytov et al., 2022).

1.3.2. Superparamagnetic property and heating efficiency

Nanosized ferromagnetic particles with small number of domains possess superparamagnetic property. The magnetization of these type of nanomaterials is vulnerable to changes in magnetic

field and temperature. This gives advantage to monitor particles' magnetic behavior for desired biomedical applications (Enriquez-Navas & Garcia-Martin, 2012). In magnetic hyperthermia treatment technique, when magnetic nanoparticles are exposed to external alternating magnetic field (AMF), they generate heat through three major mechanisms pertaining to their size and magnetic domains. The AMF induce eddy currents in multidomain nanoparticles, eventually causing heat or trigger hysteresis loss because of flipping the magnetization of the particles which causes heat(Ahmed et al., 2020). In the case of small size superparamagnetic nanoparticles, the first and most dominant heat is created from Neel and Brownian relaxations. The former refers to heat produced from energy loss due to reorientation of each magnetic moment within a particle causing displacement of domain walls and the later due to rotation of the whole particles (Figure 5 (a)) (Fatima et al., 2021; Suriyanto et al., 2017). In addition to the above properties of magnetic particles, high magnetic saturation (*Ms*) in nanoparticles is proportional to the large thermal energy release during treatment. As a result, less dose will be needed to kill many cancer cells. The treatment time will be significantly reduced(Obaidat et al., 2015). Particles with high *Ms* also allow monitoring during transport towards cancerous cells across biological medium. In both single and multidomain nanoparticles, the interaction of the nanoparticles with themselves and the surrounding medium also contributes some amount of heat into the system(Abenojar et al., 2016).

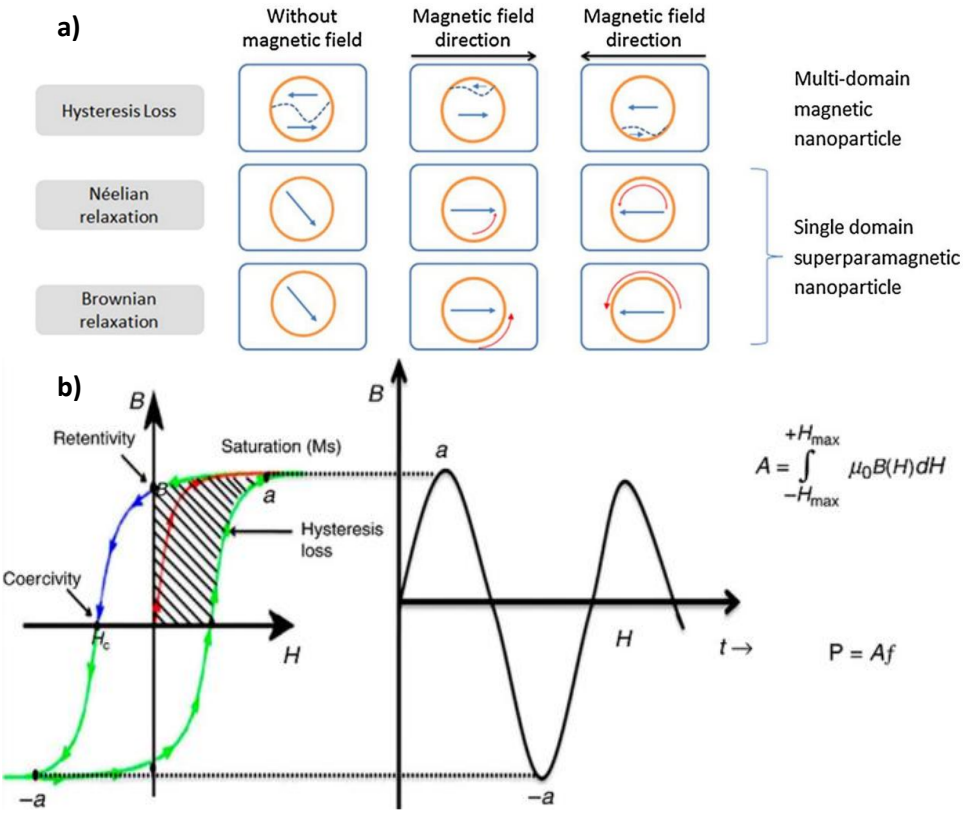
a)
Without magnetic field
Magnetic field direction
Magnetic field direction
Hysteresis Loss
Néelian relaxation
Brownian relaxation
Multi-domain magnetic nanoparticle
Single domain superparamagnetic nanoparticle
b)
B
Retentivity
Saturation (Ms)
a
Hysteresis loss
Coercivity
H_c
H
−a
B
a
H
t →
−a
$A = \int_{-H_{max}}^{+H_{max}} \mu_0 B(H) dH$
P = Af

Figure 5: Mechanisms of heat generation in magnetic nanoparticle during hyperthermia treatment (top). Short straight arrows represent the magnetic moment direction, the curved arrows represent the movement or change in direction, and the dash lines represent the domain boundaries in multi-domain particles. Estimation of hysteresis loss from hysteresis cycle of a ferromagnetic multidomain particle (bottom). Reproduced from (Ahmed et al., 2020; Suriyanto et al., 2017).

1.4. Organic and Molecular Magnets in Data Storage Applications and its Implication in Global Energy Consumption.

In the human history, data storage has evolved from storing data in memory to stone and papers to a more reliable and retrievable tools. According to Cloudesene 2022 (https://www.statista.com/statistics/1228433/data-centers-worldwide-by-country/), today, there 6334 data centers in just 15 countries of the world. Magnetic data storage is one of the recent advancements introduced around 100 years ago and has been through several advancements in access capability, storage capacity per square inch (kb/in^2) Table 1 and Figure 6 below. It is evidence that magnetic materials have a vital role in the evolution of modern data storage (Chong & Piramanayagam, 2012, p 1-9). There has been extreme demand long ago for magnetic materials with improved areal density. In modern data storage materials, magnetic particles including thin metallic films of Iron (Fe), Cobalt (Co) and Nickel (Ni) and their alloys and with other nonmagnetic metals are being extensively used in high density disk drives(Comstock, 2002). Organic and molecular magnets were introduced in late 60's with promising applications in data storage and quantum computing. Till today, they have been an area of intensive research. For example, Figure 7 shows some of the early organic and molecular magnets investigated and many are still under investigation. The reason for this is due to molecular magnets compared to

conventional magnets present novel advantages. First, data is recoded based on spin up and down and requires magnetic field instead of electric field and require minimal energy. Fifteen of the world large data centers consume 1% of global electricity. For US, it reaches around 2% (Masanet et al., 2020; W. Zhang et al., 2022). Thus, using molecular magnets means significant energy save. Second, data is secure and remains for operation even after the devices is switched off or under the absence of magnetic fields (Lapo, Bogani & Wolfgang, Wernsdorfer, 2008). It is evident that the next generation data storage devices are going to depend on this materials. This may be a revelation to IBM which revealed the scaling limitation of data magnetic storage materials at affected real density in around 20 years now. Lately, the realization of graphene based molecular magnets opens more opportunities in data storage given the remarkable properties of graphene for instance, low-temperature fabrication, low density, transparency, electrical insulation, and photo responsiveness in addition to the increase in magnetic ordering to above room temperature compared to traditional molecular magnets (Sato, 2012; Spree & Popov, 2019; Woodruff et al., 2013). Besides, molecular magnets suffer from tunneling at zero field, a major cause for their inefficiency for information storage (Wernsdorfer et al., 2002).

Table 1: The chronology of data storage devices

Year	**Storage Device**	**Capacity**	**Size**	**Materials**	**Remark**
1725	Punch Cards	960bites	7 3/8”x 3 ¼”	Card stock paper	Store data through a pattern of punched holes and blank spaces
1956	Hard drive	5MB	50 x 24”	Aluminum or glass and coated with a magnetic material	
1971	Floppy disk	80KB	8”	Magnetic film	8” read only
1979	Compact disk	700MB	4.7”	Polycarbonate plastic	Optical disks
1985	CD-ROM	900MB	4.7”	Polycarbonate plastic	Read and Write
1994	CompactFlash	100GB	6.8” x 4.7”	Semiconductor	Heavily used by DSLR Cameras
1995	DVD	8.5GB	4.7”	Polycarbonate plastic	-
2000	USB Flash	8MB	-	Metal oxide semi-conductor	Multipurpose

	Drive				
2005	Portable Hard drive	1TB	2.5”	Aluminum alloy, glass, or ceramic	Multipurpose
2006	Blue -Ray	50GB	4.7”	Polycarbonate plastic	Recording, rewriting, playing back high-definition video
2013-2020	Cloud storage	Petabytes		Spintronic devices	General purpose
2020+	Spintronic devices	1TB/In^2		Metal -insulator-metal sandwiches	Molecular magnets

Source: adapted from (Chong & Piramanayagam, 2012; Comstock, 2002; Bhushan, 2018)

Year	Magnetic storage devices development
(a) Tapes and tape drives for audio, video and data recording	
1920s	The first recorders with steel tapes made by Germans
1928	Fritz Pfleumer filed a patent for coating γ-iron oxide particles into a strip of paper as a recording medium
1935	German magnetophone exhibited in Berlin. Used a plastic base with a magnetic coating
1947	3 M shipped the first **commercial** oxide magnetic tapes coated on paper backing
1948	Ampex shipped the first **commercial** audio tape recorder (Ampex 200A)
1951	3 M demonstrated video recording. In 1953, RCA followed
1953	IBM shipped the first **commercial** magnetic tape drive for data storage (IBM 727)
1956	Ampex announced the first **commercial** rotating-head video recorder (Ampex VTR VR-1000). Used transverse format
1960	Ampex introduced helical scan recording to record a field continuously
(b) Hard disk drive for data storage with random access	
1957	IBM shipped the first **commercial** hard disk drive, called Random Access Method of Accounting and Control (RAMAC) (IBM 305)
(c) Flexible (floppy) disk drive for data storage (a cheaper alternative)	
1972	IBM shipped the first **commercial** flexible (floppy) disk drive using 8 in. flexible disk in a rectangular shell (IBM 23FD)

Figure 6: The history of magnetic data storage devices. Reproduced from (Bhushan, 2018).

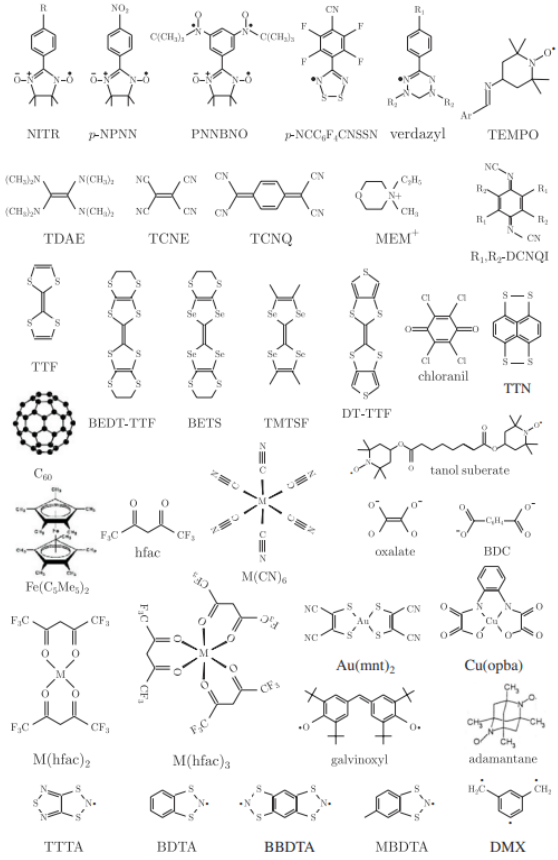

Molecule		Name	S	D (K)
	"Mn_{12}"	$Mn_{12}O_{12}(CH_3COO)_{16}(H_2O)_4$	10	0.56
	"Fe_8"	$[(tacn)_6Fe_8O_2(OH)_{12}]^{8+}$	10	0.275
	"Mn_4"	$Mn_4O_3X(O_2CMe)_3(dbm)_3$	8	0.39–0.53
	"Mn_9"	$Mn_9O_7(OAc)_{11}(py)_3(H_2O)_2$	$\frac{17}{2}$	0.42
	"Fe_{19}"	$Fe_{19}(metheidi)_{10}(OH)_{14}O_6$-$(H_2O)_{12}NO_3 \cdot 24H_2O$	$\frac{33}{2}$	0.56
	"Ni_{12}"	$Ni_{12}(chp)_{12}(thf)_6(H_2O)_6$	12	0.067

Figure 7: Some of the first studied organic magnets and precursors(left) and molecular magnets (adapted from (Blundell & Pratt, 2004)

1.5. Problem Statement and Research Goals

Relying on the core physical and properties of magnetic materials and taking advantage of tunability of those properties this study attempts to find sustainable solutions to deteriorating environmental, health and energy situation the world is facing now and expected to worsen in the future. Non-renewable energy sources are among the major causes of environmental pollutions and environmental pollution is direct threat to the life of all living things. Moreover, severe environmental factors speedup the depletion of natural resources. Given the complex and interrelated nature of these problems it is recent policy and research direction to novel material

and technology solutions (Olivetti & Cullen, 2018). Magnetic materials beginning from their first use as compasses has been progressing to advanced used in data storage materials and recently in water treatment and biomedical applications. Their intrinsic properties unfold opportunities for research and manipulation of those properties made these materials candidates in many applications. We focused on surface modification, size control, composition and magnetization to develop novel in organic and organic soft magnets suitable for water treatment, magnetic hyperthermia and energy applications. Therefore, the fundamental goal of this study is to synthesis, characterize and optimize magnetic nanoparticles for multifunctional use in water treatment, hyperthermia cancer treatment and room temperature graphene based molecular magnets for quantum computing and data storage devices.

To address the long-therm health impacts posed by chemicals used in conventional water treatment methods we suppose that;

Hypothesis:

Magnetic nanoparticles can be synthesized using green method with comparable potential in water treatment to their corresponding chemical-based treatment agents and nanoparticles.

To test this research statement, this study will address the following objectives:

Aim1:

For water treatment, recyclability and alternative recoverability we aim to producing efficient materials prepared using simple green and eco-friendly methods with improved recyclability and recoverability to treat water from various pollutants. The materials will have simultaneous degradation of multiple pollutants in very short period with high performance over wide range temperature and pH.

Objective 1:

- To synthesize nanoparticles using plant phytochemicals as reducing and caping agents capable of removal of multiple organic pollutants (MO, 4-NA) and test their recyclability, introduce alternative recoverability and efficiency at different water conditions.

Objective 2:

To synthesize ZVI@Citrate coreshell nanoparticles using coprecipitation method for rapid removal of organic and inorganic pollutants and inhibition of pathogenic and compare them with relevant studies.

To address the limitation of suitable platform and tunable size magnetic nanoparticles used for magnetic hyperthermia we hypothesize:

Hypothesis:

The right composition of core and shale substance will enhance thermal stability of the core and dispersion of the material as well as novel coating platform on nanoparticles will improve agglomeration problem. Moreover, the nature of the coating agent will ether contain the heat produced due to magnetothermal heating or involve in maximizing the heat due to electron transition.

Aim 2:

Optimize core/shell magnetic nanoparticles with different size, high magnetic properties and efficient magnetothermal heat to be used for magnetic hyperthermia as an alternative cancer therapy. To make an effort on solving agglomeration problem by functionalization of those MNPs by novel surfactants and tailoring their size to produce heat in the therapeutic limit of applied magnetic field.

Objective 1:

To synthesize Fe3O4@SM nanoparticles and examine its suitability for magnetic hyperthermia, in in-vitro.

Objective 2:

To synthesize Fe@CIT Core-shell nanoparticles with different size and examine their suitability for magnetic hyperthermia.

Despite the promising advantages to replace conventional magnets, the operating conditions of previously developed molecular magnets are far from pertinent conditions. Thus,

Hypothesis:

Creating charged/ organometallic compound will lead to emergence of electron spins within the molecule and eventually introduce magnetism into a surrounding molecule and stacking this charged intermediate between graphene layers will disseminate the charge over the six membered chain of graphene layers and sustain the magnetic property for the whole assembly.

- **Aim 3:**

To produce room temperature graphene based molecular magnets using simple coprecipitation reaction and heat treatment. A charged amino ferrocene will serve source of spin to graphene layers above and below the structure.

Objective 1:

To synthesize amino ferrocene and assemble it between graphene layers and study its morphological and magnetic properties.

CHAPTER 2

PROBLEM AND RATIONALE

2.1. Health, Water and Energy Crisis

Several studies claim that the world is in a great disaster in terms of health - so many complications, especially cancer cases are growing, clean water scarcity is seen in every corner of the world, and massive energy demand and depletion of non-renewable energy sources(Alola et al., 2019; Boretti & Rosa, 2019; S. Khan et al., 2017, 2022; Sung et al., 2021; Tipantuna & Hesselbach, 2020). At this moment in time, millions of people are experiencing water related

problems and water pollution is among the major contributors. Reports from World vision, (2021) UNESCO, (n.d.) and WHO (2019) reveal that 2 million tons of sewage drain into water every day. Out of this 300-400 megatons/year are industrial discharges. In developing countries 90% sewage are untreated. Above 673 million people defecate in the open. As a result, 2 billion people live without access to adequate sanitation, 785 million people lack access to clean water. Every day 800 children under 5 die from water borne diseases e.g. diarrhea. All problems collectively are expected to put half of the world in water stress in less than 10 years from now and to significantly diminish biodiversity. This clearly shows high demand for efficient water treatment methods. Sustainable and efficient water treatment methods are necessary, especially water used for drinking needs to be accessible and safe. With efficient recyclability, magnetic nanoparticles have been one of the best candidates in water pollution and related problems (Deshpande et al., 2020; Tom, 2021).

Cancer has become the top cause of death and a major contributor to the weakening of to increasing life expectancy in all corners of the globe. In the year of 2020 alone, there has been 19.3 million new cases and 10million deaths, and this is expected to increase by 47% and the world new cases will tool in to 28.4 million by 2040. In developing countries like Africa, the incidences may be higher (Njuguna et al., 2020; Sung et al., 2021). The global trend of rates is breast cancer (11.7%), lung cancer (11.4%), colorectal cancer (10.0 %), prostate cancer (7.3%), and stomach cancer (5.6%). In Latin America and the Caribbean, a study showed 1.5 million new cancer cases and 700,000 deaths occur annually. It is estimated that with 67% increase there will be 2.4 million new cases annually by 2040. Among the prevalent occurrences in this region are prostate (15%), breast (14%), colorectal (9%), lung (7%) and stomach cancer (5%). Globally,

female breast cancer is the most dragonized type of cancer. In 2020, lung cancer was the first cause of death in Latin America (Njuguna et al., 2020; Sung et al., 2021).

Corresponding to diverse cancer disorders i.e. lung, colon, breast and prostate cancer types, many treatment techniques exist. Deprived of the technical difficulties and side effects of the treatment techniques (CDC, 2022), complexity, site specificity and unaffordability for the general public are some of the most drawback associated with those techniques (Damyanov, 2018; Lettieri-Barbato & Aquilano, 2018). Magnetic hyperthermia is an experimental cancer treatment technique. Heat generated from magnetic nanoparticles up on exposure to alternative magnetic field is used to burst cancer cells onsite. Despite extensive research on this technique efficient heating and biocompatible surface for nanoparticles has been among drawbacks for practical application of the technique(Albarqi et al., 2019; X. Liu et al., 2020; Patil-Sen et al., 2020).

Depletion of non-renewable energy sources in contrast to increase in energy consumption and the climate impacts by which those sources pose on the planet has been an alarming issue (Bekun et al., 2019). The recent economic development is powered by use of non-renewable energy resource which always resulted in pollution of the air, water, and soil. Greenhouse gases, rapid increase in surface temperature, chronic respiratory diseases, acid rain, organic, heavy metal, pollutants and nutrients endangering the accessibility of clean water and the life plants and animals that depends in it (W.-J. Guan et al., 2016; Ibrahim & Ajide, 2021) . Solar, wind, and hydro powers has intensively introduced to tackle the problem. However, climate and geographic challenges limit their extensive use. As a result, world energy coverage from renewable energy accounts for 30% of the total(Aleixandre-Tudó et al., 2019; Bekun et al., 2019). Therefore, the urgency of the situation demanded policy action in addition to research and societal measures.

For example, upgrading the current vehicle fuel and public transportation, cooking fuel and ventilation, industrial technology, building up healthy cities, and implementing environmental policies introducing novel medications(W.-J. Guan et al., 2016).

To realize sustainable environment for forthcoming societal and economic development, preparation of energy efficient materials and renewable source of energy and technology has been the focus of policy and research. Evaluating the overall trend in health, water sand energy crisis the conventional substitute for non- renewable energy is far behind to answering climate challenge and lacks sustainability. Despite fast advancement in water treatment materials and technologies, provision of safe and affordable water to the public is a worldwide problem. The case with cancer is similar. Fast predominance, complicated, high-priced and extended medical procedures leave the issue without sustainable solution. Magnetic nanoparticles and their flexible properties have potential application in these areas and has been used for several ten years now(Aghebati-Maleki et al., 2020; A. Ali et al., 2021; Gehrke et al., 2015; Joudeh & Linke, 2022; I. Khan et al., 2019; kianfar, 2021; Meng & Li, 2018; Pasinszki & Krebsz, 2020; Sekoai et al., 2019; X. Sun et al., 2017; Yang et al., 2021). Therefore, this project with an interdisciplinary approach from Chemistry, Physics and Biomedical concepts uses magnetic nanoparticles in attempt to provide sustainable solutions to water pollution, cancer, energy storage and efficiency as part of research approach for sustainable solutions. Figure 8 lists key nanoparticles controlling parameters and prospective applications which this study is based on.

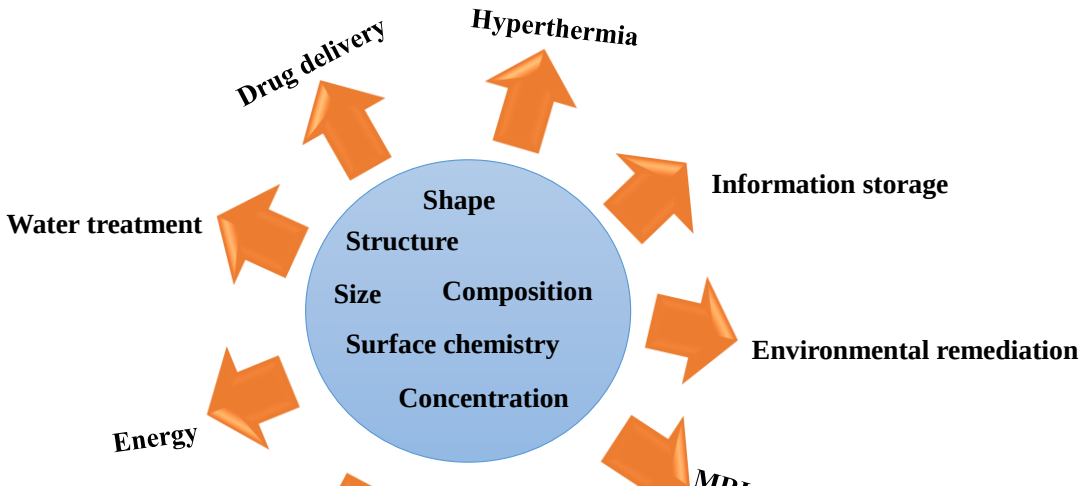

Figure 8: Control parameters of magnetic nanoparticles and sustainable prospective applications

2.2. Green and Recyclable Materials for Water Treatment

Water treatment is one of the most important technologies extensively explored due to various point and non-point sources of pollution that has been increasing parallel to agriculture and industrial developments. This made clean water crisis in every corner of the world(I. Ali & Gupta, 2006). Contaminated water cannot be used for may purposes before its pass different levels of purification. Especially, water used for domestic purposes needs to meet quality standards(Agrawal & Bhalwar, 2009; US EPA. n.d.; CDC 2020 and WHO, 2011) Consequently, many treatment technologies have been developed and are operating in large scale adhering to regulations on water quality standards. However, typical water treatment processes are full of organic and inorganic residuals from added coagulants, flocculants, disinfectants as well as biproducts resulted from reaction of those chemicals with the organic matter in addition to pollutants from non-point sources (WHO, 2011). The property of most of these substances does not allow complete recovery from water which brings an extra challenge of long-term health impact. Perhaps, the only way of managing them to meet water standards is limiting their amount while addition (WHO, 2011). Magnetic nanoparticles (MNPs) has been used in water treatment

taking their magnetic property an advantage for recyclability (J. Guo et al., 2012). Higher surface area and minimal residual after treatment are key advantages in using these the particles water treatment purposes. Additionally, less toxicity of iron oxide nanoparticles has made them excellent choice for many biomedical and environmental applications including water remediation (Mahanty et al., 2019; Malhotra et al., 2020). Moreover, the surface chemistry of MNPs can be tuned to optimize recovery as well as improve adsorption affinity to specific metal and non-metal pollutants (J. Guo et al., 2012).

Magnetic iron oxide nanoparticles are synthesized by physical, chemical, and biological methods. Physical and chemical methods involve a set of complex processes(Kostyukova & Chung, 2016; Kumfer et al., 2010). Additionally, chemical methods use hazardous chemicals during synthesis and functionalization which adds another treat to clean water (Arakha et al., 2015; J. Guo et al., 2012; Herlekar et al., 2014). In contrast, biological synthesis methods provide safer particles with simple reaction procedures. For example, bacterial enzymes can synthesize iron oxide MNPs, although the process takes several days to weeks. Many of the particles synthesized this way also suffer from weak magnetic property compared to those synthesized using chemical methods. Besides, after reduction of metal precursors, functionalization must continue in distinct process with newer compounds (Majeed et al., 2020). Some other researches have produced iron oxide nanoparticles from plants. Nevertheless, many of those studies that argue to use plant extracts also used strong alkaline solutions while synthesis or foreign chemicals during functionalization to increase the magnetic property of their products. For example, synthesis of F_2O_3 MNPs from orange peel (Bashir et al., 2020), Fe_3O_4 MNPs from *Azadirachta indica* (Samrot et al., 2020). Thus, chemicals used in processing the nanoparticles become source of their toxicity during application. In the present study, only plant extracts were

used as reducing and coating agents. Plant secondary metabolites are made up of various functional groups known for their biological activity but also capable of reducing nanoparticles (Arakha et al., 2015; Marslin et al., 2018; Mohan Kumar et al., 2013). On the top of their reducing power, those phytochemicals can serve as coating agents, both to stabilize the nanoparticles as well as for multidimensional absorption. Reduction and functionalization were done simultaneously using aqueous extracts of shade dried *Azadirachta indica* leaf. Crude leaf extracts of this plant has diverse metabolites including alkaloids, saponins, flavonoids, tannins and phenolic compounds (Samrot et al., 2018; Devatha et al., 2016). As a result, it has been used for synthesizing magnetic nanoparticles for water treatment and in various medicinal applications (Alzohairy, 2016; Kostyukova & Chung, 2016& Samrot et al., 2018). Instead of chemical modification as synthesized nanoparticles were used directly to preserve the active ingredients by growing them on a solid material to compensate the loss in magneticity that drastically diminishes their recyclability. Thus, in addition to magnetic manipulation, particles were grown on solid PVA surface to enable alternative recovery. PVA is chosen as solid support due to its thermal stability up to 354.8 ^{o}C and can withstand extreme acidity and basicity conditions (Feldman, 2020). Generally, green and one spot synthesis is preferred health, environmental and economic wise. Moreover, multifunctional group compounds on the surface of the nanoparticles improvises absorption of multiple organic pollutants as well as inorganic ions existed in the polluted water. The present findings motivated us to further study adsorption efficiency to specific heavy metals and efficacy to inhibit microbes of sample nanoparticles which is already included in our upcoming work.

Using magnetic particles as water treatment agents not only is efficient and effective but also transforms the ordinary water treatment processes to safe and cost effective as it requires much less infrastructure.

2.3. Magnetic Hyperthermia

Since the onset use of magnetic hyperthermia as an alternative technique to cancer therapy around 50's for breast cancer, it has been area of research interest till the p\resent day (Mahmoudi et al., 2018; Blazar et al., 2021). Various advantages including site invulnerability, target specific mode of action and synergy with other techniques such as chemotherapy and radiotherapy as well as anticipated affordability compared to other techniques X. Liu et al. (2020); Thiesen & Jordan, (2008), makes the technique promising especially looking at the exponential increase in cancer cases all over the globe (Sung et al., 2021). The technique uses nano sized magnetic nanoparticles (MNs) to dissipate heat that destroy cancerous cells. These particles are prepared using several methods among them reduction of metal salts is commonly employed technique(Majidi et al., 2016; Masunga et al., 2021). Among the diverse applications of magnetic nanoparticles, their ability to produce heat when exposed to alternating magnetic field made them important agents in cancer therapy. Suitable particles for hyperthermia are those with right size, high magnetic saturations and biocompatible. These particles are prepared using several methods and among them reduction of metal salts is commonly employed technique (Majidi et al., 2016; Masunga et al., 2021). Their ability to produce heat when exposed to alternating magnetic field made them important agents in cancer therapy (Gul et al., 2019; Blazar et al., 2021; X. Liu et al., 2020; Mahmoudi et al., 2018; Thiesen & Jordan, 2008). However, the technique has limited clinical trials and application in human cancerous cells and still not recognized as standard therapy Mahmoudi et al., (2018), due to inability to measure the

temperature raise with in biological medium and in consistent heating of the particles (Hergt & Dutz, 2007; Mahmoudi et al., 2018; Peiravi et al., 2022). Moreover, biocompatibility of particles with right magnetic property and ease of transport in the biological medium impacts their abundance in the tumor surrounding eventually, their efficiency (Hergt & Dutz, 2007; Peiravi et al., 2022). One way to improve their transport in \biological medium is to enhance their dispersion in aqueous medium which is done by adapting their surface properties through functionalizing with appropriate platforms. For example, iron oxide nanoparticles coated with 1,4- diaminobenzene (14DAB), 4-aminobenzoic acid (4ABA) and 3,4-diaminobenzoic acid (34DABA) and their combination Kandasamy et al., (2018), graphene oxide(GO), reduced graphene oxide [rGO], and PEGylated rGO Podolska et al., (2020); Sugumaran et al., (2019), alginate and cell-targeting ligands (D-galactosamine) Wu et al., (2015), glutamic acid (GA), citric acid (CA), polyethylene glycol (PEG), polyvinylpyrrolidine (PVP), ethylene diamine (EDA) and acetyl-trimethyl ammonium bromide (CTAB) Rajan et al., (2020) and folate-conjugated poly(ethylene glycol) Piazza et al., (2020), were found efficient for magnetic hyperthermia. Alternatively, core shell nanoparticles recently show prospective application for hyperthermia due high superparamagnetic properties(Gupta et al., 2021; Horny et al., 2021; Martinez-Boubeta et al., 2021; Patil-Sen et al., 2020; Sanad et al., 2021). However, the heat yielded was below 45^{o}C as a result week dT/dt and specific absorption rate (SAR) Horny et al., (2021); Sanad et al., (2021), attributed to shape and size differences (Vasilakaki et al., 2015). Moreover, aggregation of the particles within the medium confines heat for few of the cancerous cells thus remarkably diminish efficiency of nanoparticles to destroy maximum of those cells (Hergt & Dutz, 2007; Peiravi et al., 2022). Thus, even though materials with superior magnetic saturation that potentially produce high heat are prepared, it requires both high

superparamagnetic property and successful functionalization to be able to produce heat per individual particle to reach all malignant cells within the tumor. This research introduces novel green functionalizing material that satisfies those key properties. With consideration to biomedical application, these materials are biocompatible because compounds on the surface are secondary metabolites of a plant material prepared with water as a medium. Chemical nature of the metabolites and their effective coating ability produce efficient nanoparticles with enhanced calorimetric properties: higher rate of solution temperature and specific absorption. In this study a novel green platform is introduced and compared against the common platform used in the technique. Magnetic nanoparticles were prepared using simple coprecipitation metal precursor and further heated in a pressure reactor to yield super paramagnetic nanoparticles, then the particles were coated with two formulated platforms.

2.4. Tunable ZVI@CIT For Water Treatment, Magnetic Hyperthermia and Energy Applications

Core-shell nanoparticles of zerovalent iron (CZVI) provide a vast opportunity in water treatment, catalysis, biomedical and energy applications and has received wide attention in recent years due to their remarkable chemical and physical properties which allow easy monitoring with magnetic field, effective surface dispersion, fast reactivity and surface modification(Ghosh Chaudhuri & Paria, 2012; Kwizera et al., 2016, 2017a; X. Li et al., 2006; Tiwari et al., 2021; Yelenich et al., 2015). Today, ZVI nanoparticles are extensively investigated for environmental, biomedical and energy candidate materials due to high demand for materials of high specific area, specific heat absorption, efficient reactivity and tunable surface properties since these problems are amongst the major current problems across the globe (Kumar et al., 2013; X. Li et al., 2006). As a result, several kinds of core-shell nanoparticle have been introduced suitable for each application. With

respect to the nature of the core and the shell, nanoparticles are grouped in to four categories namely metal/metal, metal/non-metal, non-metal/metal and non-metal/non-metal in order of core and shell component of the core-shell nanoparticles(Adamiano et al., 2018; Dembski et al., 2018; Ghosh Chaudhuri & Paria, 2012; Nomoev et al., 2015). Amongst them metal/metal and metal/non-metal are commonly used core-shell nanoparticles due to simple and efficient synthesis including various synthesis options as well as wider range applications. Choice of proper synesthetic procedure is an important step for preparation these particles for the desired purposes(Ghosh Chaudhuri & Paria, 2012). Much research use both bottom-up and top-down synthesis methods. Indeed, bottom up synthesis approaches is preferred at it allows complete control over the process at minimal energy expense(Dodd, 2009; Khatami et al., 2018). Some of the bottom up synthesis approaches include, hydrothermal synthesis, solvothermal synthesis, sol-gel method, emulsion polymerization, microemulsion polymerization, chemical synthesis, chemical vapor deposition, laser-induced assembly, self-assembly, colloidal aggregation, film deposition and growth and co-precipitation (Baig et al., 2021; Ghosh Chaudhuri & Paria, 2012; Kumar et al., 2013; Rane et al., 2018). However, most of these approaches are complex, energy-demanding and uncontrollable. If conducted cautiously, co-precipitation is possibly a very facile and convenient way for preparation of homogeneous small size core-shell nanoparticles because synthesis of the core and attachment of the shell is achieved in controllable surface adsorption, ion exchange, surface precipitation or occlusion mechanisms. In preparation of ZVI nanoparticles, oxidation in to oxidized iron compounds and aggregation of product particles are two major challenges(Alterary & AlKhamees, 2021; Chekalil et al., 2019; Primc et al., 2016; Salehizadeh et al., 2012). While, previous research demonstrated running coprecipitation reactions to prevent oxidation this approach is still cost-ineffective and time consuming. Another

important factor in synthesis using coprecipitation to control the pH of the solution (Dembski et al., 2011; K. Wu et al., 2015). The means to control pH is by controlling the addition of reducing agent. Nevertheless, controlling pH neither avoids oxidation nor determines the size and homogeneity of the particles. Nevertheless, small and narrow size distribution of particles are efficient candidates for removal of wide range of pollutants from contaminated water and show efficient heat capacity in magnetic hyperthermia(Abenojar et al., 2016; Guibert et al., 2015; Yelenich et al., 2015). In consideration of the above challenges the present study attempts to achieve comprehensive textural and magnetic properties by monitoring source of the core and shell materials as well as the reducing agent.

2.5. Room Temperature Molecular Magnets

Graphene based molecular magnets (G-MMs); especially those with near room temperature magnetic susceptibly are in need at most in prospective applications to replace recent magnets in spintronic and quantum computing. They exhibit longer magnetic order than ligand based molecular magnets. Besides, ligand based molecular magnets suffer from tunneling at zero field, a major cause for their inefficiency for information storage (Wernsdorfer et al., 2002). Even though, graphene sheets lack magnetic property, structural change due to oxidation to graphene oxide and structural defects introduces ferromagnetism. In both graphene oxide and reduced graphene oxide Diamantopoulou et al. (2017) and Sarkar et al. (2014) reported weak superparamagnetism at room temperature. Epoxide functional groups, composites are responsible for magnetic susceptibility of graphene oxide Galpaya et al. (2014), creating unpaired spins on the carbon radicals (Lee et al., 2015a; M. Wang & Li, 2010). Surface N-doping also increases magnetization in graphene oxide sheets to ca. 1.66 emu/g (Y. Liu, Tang, et al., 2013) and by 64.1% when annealed at 500 °C (Y. Liu, Feng, et al., 2013a). Hong et al.

(2013) has published nitrophenyl functionalized graphene based molecular magnet with long-range magnetic order above 400K. The high surface area in graphene integrated with aryl radical on the surface created out-of-plane antiferromagnetic ordering. In recent study, attachment of electron withdrawing substituted ligands to the graphene enhanced charge transfer revealing magnetic and electronic properties (Zhu et al., 2020). Similar to this study, magnetic property of graphene oxide surface functionalized by amino ferrocene revealed magnetization as collective effect of the sheets and the ferrocene moiety (Sakurai et al., 2019). The research trend in this area indicates, molecular magnets are expected to be available with several characteristics including low-temperature fabrication, low density, transparency, electrical insulation, and photo responsiveness in addition to the increase in magnetic ordering to above room temperature. That is, if they are to be used in practical applications (Sato, 2012; Spree & Popov, 2019; Woodruff et al., 2013). In this study, we aimed to solve two major gabs in G-MMs. First, to synthesize the molecular magnet that can operate at room temperature. Second, to increase magnetic order stability by attempting to locate the ligand inside graphene layers. For this reason, we select ferrocene as magnetic ligand to be embedded to graphene oxide layers. Graphene oxide layers are stable single chemical based structural frameworks, which will behave uniformly throughout the assembly. Ferrocene is a choice of ligand for its efficacy to participate in electron transfer (L. Guan et al., 2005). The more favorable interaction of the graphene oxide layer and the ferrocene in a way that does not alter their chemical properties is a noncovalent week interaction resulted from near proximity of delocalized $\pi -$ electrons (Lopes et al., 2010). Moreover, the use of amino ferrocene charged is crucial for the formation of our molecule-based magnet (Wainwright, 1999).

2.6. Conclusions

Contemplating the nature of our research problems, it requires manipulation of surface and grain size (for both water treatment and magnetic hyperthermia) and magnetic properties in all applications. In water treatment the magnetic materials are recycled by a magnet after treatment while in magnetic hyperthermia particles need magnetic property for easily transport on biological medium and to provide magnetothermal heat for destroying cancer cells during the treatment. For molecular magnets imposing spin coupling thus stable moment in the molecule is important part of the investigation. On assembly of an organometallic compound to a graphene framework a charge transfer from the organic moiety to graphene is targeted to produce long rearrange magnetic order. List of the parameters controlled here and corresponding applications are listed in Figure 9 below.

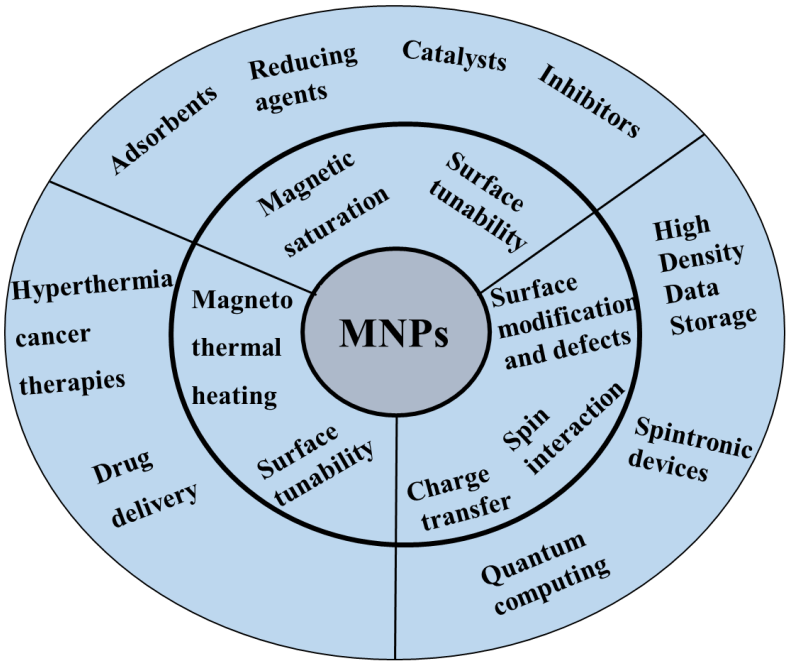

Figure 9: Selected controlling parameters of inorganic and organic(molecular) magnetic materials and their respective applications in this project.

CHAPTER 3

METHODS

3.1. Materials

Chemicals used in this study include iron (III) chloride ($Fe(Cl)_3.6H_2O$), iron (II) chloride ($Fe(Cl)_2.4H_2O$), methylene blue, sodium hydroxide (NaOH), and hydrochloric acid (HCl), Sodium chloride (NaCl), sulfuric acid (H_2SO_4), phosphoric acid (H_3PO_4), potassium permanganate (KMnO4), iron sulphate heptahydrate ($FeSO_{11}H_2$), Sodium citrate dihydrate($C_6H_9Na_3O_9$), $NaBH_4$, sodium sulphate (Na_2SO_4), sodium nitrate ($NaNO_3$), sodium bicarbonate ($NaHCO_3$), magnesium sulphate ($MgSO_4.7H_2O$), calcium sulphate ($CaSO_4$) and potassium chloride (KCl), hydrogen peroxide (H_2O_2), nitric acid (HNO_3), 4-nitroaniline, Tin granules, single layer graphene, graphite, ferrocene were purchased from Sigma Aldrich and Fisher scientific (USA). Ultra-pure Argon gas (analytical grade) was obtained from Air Gas, El Paso, USA). All chemicals were analytical grade and used in this study without further purification. Distilled water and Milli Q water were used as a solvent in all the experiments while distilled water and mixture distilled water and ethanol was employed for washing nanoparticles.

3.2. Methods

3.2.1. Preparation of secondary metabolites in crude extracts

Fresh leaves of Neem (*Azardica indica*) were collected and washed with distilled water and shade dried for ten days. Then, dried leaves were hand crushed and stored at 20^{o}C. In a 250ml Erlenmeyer flask, 10g of power leaf was soaked in 100ml distilled water for 10 minutes and then

heated with incessant stirring for one hour at 80^{o}C. Extract solution was double filtered using Whatman filter paper and centrifuged to remove any unfiltered dusts and stored at -10^{o}C for further use (Hashim et al., 2021; Naz et al., 2022).

3.2.2. Green synthesis of bare and secondary metabolite coated iron oxide coated with nanoparticles

Solution of metal precursors: 0.1M of Fe $(Cl)_3.6H_2O$ and 0.2M of Fe $(Cl)_2.4H_2O$ (1:1) were prepared in one flask. Plant extracts were added to the flask dropwise with vigorous stirring. The solutions turned black in each addition until completely became black when the whole volume of extracts (1:1) was added. This black suspension of nanoparticles was divided in to two portions. The first half (Y0PL) were immediately centrifuged and washed then dried at 60 ^{o}C for 6hr before further analysis. The second half was introduced into pressure reactor and heated at 250 ^{o}C and 1000psi for two hours. The reactor chamber was allowed to cool, and particles were collected with ethanol and then washed several times in distilled water and then in mixture of distilled water and ethanol. Oven dried nanoparticles were characterized and studied for absorption. In the case of plant-based nanoparticles (Y0PL), two solutions that vary in the ratio of plant extracts, 1:1 and 1:2 metal - plant ratios were prepared. However, both samples showed the same performance in absorption and similar spectra in UV and XRD but the former one has higher yield. As A Result, only the first solution i.e., 0.1M of Fe $(Cl)_3.6H_2O$ and 0.2M of Fe $(Cl)_2.4H_2O$ and plant extracts (1:1) was used in all experimentations in the study.

3.2.3. Functionalization of magnetic nanoparticles

During the synthesis process, plant phytochemicals serve as reducing and functionalizing agents in concerted process. Hence, as synthesized nanoparticles are produced with their surfaces

modified. However, magnetic moment of these particles is very low. To enhance their magnetic property the particles were put in the pressure reactor at elevated conditions. The conditions have transformed the particles into complete phase iron oxide nanoparticles with enhanced magnetic property but lost their surface modifiers in the process. These particles are labelled Y0PR. Thus, subsequent functionalization was necessary to recover plant-based compounds on the surface of the nanoparticles. For this purpose, 50mg of the nanoparticles were taken and added in to 3ml solution of extracts and stirred overnight for 12 hours. Then, particles were washed first with distilled water then with the mixture of distilled water and ethanol and dried at 60^{o}C(Y0PRP).

3.2.4. Synthesis of Fe_3O_4@GO nanoparticles

To 20 mL of solutions of iron dichloride ($FeCl_2$. $4H_2O$), iron trichloride ($FeCl_3$. $6H_2O$) (2:1) 2.5mL (50mg/L) of graphene oxide was added and stirred vigorously. Then 1M of NaOH was added until pH of the solution reaches 12. The whole process was done inside a chamber of glove box flashed by Argon. Dark brown particles started to form after pH 10 and finally they were collected and washed with ethanol several times and dried at room temperature for 8hrs (Hanh et al., 2018).

3.2.5. Synthesis of Fe@CIT nanoparticles

In 15ml centrifuge tubes, various concentrations of reactants were dissolved in 10 milliliters of distilled water. Concentration of iron sulphate were pre-prepared in 111.2, 55.6, 27.8, 18.5, 13.9, 11.12, and 9.27 mole/L and sodium citrate in 73.53, 49.01, 36.76, 29.41 and 24.50 mole/L and that of sodium borohydride in 18.92, 9.45, 6.30, 4.72, 3.78, 3.15mole/L. Synthesis was conducted in four batches. The goal of the first batch is to research the optimum concentration of metal core. Thus, reactions were run at variable concentrations of iron sulphate heptahydrate and fixed concentrations of sodium citrate and sodium borohydride as well as time of addition of the

reducing agent. Iron sulphate heptahydrate and sodium citrate were mixed by magnetic stirring at 1500rpm for 5 minutes while sodium borohydride was dissolved separately and added after the five minutes, drop wise 1drop/second. Additions were made in 150ml three necked round bottom flask to give final ratio of 1.25:1:5, 2.5:1:5, 5:1:5, 7.5:1:5, 10:1:5, 12.5:1:5 for Iron sulphate heptahydrate, sodium citrate dihydrate and sodium borohydride respectively. Similarly, to identify suitable concentrations of the shell material (sodium citrate) different concentrations of sodium citrate mentioned above to attain a final ratio of 10:1:5,10:2:5, 10:3:5,10:4:5 and 10:5:5(second batch). The third batch aims to study the right amount of reducing agent. For this end, seven concentrations of sodium borohydride were mixed with iron sulphate heptahydrate and sodium citrate in a solution to give a final ratio of 10:1:1, 10:1:2, 10:1:3, 10:1:4, 10:1:5, 10:1:6 as shown in Table SA1 of the supporting information. Except for the study of effect of reaction temperature, all other reactions were conducted under the laboratory temperature(21-25^{0}C). Effect of sodium citrate dihydrate and sodium borohydride were studied in similar manner by varying the concentration of target reactant and the ratio of the reactants as shown in the supplementary material, Table SA1. The first batch of experiments for optimization of iron sulphate heptahydrate concentrations were run with and without argon atmosphere while all other reactions were conducted under standard conditions. Effect of temperature was studied on selected sample ratio (10:1:5) which showed ultra-high magnetic properties. For this approach, reaction temperature was adjusted to 0, 10, 30, 40, 60 and 80^{o}C through the entire reaction process.

3.2.6. Synthesis of graphene oxide

The synthesis of graphene oxide was done using the modified Hummer method mentioned elsewhere (Zaaba et al., 2017). To be specific, we added 3ml of phosphoric acid (H_3PO_4) to 27ml

of sulfuric acid (H_2SO_4) and stirred for ten minutes. While stirring, 225 mg of graphite powder followed by1.32g of potassium peroxide ($KMnO_4$) was added and the mixture was allowed to stir for seven hours. Finally, 0.675 ml of hydrogen peroxide (H_2O_2) was added and stirred for 10 minutes. The product was centrifuged five times with hydrochloric acid in distilled water and finally with ethanol and left to dry overnight.

3.2.7. Synthesis of amino ferrocene

The cyclopentadienyl ligands in ferrocene are aromatic (considering the cyclopentadiene anion) hence can undergo electrophilic aromatic substitution reactions which is characteristics of aromatic compounds mainly benzene (Rausch, 1963; Woodward et al.,1952). However, nitration of ferrocene has been deemed un-attainable (Woodward et al., 1963). Regard as the aromaticity character of the ferrocene, the well-known mechanism of nitration of benzene with slight modifications was followed (Olah et al., 1987). First, 1ml of sulfuric acid (H_2SO_4) and 3ml of nitric acid (HNO_3) were mixed in a 250 round bottom flask and placed in in ice bath for 15 minutes. To this mixture, 0.8 g of ferrocene was added slowly in portions. This nitro-ferrocene was transferred to three neckd round bottom flask for reduction. By the opposite arm of the flask, 1g of Tin granules and 7ml of hydrochloric acid (HCl) was poured and closed by a cork fitted with thermometer. With drop wise release of the nitro ferrocene, the mixture was refluxed for 45 min at 75 ^oC, the set up was allowed to cool and then disassembled. The product was washed and centrifuged several times. The final product $[C_{10}H_9FeN]^+$ was formed by the mechanism as shown as Figure 10.

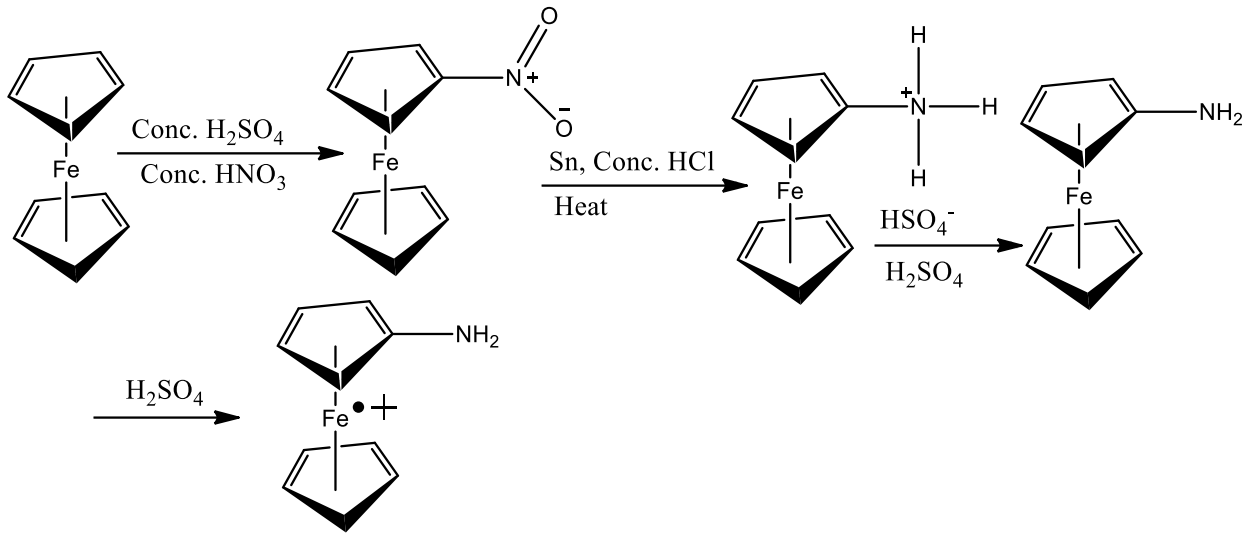

Figure 10: Reaction mechanism for synthesis of amino ferrocene $[C_{10}H_9FeN]^+$

3.2.8. Synthesis of G-MMs

Similar setup was assembled as above, this time, to the supersaturated solution of amino ferrocene semi-crystals in the flask, 0.02 graphene oxide dissolved in 10 ml of dimethyl formal amide (DMF) was added. After refluxing for 45 minutes at 60^{o}C, the product was centrifuged and washed several times before further analysis. The chemical structure of the anticipated final product is illustrated in Figure 11.

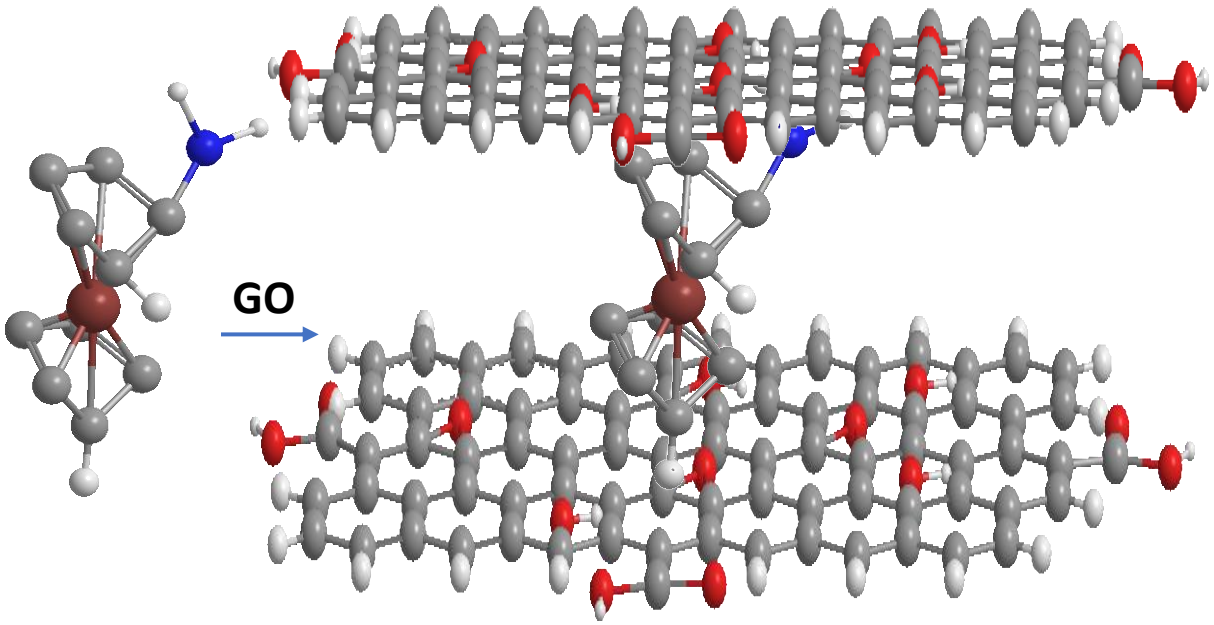

Figure 11: Reaction Mechanism for synthesis of GOFR-MM1

3.2.9. Growth of magnetic nanoparticles on solid support

Using lesser cutter, PVA disks of diameter 7mm and 2mm thickness were prepared first. Next to that, Y0PL was synthesized following similar procedure as above. Then, some amount of Y0PL was dispersed in Mili Q water in 50ml centrifuge tube to give 5mg/L concentration. After that, PVA sponge disks were inserted into solution and stirred overnight in orbital shaker at 150rpm. The disks were white at the beginning but then turned black same as the solution containing the nanoparticles in the first 10minutes indicating growth of the nanoparticles on their surfaces. For the sake of stability however, the disks were allowed to stir for 15 hours. They were then takeout from the flask and air dried for 14 hours after rinsing them with distilled water.

3.2.10. Assembly of particles grown on PVA into microfluidic chip

The chip was prepared from 1.5 mm an acrylic glass (Poly (methyl methacrylate), (PMMA)) and designed with inlet, outlet channels and nanoparticles grown on PVA surface in the middle, and all connected in channels as shown in Figure SA 3. After nanoparticles/ PVA is inserted in the

middle section, clamped with flat mechanical compressors and placed in the oven for 30 minutes at 120^{o}C. The final chip would look like as shown in Figure 12 below.

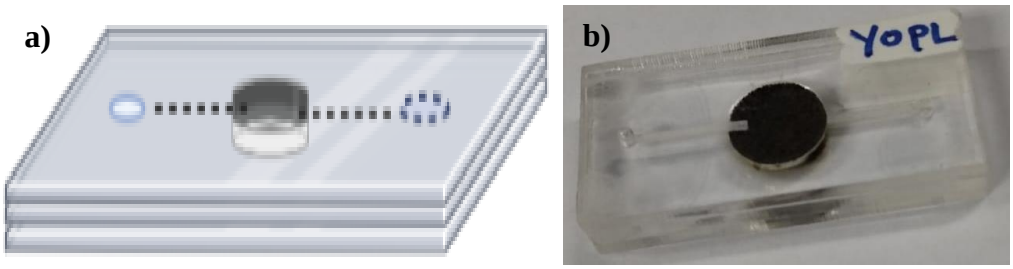

Figure 12: Continuous single adsorbent Microfluidic chip design: a) 3D-model and b) image of the actual chip.

3.2.11. Characterization

Except molecular magnets and the first green synthesized particles (also semi-crystalline), all particles are crystalline as confirmed by advanced instrumental technics. Our aim is to study their property label them as candidates for water treatment, magnetic hyperthermia and data storage. Thus, we used some of the powerful tools to examine their structural, elemental, and magnetic properties to strengthen our argument and before proceeding to their actual application assay.

X-ray diffraction (XRD)

After purification and drying at desired temperature all sample nanoparticles are powders thus powder XRD measurements were carried out using a PANalytical X'Pert PRO XRD with Cu K radiation (lamda= 0.1548 nm). Each run was set between 20 degrees and 90 dgrees of reflection angle (2θ) in a scan rate between 0.01 to 0.3 second which account 10 minutes to 120 minutes Of scanning time and results were analyzed in Origin software. Average size was calculated using Scherer formula:

$D=K\lambda/\beta Cos\theta$……1

Where: D is , K is a constant, λ is the X-ray wavelength, β is the line broadening at half the maximum intensity (FWHM), in radians and θ is the diffraction angel.

Scanning electronic microscope (SEM)

Sample nanoparticles were mounted on a carbon tape and their SEM image of was recorded. The topography of powder particles was studied using Hitachi S-4800 Field Emission Scanning Electron Microscope (FE-SEM) detector type XFlash 6|60 ex, equipped with EDX from Bruker Nano GmbH Berlin, Germany at 15keV primary energy and current 7mAm. From the resulting images size distribution was estimate and number of atoms were calculated by the following formula.

No. Atoms = $\frac{4/3\pi r^3}{a^3}$……1

Where, *r* is the radius of particles and *a* is lattice constant (El-Gendy et al., 2010).

Energy dispersive X-ray spectroscopy (EDS)

Simple operation on SEM machine also serves as EDX which provides information related to elemental composition. From each sample, an SEM image between 1 to 5 micrometers was scanned by the detector and surface analyzed for composition and abundance of elements by EDS immediately. Most compositions are average taken from larger area in 5μm resolution. Moreover, particle distribution was analyzed using ImageJ and data were processed in Origin software.

Ultraviolet-visible spectroscopy (UV-Vis)

Nanoparticles excites electrons at certain wavelength which the resultant λ- max is taken as characteristic identification for that particle. For identification of nanoparticles and determination of their Band gap energy (Eg) we used V-770UV-Visible/NIR spectrophotometer (a single monochromators and dual detectors, 190 to 2700nm, Jasco) in 200 to 800nm range. For adsorption assays SpectraMax Plus 384 Absorbance Plate Reader was used.

Fourier Transform Infra – Red spectroscopy (FTIR)

For understanding surface functional groups in nanoparticles and major bonds in molecular magnets infrared vibration measurements were carried out between 400 and 4000 cm^{-1} with a vacuum based Bruker IFS 66v spectrometer, equipped with a DTGS detector and a KBr beam splitter. The samples for the IR studies were prepared in form of pellets by embedding the nanoparticles in a transparent polycrystalline CsI matrix. An accumulation of 256 scans was performed for each spectrum. The data were normalized at each frequency to a vacuum throughput spectrum. The spectra were matched to the standard vibration and bending wavelengths for various functional groups.

Raman spectroscopy

When analyzed by Raman spectroscopy graphene has two distinctive bands regardless of small modifications or attachments. We used this tool to detect the quality of D and G bands for our molecular magnets. Interpretation was made by reference vibrational, rotational, and other states given wavelengths.

Vibrating sample magnetometry (VSM)

Magnetic saturations (Ms) and temperature dependent magnetizations at 300K and 50K was obtained from vibrating sample magnetometry (temperature:50 – 400 K and 3 tesla platform),

Quantum Design PPMS® VersaLab, North America. Both coercivity (Hc) and domain size (Dmag) were obtained from hysteresis loops at 300K. To calculate grain size, we used the following formula(El-Gendy et al., 2010; Glaspell et al., 2006).

$$Dmag = \frac{18K_B T\frac{(dM)}{(dH)}}{\pi\rho Ms^2} \quad \text{.....2}$$

Where, K_B is Boltzmann constant, T is temperature in Kelvins, dM/dH is the initial slope

near zero field, ρ is the bulk density and Ms is magnetic saturation of the sample.

3.2.12. Adsorption assay

Nanoparticles were examined for their absorption efficacy towards methyl blue, a model industrial contaminant and 4-nitroanilline, an additional organic pollutant that exist in polluted water which also has serious health consequences. Stock solution of methylene blue (MB) was prepared in Milli Q water at 10, 20, 40, 80 and 140mg/L and that of 4-NA at 0.5mM and 1mM concentration. Following this, as synthesized, bare, and functionalized nanoparticles were dispersed in each pollutants concentration to give final concentration of 5mg/L. Before the absorption experiment, mixture solutions were sonicated for 1minutes. This mixture was then put in orbital shaker from 5 to 160minutes where sample were taken at 5, 10, 20, 40, 80 and 160minutes. Magnetic particles were removed easily from eluates using a magnet whereas non-magnetic nanoparticles were removed by centrifugation at 12800rpm for 10minutes. Absorbance of the final solutions was measured in UV-spectroscopy at 200-800nm for MB containing solutions and 250 to 550 for 4-NA containing solutions. On the other hand, PVA disks with nanoparticles grown on their surface were assembled into microfluidic chip system. The system comprises inlet, outlet and the disk connected in a linear fashion. An appropriate amount of MB

solution(5ml) was transferred to a syringe and fixed at the plumber. The needle is connected to the inlet by polyethylene tube and the outlet to receiving clean vial with the same tube. At the same concentration of MB used above, absorption performance of sample nanoparticles was studied. Furthermore, time elapse was reduced to a range of 2-12minutes. Optimum temperature and pH conditions for the performance of nanoparticles incorporated in PVA sponge was also analyzed in a similar setting. Finally, removal efficiency of nanoparticles was calculated as follows (J. Guo et al., 2012):

$$Removal\ Efficiency = (1 - \frac{C_i}{C_e})x100\% \quad \text{.....(1)}$$

Where C_i and C_e are initial and equilibrium concentrations of adsorbent.

Similarly, concentration of pollutants at equilibrium by sample absorbents was calculated by the following formula(Ayawei et al., 2017).

$$qe = (\frac{C_e - C_i}{m})xV \quad \text{.....(2)}$$

Where C_e is adsorbate concentration at equilibrium(mg/L) and C_i is initial adsorbate concentration in solution respectively, *m* is mass of the adsorbent in grams per unit volume and V is the volume of the mixture solution in litters.

The nonlinear Langumir model was calculated as:

$$qe = \frac{q_m K_L C_f}{1 + K_L C_f} \quad \text{.....(3)}$$

3.2.13. Investigation of specific heat adsorption of nanoparticles

To assess feasibility of each nanoparticle for hyperthermia application, 5mg of each nanoparticle was added to a 2ml vial with 1ml distilled water and sonicated for 10minutes. The vial was

cupped with water-cooled magnetic coil and inserted into hyperthermia chamber. Then, an alternating magnetic field was released in a range of 100 to 400Oe at 304 kHz frequency for the period of 120 seconds. The fiber-optical sensor measures temperature raises against time and displays it for every temperature increase in a second (El-Gendy et al., 2009a).

CHAPTER 4

GREEN SYNTHESIZED IRON OXIDE NANOPARTICLES FOR WATER TREATMENT WITH ALTERNATIVE RECYCLABILITY

4.1. Introduction

Widely used water treatment methods are based on chemicals that leave residual unwanted impurities, instigating long-term health impacts. Hence, functionalized **m**agnetic **n**ano**p**articles (MNPs) have been used to fill those gabs and are commonly used for metallic adsorption in contaminated waters(Archismita et al., 2020; Pinto et al., 2020; Tom, 2021). High surface to volume ratio of those MNPs allows for a larger capacity of pollutant adsorption. In this study, functionalized iron oxide MNPs are synthesized by novel green approach using plant phytochemicals with the capability of absorbing multiple organic pollutants. Herein, we studied synthesis of iron oxide MNPs with crude plant extracts using simple maceration technique. The reaction was supported further by heat treatments to complete the reduction process to superparamagnetic iron oxide nanoparticles. Our XRD result show formation of spherical and cubic Fe phase, goethite (before treatment-Y0PL) and magnetite (after treatment -Y0PR) and magnetite (after treatment and functionalization-Y0PRP) with average size ranging from 29 to 277nm. Phytochemicals increased the size and altered texture of nanoparticles. The magnetic properties were measured for magnetization dependence on external magnetic field to show ferromagnetic behavior with Ms =43.6(HC=0.015 Oe), 36.41(HC=0.01 Oe) and

13.12(HC=0.001 Oe) emu/g for Y0PR, Y0PRP and Y0PL respectively. Absorption/reduction efficiency of nanoparticles was studied against MB (10-140mg/L) and 2-NA (0.5-1mM). As synthesized green nanoparticles absorbed the model dyes above 80% efficiency under wide range conditions in a very short time and 94% under optimum conditions. Moreover, this paper introduces successful alternative recyclability especially, for weak magnetic nanoparticles by growing them on the surface of polyviniyl alcohol solid support. Green synthesized magnetic nanoparticles prepared in this study are easy to synthesize, cost-effective and enviro-friendly water treatment agents also illustrated in Figure 13 below.

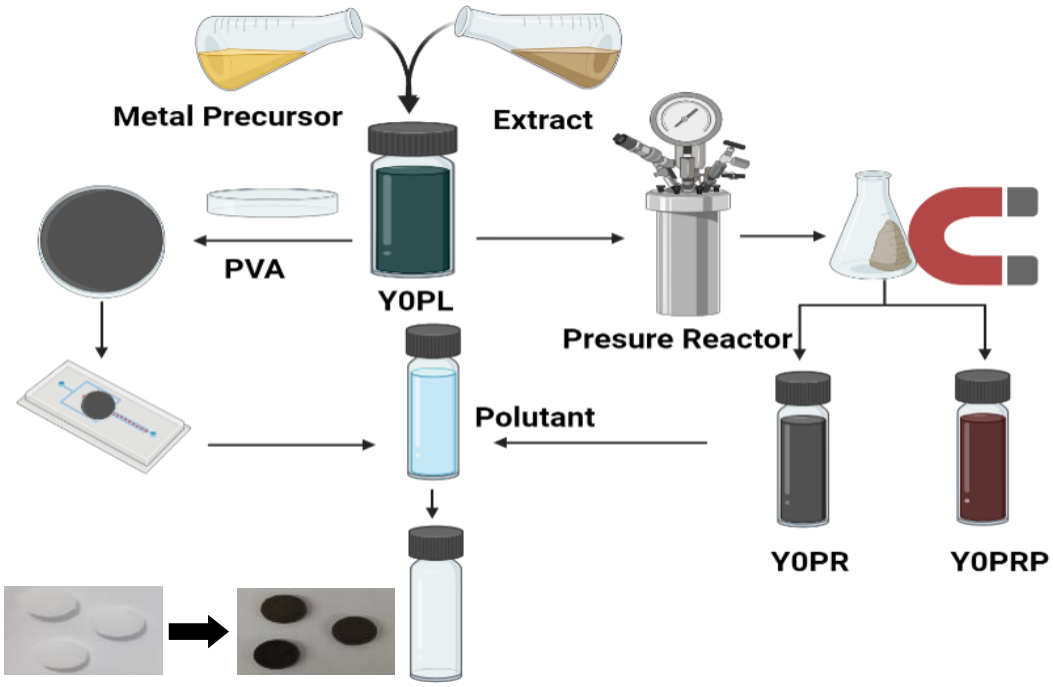

Figure 13: Green synthesis and preparation of alternative recyclability. PVA = polyvinyl alcohol.

4.2. Structural and Morphological Properties

X-ray diffraction (XRD)

XRD measurements were carried out using a PANalytical X'Pert PRO XRD with Cu K radiation (lamda= 0.1548 nm). Average size was calculated using Scherer formula: D=Kl/βCosθ. As synthesized nanoparticles are larger size goethite iron oxide with characteristic hkl plans (120, 130, 041, 151). This size increment is due to concentrated solution of crude extracts possesses as many as compounds for the solvent molecules used during extraction. Thus, the surface of nanoparticles is covered by a group of these compounds resulting in a significant transformation of their sizes (Borowik et al., 2019). Bare and functionalized nanoparticles have comparable sizes because they are same phase nanoparticle except thin layers of surface compounds from plants during functionalization after they transformed to stable magnetic nanoparticles.

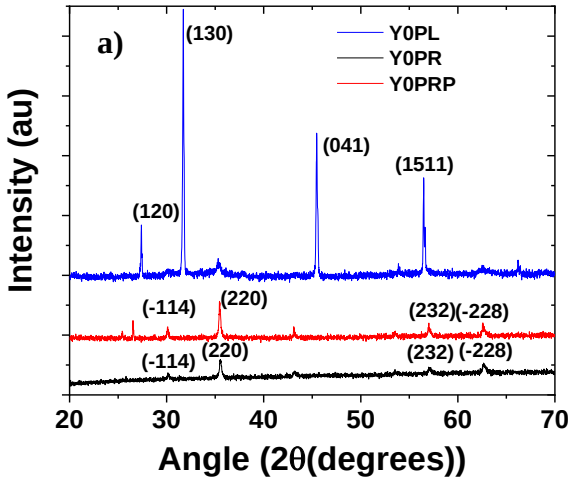

b)

Material	Crystalline size (Av.) in (nm)	Phase structures
Y0PR	29	Fe3O4- magnetite
Y0PRP	45	Fe3O4- magnetite
Y0PL	277	α-FeOOH- goethite

Figure 14: XRD pattern of green synthesized nanoparticles(a) crystalline size and phase derived from XRD data (b).

Scanning electronic microscope (SEM) and size distribution

Shown below are the SEM image of nanoparticles at two different resolutions recorded on Hitachi S-4800 Field Emission Scanning Electron Microscope (FESEM) detector type XFlash

6|60 ex, equipped with EDX from Bruker Nano GmbH Berlin, Germany. As synthesized iron oxide nanoparticles display majority of spherical with a few of cubic particles. When these particles were exposed to high pressure and temperature, this texture would be lost getting down to agglomerated mixtures of spherical and cubic texture with larger surface area but higher magnetic attraction. In the first phase nanoparticles, surface modification by plant extracts meaningfully impacted their complete synthesis to magnetic particles, increased size and interaction. Plant phytochemicals are composed of large number of functional groups that would chelate the metallic nanoparticles eventually building strong shell that lessens the magnetic property and crystallographic presentation of particles blocking the electron beams in the SEM machine, hence blurry images (Figure 15).

Energy dispersive X-ray spectroscopy (EDS)

Simple operation on SEM machine also serves as EDX which provides information related to elemental composition. Prominent peaks with Fe and O label are for iron and oxygen which are the primary elements in the synthesized sample magnetic nanoparticles, which indicates formation of iron oxide nanoparticles. Other peaks with different elements must have originated from the metal precursors and plant during synthesis or functionalization. Due to their magnetic nature, samples were attached on carbon tape before measurement. Due to that a peak for carbon is shown in the far left in all the EDX graphs.

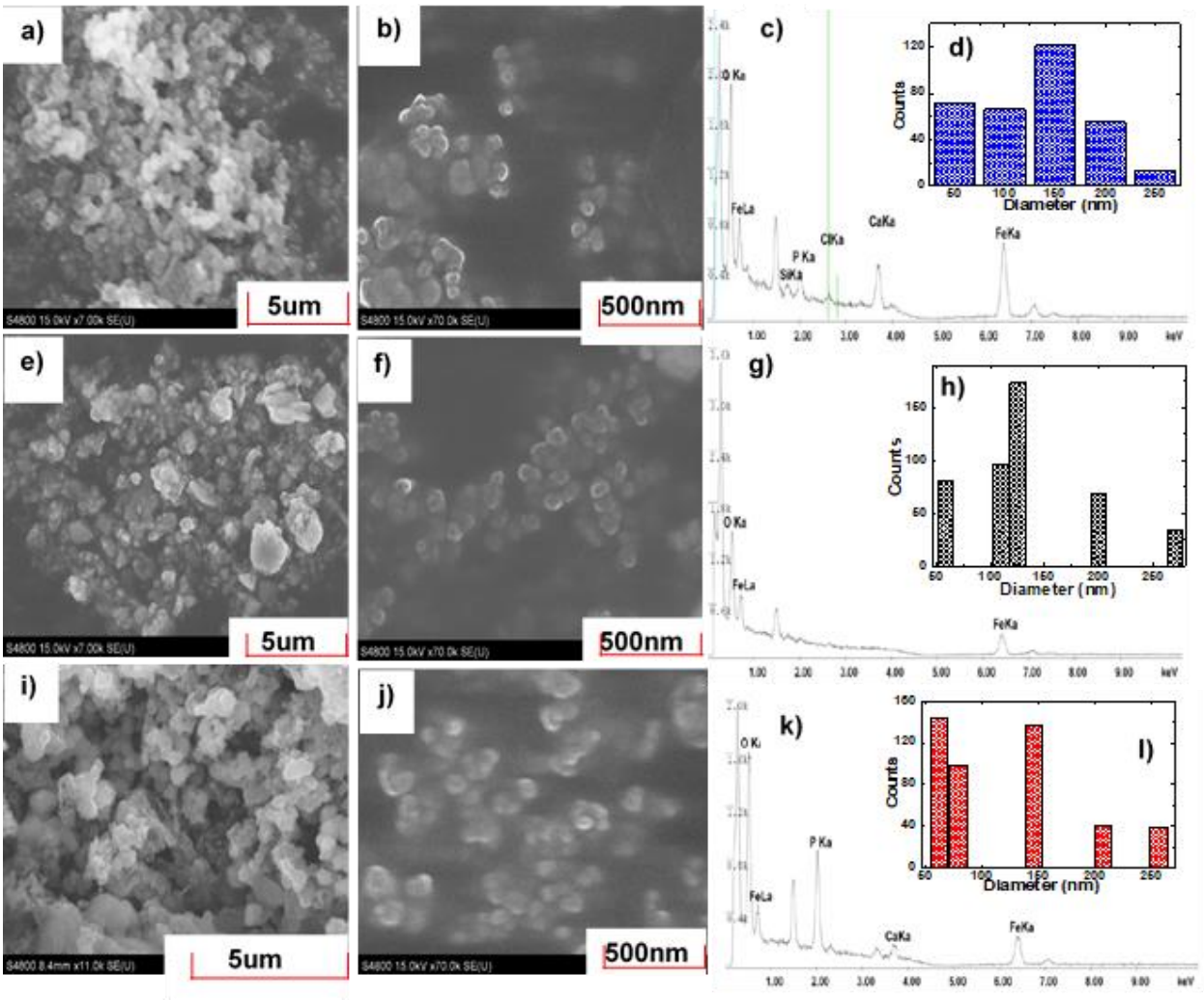

Figure 15: Morphological structure measurement including SEM images, EDX analysis and size distribution of Y0PL (a-d), Y0PR (e-h) and Y0PRP (i-l).

4.3. Absorbance and Bandgap Energy

Iron nanoparticles typically display maximum absorbance (λ max) between 300 and 450 which is also shown on the sample nanoparticles synthesized in the present study (Figure 16 (b)). The difference between Y0PR and Y0PRP is in the surface property since the latter is modified by plant phytochemicals. Thus, both Y0PR and Y0PRP has similar absorbance maxima. Similarly, Y0PL has identical λ max but narrow peak. Owing to all samples were measured at the same

scan rate, the peak broadening could have been caused by distortion of the electrons while collision at extreme conditions in the pressure reactor (Jiang et al., 2010).

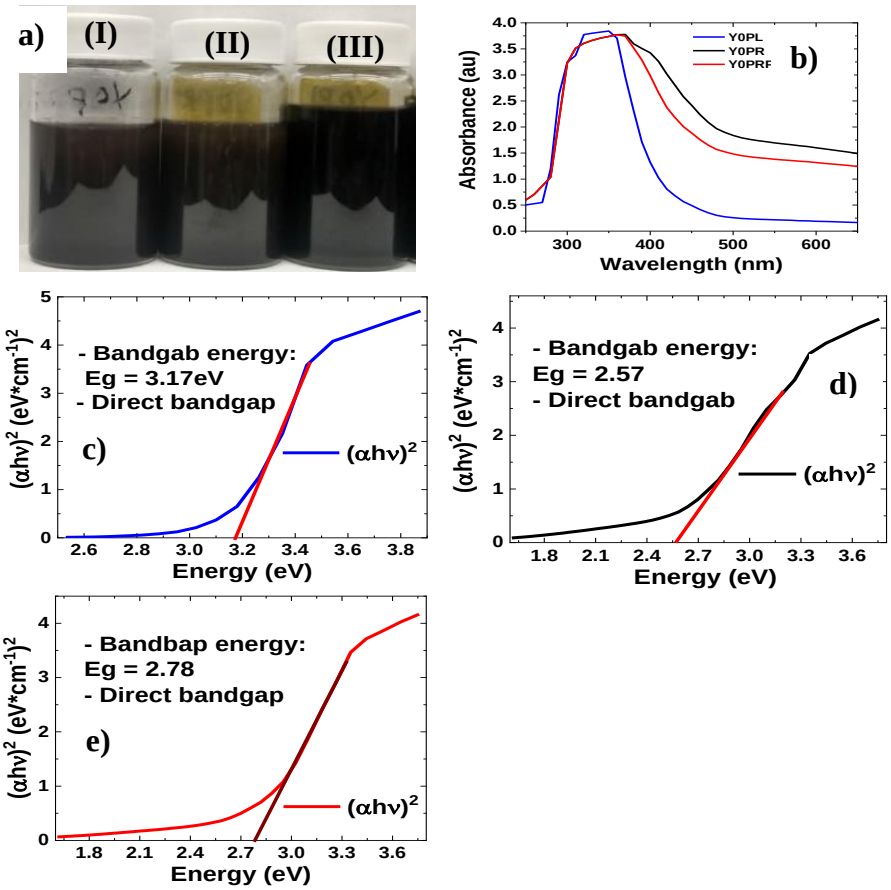

Figure 16: Green synthesized magnetic nanoparticles: a) Image after synthesis and dispersion (I=Y0PR, II=Y0PRP and III(Y0PL) and b) UV-Vis spectra of the nanoparticles. Band gap energy of nanoparticles(c).

Bandgap energies of nanoparticles were determined from the absorbance curves Fig 4b. It can be shown that all particle has bandgap energy above 2.5 i.e., 3.17, 2.57, 2.78 eV for Y0PL, Y0PR and Y0PRP respectively as shown in Figure (4c-d). Some efficiency of a photocatalyst is in its capability to absorb light up to visible region and complete use of the solar energy. To do so,

nanoparticles must have bandgap energy less than 3 eV. In this regard, only Y0PR and Y0PRP will be efficient for photocatalytic degradation of organic compounds. Which is also in agreement to their efficient degradation of 4-NA to 1,4-diaminobenezen (Ansari & Cho, 2016; Olivetti & Cullen, 2018).

4.4. Surface Properties

The infrared transmission measurements were carried out between 400 and 4000 cm^{-1} with a vacuum-based Bruker IFS 66v spectrometer, equipped with a DTGS detector and a KBr beam splitter. The samples for the IR studies were prepared in form of pellets by embedding the Goethite (Y0PL), Magnetite (Y0PR), and Magnetite (Y0PRP) nanoparticles in a transparent polycrystalline CsI matrix. An accumulation of 256 scans was performed for each spectrum. The data were normalized at each frequency to a vacuum throughput spectrum. In Figure 17, the hydroxyl liberation and the changes in the Fe-O or O-H bonding associated with rearrangement of the oxygen close packing during thermal dihydroxylation from goethite (blue line spectrum) to magnetite (black and red line spectra) are observed. For example, the strong hydroxyl vibrations at 3392 cm^{-1} (stretching), 1629 cm^{-1} (bending), 1398 cm^{-1} (deformation), and 1070 cm^{-1} (deformation) almost disappear in the magnetite spectra of YOPR and YOPRP samples after heat treatment. The Fe-O bands at 687 and 501 cm-1 associated with a goethite structural configuration transition to two vibrational modes of FeIII -O at 584 cm^{-1} and 402 cm^{-1} (see black spectrum of YOPR) that correspond to a magnetite structure. With nanoparticle functionalization, a downshift in the 584 cm-1 vibration to a value of 574 cm^{-1} and disappearance of the 402 cm^{-1} features are also observed, demonstrating a further structural transformation.

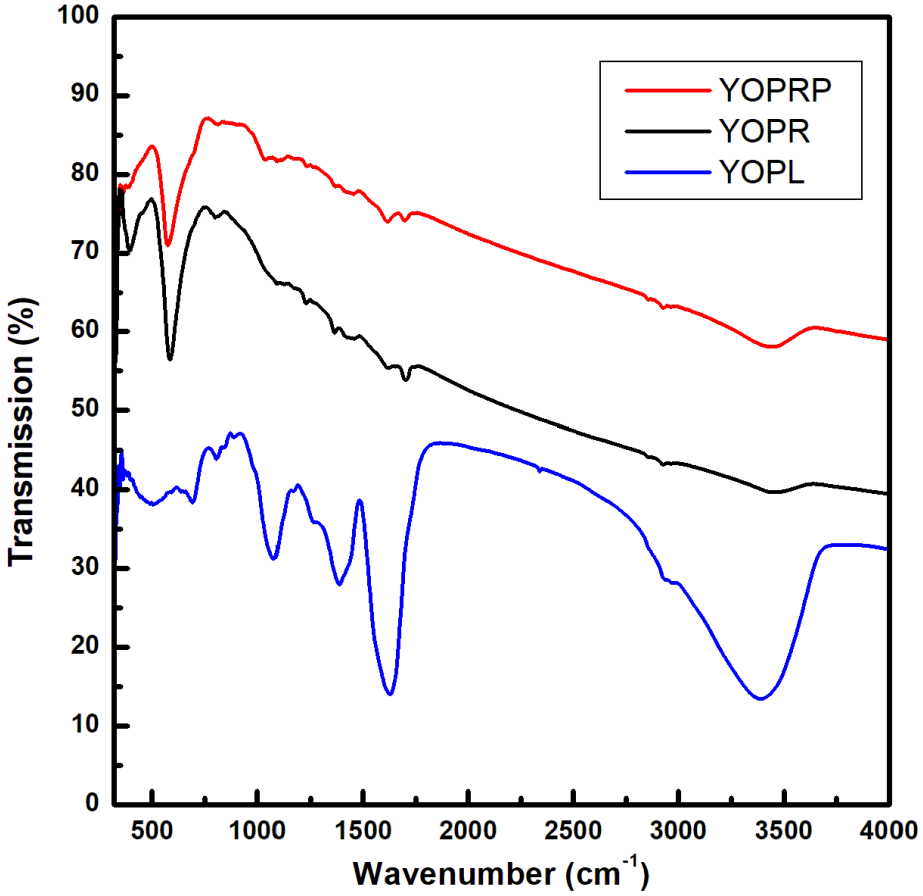

Figure 17: FTIR measurements of Y0PL, Y0PR, Y0PRP samples.

4.5. Magnetic Properties

A single step addition of extracts to metal precursors did not result in superparamagnetic nanoparticles suitable for water treatment application at room temperature. Hence, supporting the reaction by further heat treatments was necessary. A portion of these particles was thus heated in pressurized environment. All particles were magnetic and further their magnetic property was quantified in vibrating sample magnetometry (VSM) at 300K and 50k. At that temperature(250^{o}C) where the nanoparticles are formed, it is unlikely plant phytochemical will exist in their natural form. Thus, particles were immersed in extract solution and functionalized

over 12 hours period at room temperature while stirring at 850 rpm. Similarly, these particles were washed and dried before analyzed in the VSM.

Magnetic saturation (Ms) of both heat-treated nanoparticles has been more than adequate for the intended application. Which was possible to easily manipulate the particles in water by a physical magnet as less as 0.5 Tesla. Moreover, magnetic property did not show such a change over a wide range temperature difference from far below room temperature to 450K. However, magnetic property of functionalized nanoparticles was lower by about 7emu/g compared to bare counterparts. It is important to note that the first plant-based nanoparticle has Ms=13.12emu/g which is not feasible for environmental application. For example, water treatment and hyperthermia or other applications (Blazar et al., 2021).

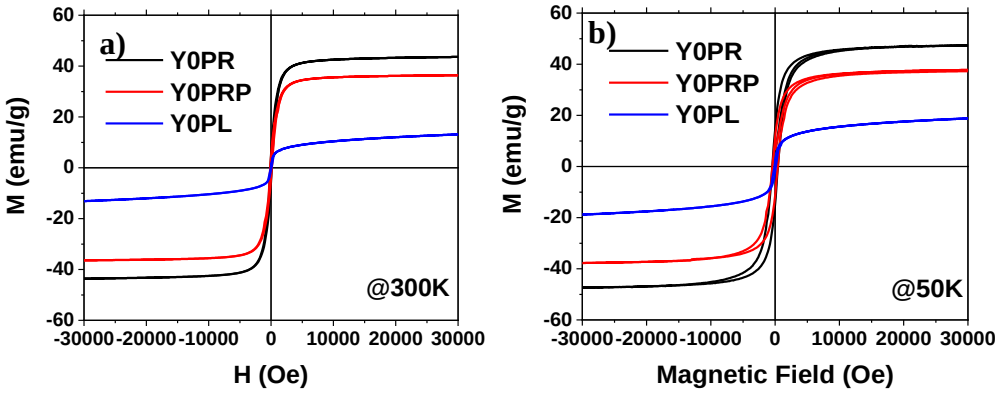

Figure 18: Hysteresis loop of sample magnetic nanoparticles at room and below room temperature.

4.6. Dispersion in Water

Well dispersions of nanoparticles in aqueous medium enables effective interaction with pollutants in water. Non- functionalized iron oxide nanoparticles are believed to weakly disperse

pertinent to metal surface with no binding sites, lacking affinity to water. Good dispersion is also a measure of successful surface modification. In the case of the present magnetic particles, functionalized nanoparticles stood comparatively well dispersed after they were sonicated for 1hour and allowed to stand for another hour. An important finding worth mentioning here is as synthesized nanoparticles (Figure 19 (III)) were highly dispersed for more than 72 hours even after the dispersion. Simultaneous reduction and coating tend to form stable nanoparticles allowing functional groups to grow on the surface during synthesis than attaching on previously stabilized nanoparticles because the attachment is stronger. Nevertheless, their weak magnetic properties would have also significant contribution in weakening fast aggregation.

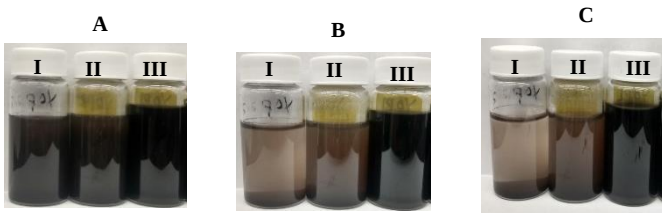

Figure 19: Dispersion of sample nanoparticles in water at 1min(A), 30min (B) and 60min(C). Where, I=Y0PR, II=Y0PRP and III=Y0PL.

4.7. Adsorption Efficiency of Nanoparticles Towards Organic Pollutants

4.7.1. Absorption efficacy of nanoparticles towards methylene blue

The graphs in Figure 20 represent outputs from absorption experiments of nanoparticles (5mg/L) added as powders against solution methylene blue at different concentrations (10 to 140mg/L-Figure SA1) and times (5 to 160minutes) without addition of catalysts. Despite its weak magnetic property, Y0PL showed super performance at all concentrations with above 85% removal efficiency in less than 20 minutes time. Same amount of adsorbent removed wide range

concentration of methylene blue from polluted water. As shown in Figure 20 (a-f) and Figure SA4, all nanoparticles have high rate of adsorption at their optimum adsorbate concentrations. Both high magnetic samples also showed comparable efficiency for removal of methylene blue at 10mg/L concentration. Above this concentration, however, Y0PL has better efficiency than both bare and functionalized nanoparticles. Y0PR and Y0PRP have comparable small size hence higher surface area, an important factor in absorption mechanism of particles. However, less hydrophilic surfaces prevent them from excellent dispersion in water. This further limit their interaction with pollutants in water at reasonable appropriate time. Even though Y0PRP is functionalized with same solution of extracts, the interaction of the phytochemicals and the nanoparticles should be inadequate due to lack of functional surface on nanoparticles from the pressure reactor.

The adsorption of methylene blue on to sample adsorbent follows Langmuir isotherm. Moreover, calculation of separation factor (R_L) by the formula (3) gives 0.798. R_L value between 0 and 1 signifies favorable adsorption(Ayawei et al., 2017).

$$R_L = \frac{1}{1+K_L C_o} \quad \text{.....(4)}$$

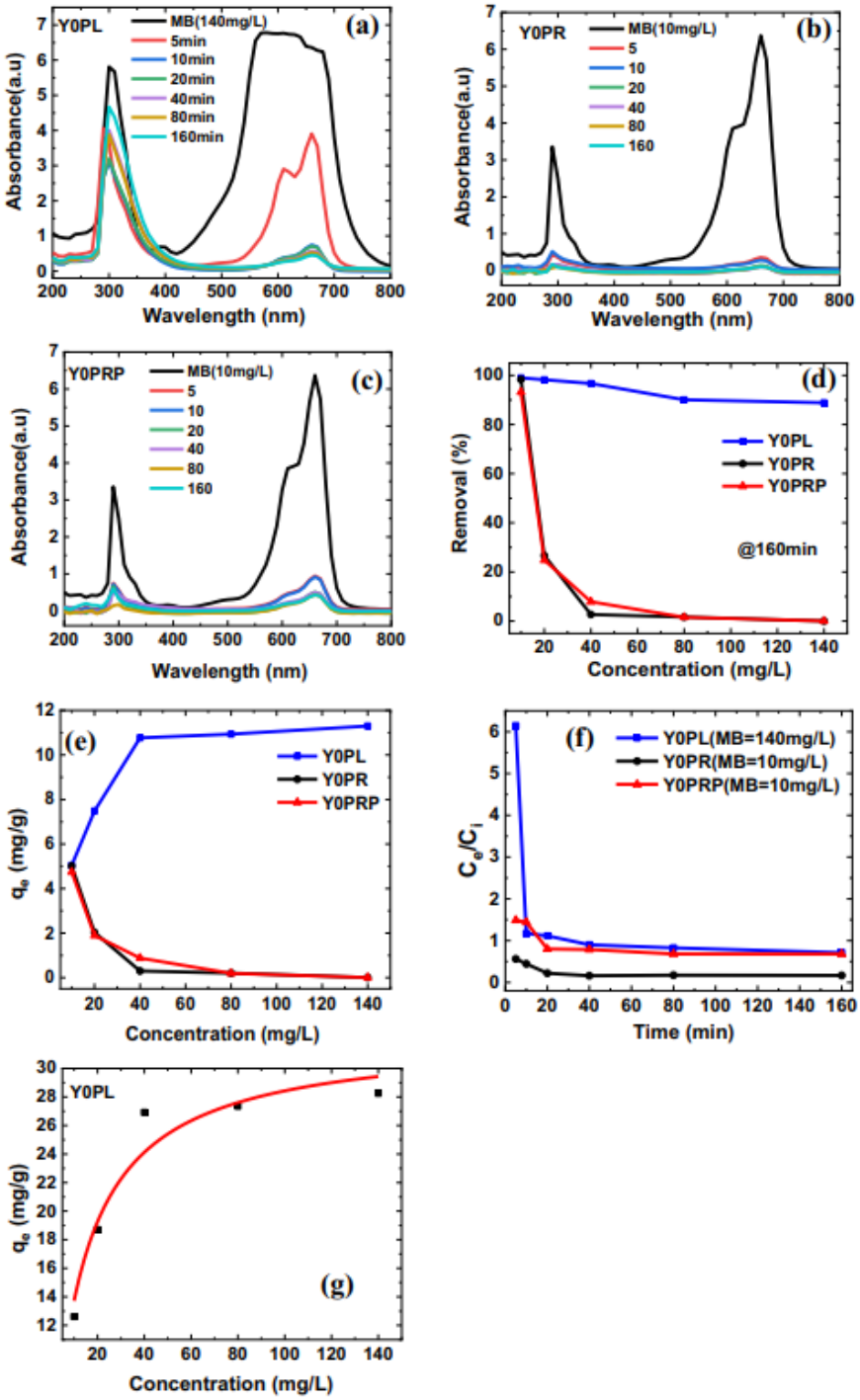

Figure 20: Absorption efficiency of magnetic nanoparticles towards methylene blue at different time and concentrations (a to f) and non-linear Langmuir isotherm of the highest efficient nanoparticle(g).

4.7.2. Absorption Efficacy of Nanoparticles Towards 4-Nitroaniline

Nanoparticles capable of removing multiple organic pollutants are most preferable in water treatment the fact that contaminated water is rich of many organic and inorganic pollutants. 4-Nitroaniline(4-NA) is another organic pollutant targeted here because of its abundance in the environment and serious health consequences. Removal of 4-NA was studied at 0.5 and 1mM (Figure SA2) over an interval of time ranging from 5 to 160 min. Findings indicate, Y0PR, Y0PRP and Y0PL absorb/reduce 2-NA 96%, 85% and 26% respectively at 0.5mM concentration. Absorption/reduction increased with increase in contact time but decreased with increase in concentration. Looking at the transformation of the peaks it is important to conclude that the absorption process incorporates reduction of 4-NA to 1, 2- diaminobenzene. Because, before treatment, 2-NA has two prominent peaks with λ max at 290 and 410nm. After the treatment, the peak at 410 disappears whereas, the peak at 290nm increases in intensity. This indicates the reduction of nitro into an amine group. The reduction process has non-linear isotherm with R_L= 0.9542.

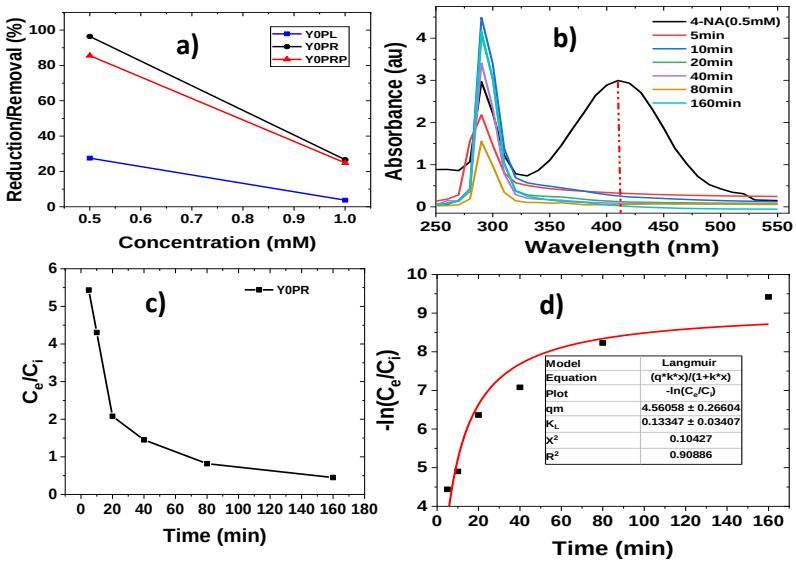

Figure 21: Absorption/Reduction efficiency of all samples against 4-NA(a), time dependent degradation of 4-NA by Y0PR(b), absorbance of degradation of 4-NA by Y0PR at different times(c), Langmuir isotherm for the degradation of 4-NA by Y0PR(d).

4.7.3. Absorption efficacy of nanoparticles grown on PVA sponge

Effective recyclability of nanoparticles after absorption is the other most important goal of this study. Although, Y0PL were targeted for this part of the study, all particles grown on PVA disks for comparison purposes between the particles as well as between the methods. Removal efficiency of Y0PL is almost similar whereas, that of Y0PR and Y0PR was substantially increased to above 80%. Additionally, contact time have improved for all nanoparticles to two minutes. As a result, the rate of pollutant removal also improved. This is because the microfluidic system removes the factor of dispersion out of the equation. First, the particles are localized on PVA disks at the beginning and fixed in adsorbent hole having the size of the disk. Moreover, the system allows small amount of adsorbate to pass through adsorbents at specific time making many active sites available. When particles are grown on PVA surface during

synthesis, excess particles synthesized in the solution may also settle on the top for grown nanoparticles. Some of these do not go even washed away with distilled water. Nevertheless, after the disk is dried and placed in the chip system, pollutant solution tends to wash these particles because of pressure. Hence, loosely bound particles along with the die elute in the first two minutes. At optimum conditions, Y0PL has the highest absorption efficacy followed by Y0PR and Y0PRP nanoparticles with comparable performance. The temperature of pollutants during the experiment was from 21.3 to 23.2 ^{o}C and pH of methylene blue solution was 6.5.

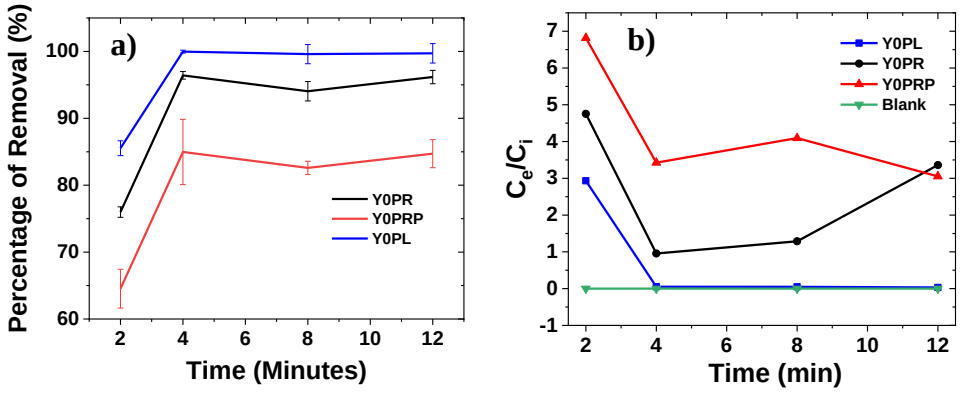

Figure 22: Percentage of removal of nanoparticles grown on PVA sponge against MB (10mg/L), pH=6.6, temperature 21.5 to 23.2.

4.7.4. Effect of pH and temperature on absorption performance of nanoparticles

Effect of temperature and pH on efficiency of nanoparticles both coated with plant phytochemicals and bare was investigated in normal and anticipated extreme conditions in water environment. Absorption results of the particles with respect to temperature and pH reveals temperature between 20 to 30^{o}C and pH between 8-12 are conditions for optimum performance for all nanoparticles. Lower temperature affects the affinity of pollutants towards the adsorbent due to pollutants agglomeration in condensed water. Similarly, lower pH can dissolve

nanoparticles as well as alter the surface binding sites of the adsorbent. Since methylene blue is a cationic dye, hydrogen ions must have protonated heteroatoms of surface functional groups creating repulsions between the adsorbent and adsorbate (Amode et al., 2016). Hence, reduced adsorption.

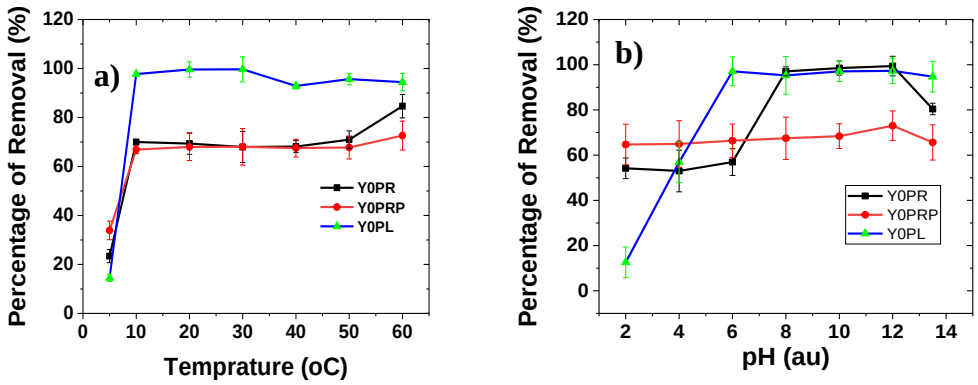

Figure 23: Optimum conditions for performance of nanoparticles grown on PVA disk. a) temperature and b) pH

4.7.5. Effect of ions on removal MB from contaminated water

To investigate performance of nanoparticles under both organic and inorganic pollutants multiple ions with concentration that resemble brackish water has added to solution of methylene blue (The concentration of the added ions can be found in the supporting information Table SA1. All other conditions were kept the same with the treatment process done above. No significant change observed at all contact times and concentrations. On one hand it signifies strong affinity of nanoparticles towards multiple organic pollutants. On the other hand, it is a clue that sample nanoparticles would have similar efficiency if tested against inorganic ions.

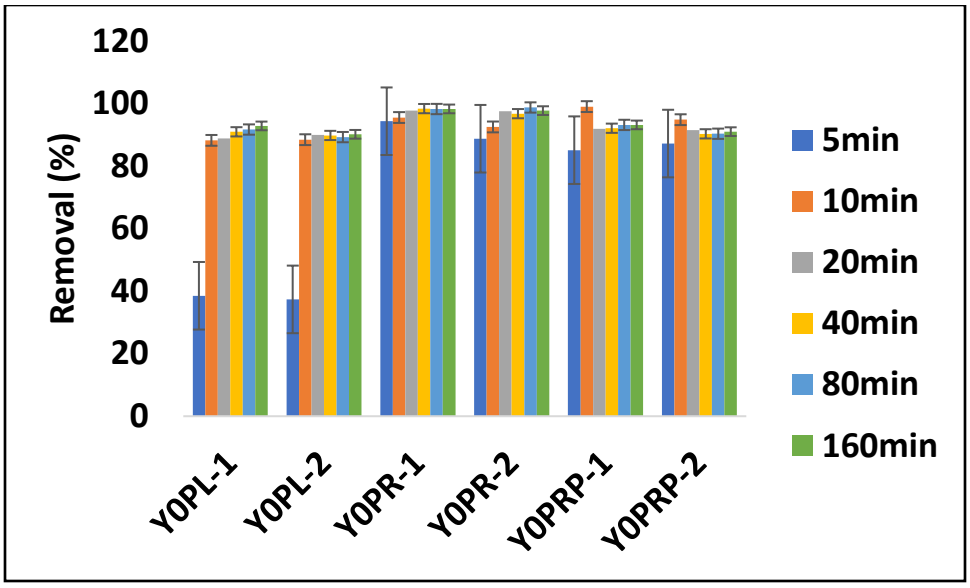

Figure 24: Effect of ions in the absorption performance of nanoparticles towards methylene blue. NPs-1 is without ions and NPs-2 is in the presence of ions.

4.8. Recyclability

After each treatment, powder nanoparticle was soaked in acetone overnight with vigorous stirring. Then the particles were collected, washed and centrifuged several times with acetone, distilled water and finally with ethanol and allowed to dry over nigh at 120^{o}C in an oven. Power nanoparticles were recovered without losing their efficiency for 5 cycles while particles grown on PVA sponge were washed out after four cycles. As a result, their absorption capacity declined below 50% after four cycles as shown in Figure 25 below. Performance of the particles at their highest efficiency can be seen in color photo in Figure SA5.

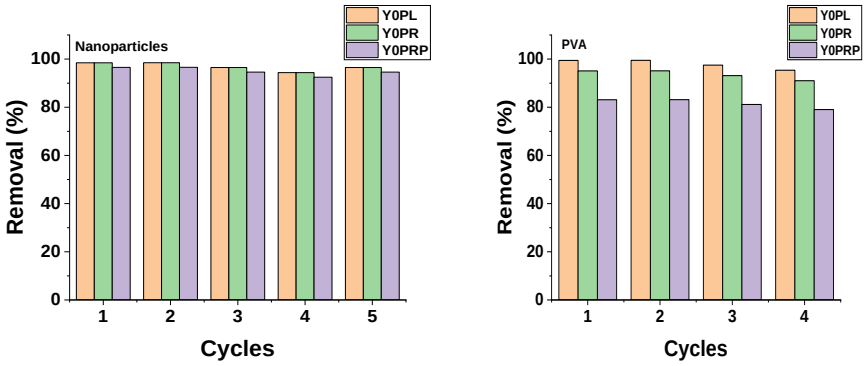

Figure 25: Recyclability efficiency of powder nanoparticles(left) and when nanoparticles are grown on PVA surface (right)

4.9. Comparison with other studies

Table 2: Pollutant removal comparison of our nanoparticles with recent published work

Material	**Concentration**		**Optimum conditions**		**% Removal /Reduction**	**Contact time**	**Ref**
	Adsorbent(m)	Absorbate (MB/2-NA)	pH	Temperature (^oC)			
γ-Fe_2O_3@Cynometra ramiflorafruit	30mg	20mg/L(MB)*	-		94%	120min	(Bishnoi et al., 2018)
γ-Fe2O3@ cellulose	0.4mg/ml	20mg/L(MB)	5.7	-	~40%	420min	(Xiong et al., 2014)
Fe_3O_4@graphene oxide	15mg/L	50mg/L(MB)	-	30	90%	180min	(Othman et al., 2018)
Fe3O4/Fe/Fe3C@PCNF[1]	40mg + H2O2 catalyst(0.32 M)	100mg/L	-	85		30min	(Zhang et al., 2015; Jang et al., 2016)
Fe_3O_4-GO@Polyacrylic acid (PAA)	8mg/ml	20mg/L	11	-	100%	1500	(J. Zhang et al., 2015)
IL/ Fe_3O_4/Ze	0.2mg/ml + $NaBH_4$(0.5 M)	0.05M(2-NA)	-		~28%	-	(Arumugam et al., 2021)31w
		0.005M(MB)	-	-	~47%	-	
NiO	5mg	0.0145mM(2-NA) + $NaBH_4$(13.4mM)	-	40.15	97%	100min	(Jeon et al., 2020)
Ag@Polymer Microgels	25.2 µg/mL	0.06mM(2-NA) + NaBH4 (12.64 mM)	9.42	21.1	~90%	22min	(Farooqi et al., 2015)
AgNPs-rGO	1mM	2mM(2-NA) + NaBH4 (0.2 mM)	-	-	~87%	20min	(Y. Zhang et al., 2012)
AgNPs					~88%	55min	
Fe_3O_4/α-FeOOH@Azadirachta indica extract	**5mg/ml**	**140mg/L(MB)**	**6-12**	**10-30**	**99.96% %**	**4min (Chip)/20min (Powder)**	**This study**
		0.5mM(2-NA)	**-**	**-**	**83%**	**160min (Powder)**	

4.10. Conclusion

In this study, iron oxide nanoparticles are synthesized using green method free of additional chemicals at all process. Plant phytochemicals acted as reducing and caping agents to form stable nanoparticles. All nanoparticles showed significant pollutant removal efficiency towards methylene blue and 2-Nitroaniline at wide range time. Despite their week magnetic property, as synthesized nanoparticles showed high percentages of removal even at high concentration of pollutants. Whereas, bare nanoparticles more efficient in reduction of 2-NA to 2-AB. Particles are efficient at higher pH's of pollutant solution and temperature from 10 to 30^{o}C which makes them good candidates in water treatment pertinent to their efficient performance and recyclability at conditions that resemble the actual waste water. Moreover, this paper introduces successful alternative recyclability especially, for weak magnetic nanoparticles by growing them on the surface polyvinyl alcohol sponge as solid support. In general, green synthesized magnetic nanoparticles in this study are easy to synthesis, cost-effective and enviro-friendly water treatment agents. In our next projects we plan to further investigate absorption efficacy of nanoparticles towards heavy metals as well as study their toxicity to pathogenic microorganisms believed to exist in water.

CHAPTER 5

SUPERPARAMAGNETIC NANOPARTICLES COATED WITH NOVEL BIOCOMPATIBLE MATERIALS PRODUCED HIGH SPECIFIC ABSORPTION RATE IN MAGNETIC HYPERTHERMIA

5.1. Introduction

With the growing cancer cases and prevalence of various cancer types, cancer treatment methods are many but complex and expensive (Kantarjian & Rajkumar, 2015; Mariotto et al., 2011). Despite its promising applications for various cancer types, magnetic hyperthermia (MH) lacks adequate clinical reports (X. Liu et al., 2020; Thiesen & Jordan, 2008). Two of the important factors worth of study are superparamagnetic nature of the particles and the platform by which the particles are coated (Albarqi et al., 2019; Kandasamy et al., 2018; Patil-Sen et al., 2020). In this study a novel green platform is introduced and compared against the common platform used in the technique. Magnetic nanoparticles were prepared using simple coprecipitation metal precursor and further heated in a pressure reactor to yield super paramagnetic nanoparticles coercivity = 0 at 300 and 50K, then the particles were coated with two formulated platforms. XRD peaks look a lot like characteristic magnetite iron oxide nanoparticle for all the particles. SEM images further proof spherical shaped face-centered cubic spinel iron oxide structure. Compared to non-functionalized and graphene oxide functionalized particles those with secondary metabolites in their surfaces showed a temperature in the therapeutic limit, Tmax=45^{o}C, higher dT/dt and SAR and improved dispersion in distilled water in longer period after the assay.

5.2. Characterization

X-ray diffraction (XRD)

As shown in the XRD peaks in Figure 26 below It is evident that all the nanoparticles are iron oxide nanoparticles with prominent peaks at 30, 37, 44, 57 and 62 degrees corresponding to 220, 311, 400, 511,440 and 533 crystal plans which in turn are characteristic peaks for crystalline iron oxide nanoparticles (Zhuang et al., 2015). Non-functionalized nanoparticles tend to show more, and high intensity peaks due functionalizing agents are amorphous organic compounds.

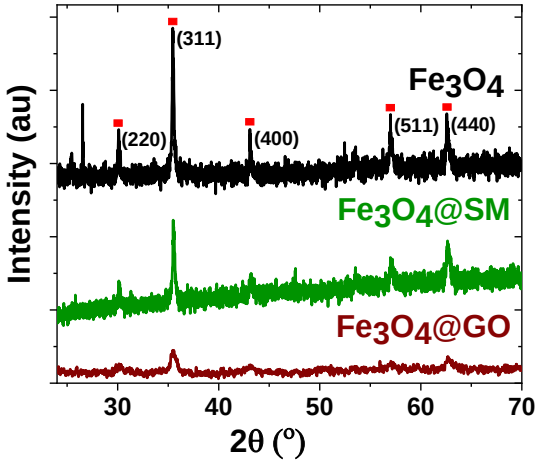

Figure 26: XRD spectra of synthesized nanoparticles. Red rectangular dots are peaks common in all nanoparticles also characteristic peaks of Fe_3O_4 nanoparticles.

Scanning Electron Microscope (SEM)

SEM is a strong tool for physical visualization of the nanoparticles and efficient for shape and size evaluation. All the nanoparticles were spherical in majority. In particles resulted from the pressure reactor and those synthesized in an inert atmosphere, uniformly dispersed nanoparticles are seen compared to those particles synthesized under ambient conditions. Particles sizes range from 29 to 357 nm where, secondary functionalized nanoparticles have relatively homogeneous

size distribution with majority of their nanoparticles between 50 to100nm. Graphene oxide functionalized nanoparticles show most of their particles greater than 29 less than100nm but with few particles nearly three times larger than average. Similar to SM functionalized nanoparticles, non-functionalized particles have majority of their particles with size between 50 to 140nm (Figure 27. c), f), and i)).

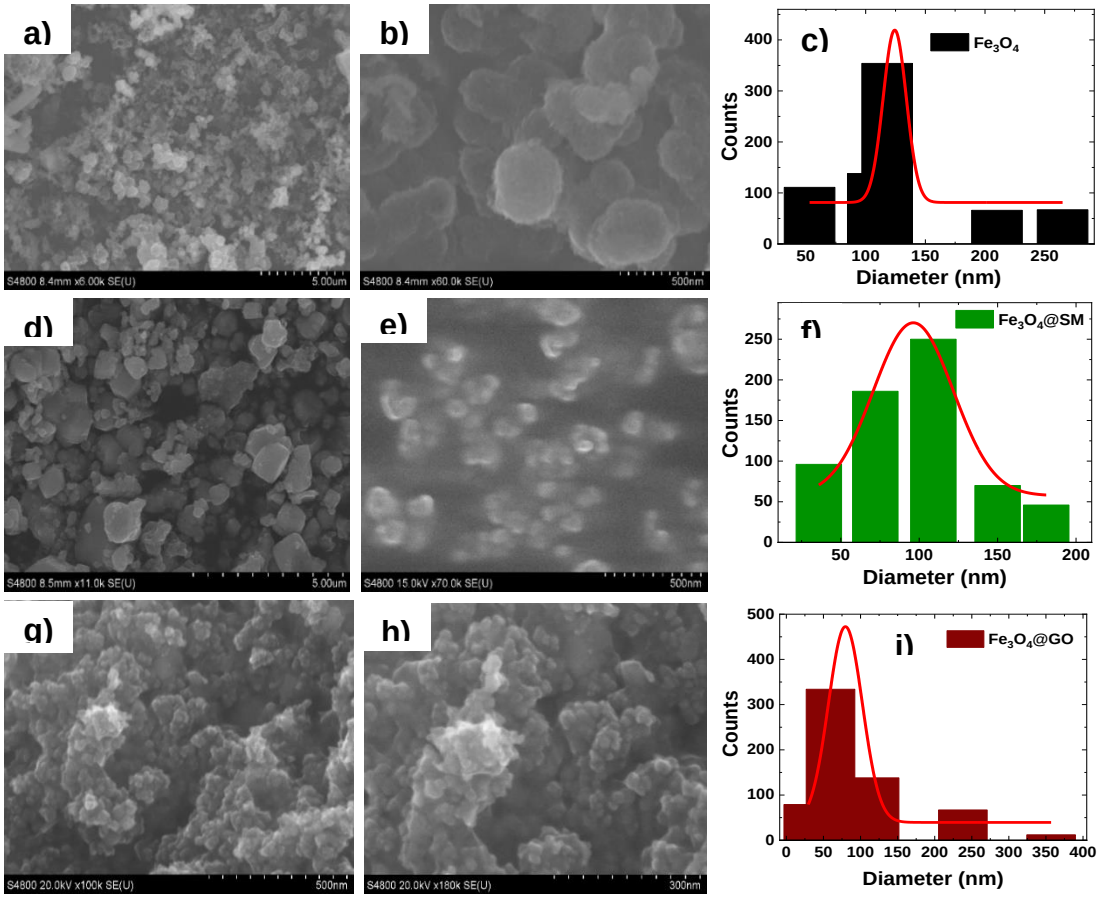

Figure 27. SEM images at different resolutions Fe_3O_4(a and b); Fe_3O_4@SM (d and e) and Fe_3O_4@GO (g and h) and their size distribution c), f) and i) respectively.

5.3. Magnetic Properties

Particles were superparamagnetic above room temperature which is also confirmed by ferromagnetic property below room temperature. With respect to magnetic property, graphene functionalized nanoparticles have higher magnetic saturation, Ms=70.99 emu/g compare to bare

and particles with secondary metabolites which were 60.29 emu/g and 50.51 emu/g respectively. Fe_3O_4@GO were synthesized under inert atmosphere thus less susceptibility to oxidation hence fewer other forms of less magnetic iron oxide nanoparticles. Similarly, the pressure reactor is filled with vacuumed and the particles were dispersed in ethanol before inserted to the pressure reactor which limits oxidation of particles while being transformed to Fe_3O_4 iron oxide nanoparticles. The secondary metabolites on the other hand are extracted with distilled water and possibly will add up more oxygen to the particles during functionalization unbalancing the ratio of oxygen i.e. exceeds than the empirical formula which impacts the magnetic property. As an indication, both Fe_3O_4 and Fe_3O_4@GO were dark whereas Fe_3O_4@SM nanoparticles were brown.

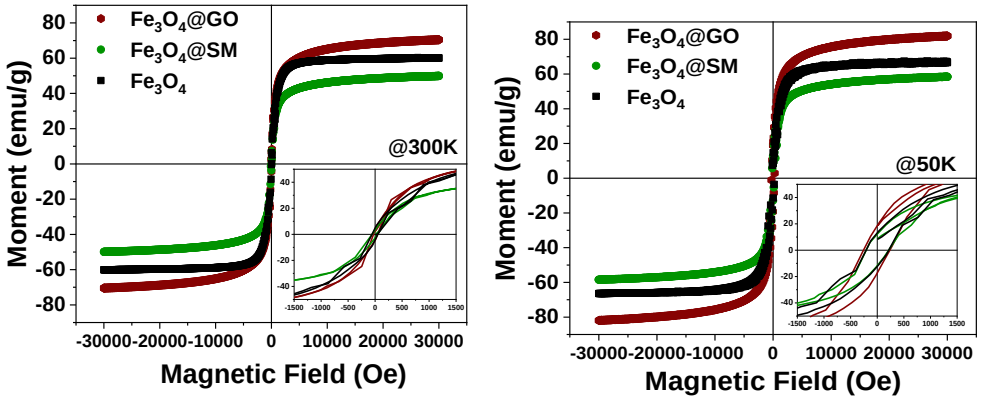

Figure 28: Magnetic property of nanoparticles at 300K(right) and 50K(left) for Fe_3O_4(black); Fe_3O_4@SM (green) and Fe_3O_4@GO (maroon)

5.4. Heating Efficiency Under Magnetic Field

Nanoparticles suitable for hyperthermia application would respond to alternating magnetic field and the temperature of the solution with the nanoparticles shall rise with increase in magnetic field and frequency of the field. As shown in Figure 29 a), b) and c)), increase in temperature

proportional to raise in magnetic field substantiates this situation. Therefore, in terms of magnetic saturation all particles are super paramagnetic strong enough to produce heat within the allowed limit during treatment (Mahmoudi et al., 2018). Despite its higher magnetic property and successful coating, the case with graphene is that multilayer graphene prevents effective dissipation of temperature to the surrounding even at higher magnetic fields thus temperature raise saturates after short time during the treatment.

Compared to all other nanoparticles SM functionalized particles has higher localized temperature (45.376 ^{o}C) which vastly acceptable in in-vitro or in-vivo hyperthermia application as temperature between 40 and 44 ^{o}C is adequate to inhibit cancer growth or incapacitate tumors(Mahmoudi et al., 2018). SM possess polar functional groups which enhanced dispersion in water which in turn elevate the temperature of the solution because of collective heating from each nanoparticle. In connection with actual test for cancerous cells this means enough heating to destroy most cells or make them susceptible to further treatment(Rajan et al., 2020).

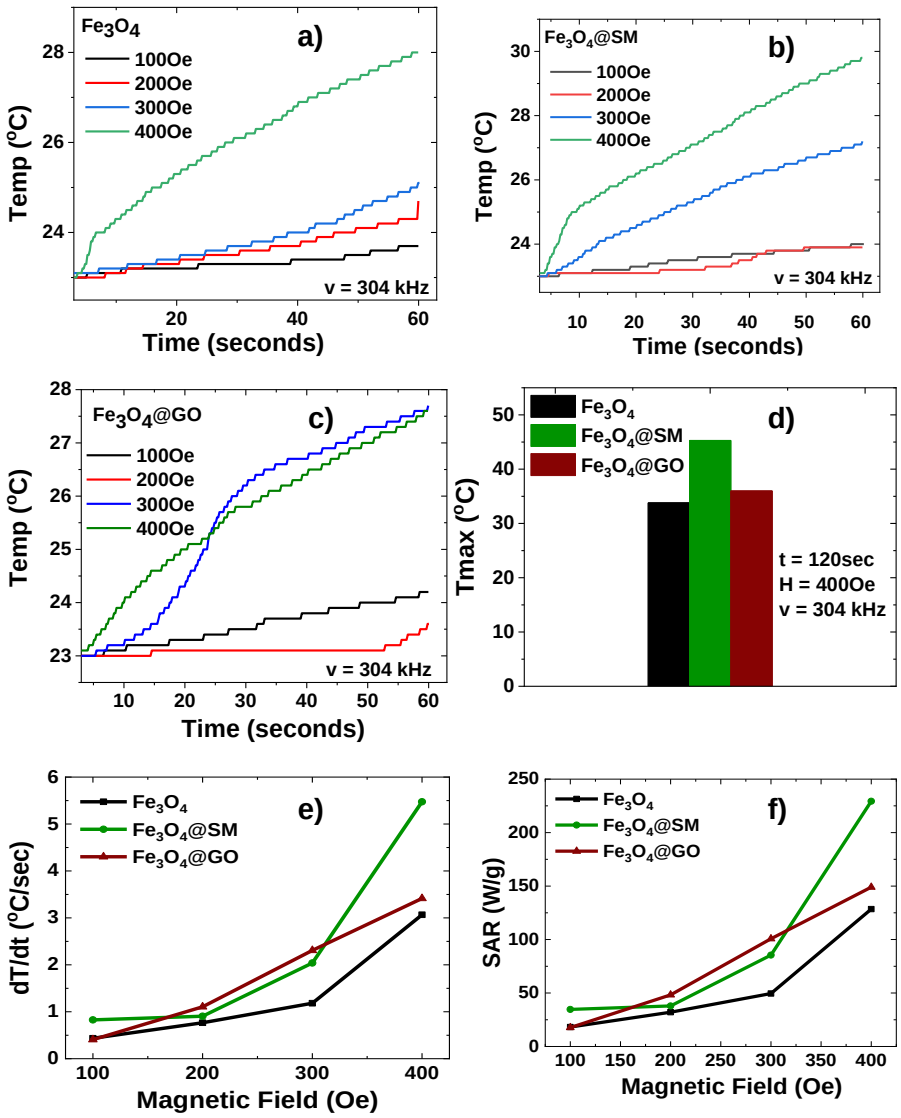

Figure 29: Magnetic hyperthermia feasibility of nanoparticles. Time dependent temperature raise of nanoparticles at different filed strengths(a) to c)). Observed maximum heating capacity of nanoparticles(d)); rate of change in temperature per time(e)) and specific absorption rate of nanoparticles in watt per gram at various magnetic field strengths; where all those parameters for Fe_3O_4, Fe_3O_4@SM and Fe_3O_4@GO are labelled black, green and maroon respectively.

Moreover, looking at time dependent heating and specific absorption rate of the nanoparticles a gradual increase of temperature over time with increase in magnetic field shows the stability of the nanoparticles for this application where the most favorable result is seen for Fe_3O_4@SM nanoparticles. Our SAR is even higher than our previous work with highly superparamagnetic (165emu/g) for similar application Sanad et al. (2021) due to surface properties rather than geometry (Sugumaran et al., 2019).

5.5. Related Studies and Significance of The Present Finding

We attempt to compare our findings with similar studies by other researchers as shown in Table 3 below. Our particles are higher in their heating capability taking average size, and the parameters used during the study into account.

Table 3: Comparative study of the present research with similar research done elsewhere

Particles	Concentration	H	Contact time	Frequency	SAR	References
Fe_3O_4@ 34DABA*	4mg/mL	130.654Oe	1800 s	330.3	37.2(W/g)	(Kandasamy et al., 2018)
Fe_3O_4@GO**	0.167mg/mL	257.55 Oe	100s	400 kHz	705^{ab}(W/g)	(Sugumaran et al., 2019)
Fe_3O_4@PVP***					323^{ab}	
Fe_3O_4@folate-conjugated PEG#	13mg/mL	125.66 Oe		420kHz	10.3(W/g)	(Piazza et al., 2020)
Fe_3O_4@GO	**5mg/mL**	**400Oe**	**60s**	**304kHz**	**147.84(W/g)**	**This study**
Fe_3O_4@SM					**230.61(W/g)**	

- *34DABA= 3,4-diaminobenzoic acid ** GO= graphene oxide, ***PVP = poly(vinyl)-pyrrolidone a= particle size = 20nm, b = invitro study, # PEG = poly (ethylene glycol).

5.6. Conclusion

Iron oxide nanoparticles are produced through simple and enviro-friendly method. Powerful tools were used confirm formation of spherical iron oxide structures. Furthermore, these particles were functionalized with biocompatible secondary metabolites introduced for the first time for magnetic hyperthermia application. Time dependent temperature rise, and SAR indicates Fe_3O_4@SM is higher than graphene oxide coated nanoparticle and bare nanoparticle. This efficiency is directly associated to appropriate magnetic properties, successful coating and interaction with aqueous medium during the treatment process. Therefore, it is possible to say that these particles can be promising for magnetic hyperthermia application. The authors also anticipate to further study the nanoparticle in-vitro and in-vivo.

CHAPTER 6

PREPARATION OF NANOENGINEERED ZVI@CIT CORE SHELL WITH ULTRA-HIGH MAGNETIC SATURATION AND TUNABLE MAGNETIC PROPERTIES AS CANDIDATES FOR TREATMENT WATER, BIOMEDICAL AND ENERGY APPLICATIONS

6.1. Introduction

Nanomaterials with superparamagnetic properties based on nanoscale crystalline zero valent iron (cZVI) have generated a great deal of interest in recent years due to their potential in water treatment energy and biomedical applications with enhanced performance at lower magnetic field gradients (Adamiano et al., 2018; Chatterjee et al., 2014; Ghosh Chaudhuri & Paria, 2012; Gupta et al., 2021; Khatami et al., 2018; Kwizera et al., 2017b). Iron based core-shell magnetic nanoparticles are one of the most intensively studied nanomaterials due to their non-toxicity especially in environmental and biomedical conditions (Galdames et al., 2020; Koo et al., 2012; X. Li et al., 2006; W. Xu et al., 2022; Zambrzycki et al., 2021; G. Zhang et al., 2010). To find out candidates for water treatment, hyperthermia and in energy applications as anode materials in lithiumion batteries, as catalysts and for oil purification, the present study demonstrates synthesis and elucidation of Fe (core) and citrate (shell) based nano-systems prepared at various temperatures and concentrations of the core metal, ligand and reducing agent at standard conditions. We studied the effect of reactants ratio and reaction temperature on magnetization of nanoparticles and their crystal structure. We found out that, at optimal metal concentrations, magnetic saturation increases with increase in concentrations of capping and reducing agents but decrease as the temperature of the reaction increases. Particles have average size (D_{SEM} = 39±13

nm) with spherical shape. Ultra-high magnetic saturation (241 emu/g) observed in response to low reaction temperature is associated with relaxation of magnetization behavior. Hence, we demonstrate that the concentration of the reducing agent and temperature of the reaction environment are crucial for monitoring the tunability of magnetization in ZVI@CIT core-shell nanoparticle systems. This work uncovers essential information on tuning magnetization and crystal properties of nano-scale core-shell particles for the purpose of using them in various applications.

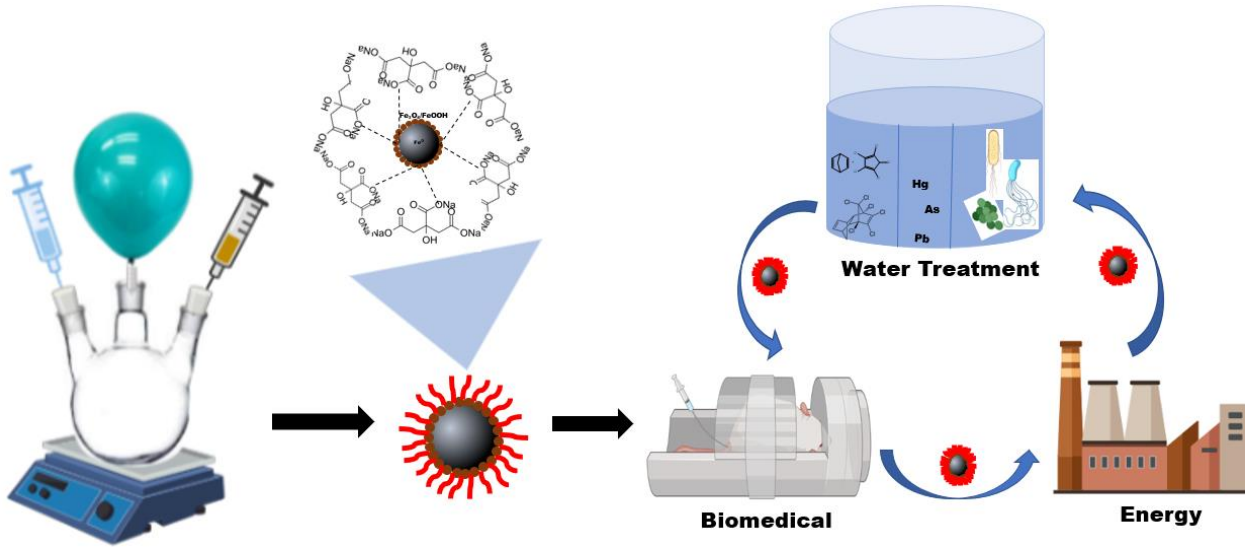

Figure 30**:** Schematic illustration of synthesis, functionalization and application of ZVI@CIT core shell

6.2. Structural and Phase Properties

XRD patterns of ZVI(Fe^0) coated in citrate are displayed in Figure 31. Peaks at 44.48, 65.72 and 83.12 reflection angle (2θ) correspond to 110, 200 and 211 miller indices for body-centered cubic crystal (bcc) iron (Araújo et al., 2019; Gaona et al., 2021; Kržišnik et al., 2014; Mühl et al., 2003). Low intensity peaks at farther reflection angle tells us the position of atoms within a lattice structure which signifies variations in morphology. However, SEM images show uniform

to morphology in average. Thus, lower intensities seen are associated with variable size shown in size distribution bar graphs in Figure 32 and lattice defects. This defect can arise form impurities and the organic ligand on the surface. Citrate is a five-carbon organic molecule that contribute to peak broadening and dropped intensity especially, subsidence of all Fe^0 peaks at higher concentration of citrate. Figure 31(b) supports this argument. Minor peaks to the left of 40 degree are possibly from iron oxide nanoparticles (Kržišnik et al., 2014).

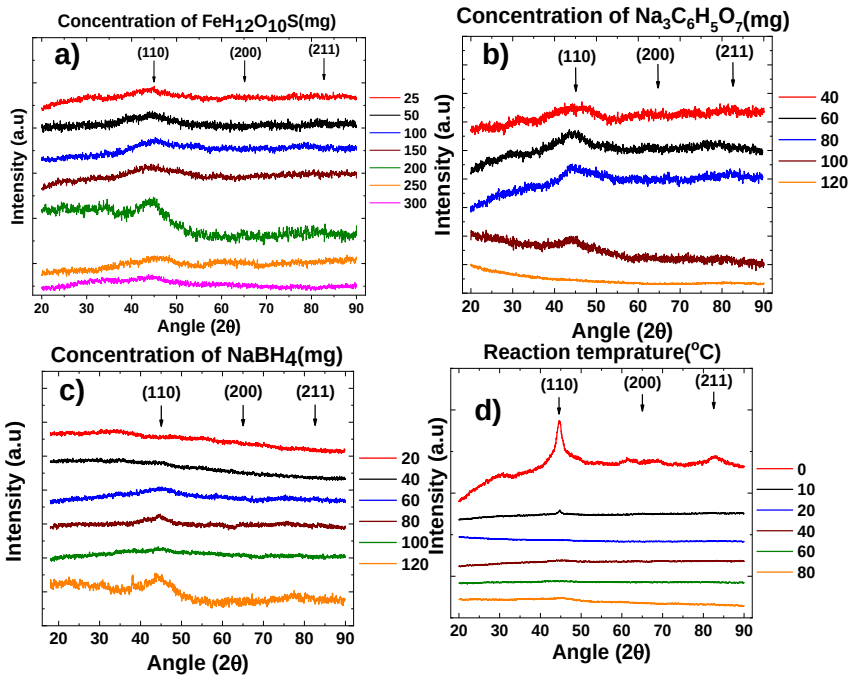

Figure 31: XRD patters of core shell nanoparticles. Particles prepared at variable concentrations of iron sulfate heptahydrate (a), sodium citrate dihydrate (b), sodium borohydride (c) and at variable reaction temperatures(d)

6.3. Morphology, Size and Elemental Composition

The morphology of ZVI was examined employing scanning electron microscope (SEM). For the output, we were able to identify shape of particles, determine area and average size of nanoparticles. As shown from Figure 32 (a-f), Figure SA6 (a -g), Figure SA7(a -e) and Figure

SA8 (a -f) particles are spherical in shape with an average size between 36 and 81 nm. Increase in average size is linked to the increase in reaction temperature, concentration of sodium citrate (Figure SA7) and decrease in concentration of iron sulphate heptahydrate (Figure SA6) and decrease pH of the solution (Figure SA8, Figure SA12).

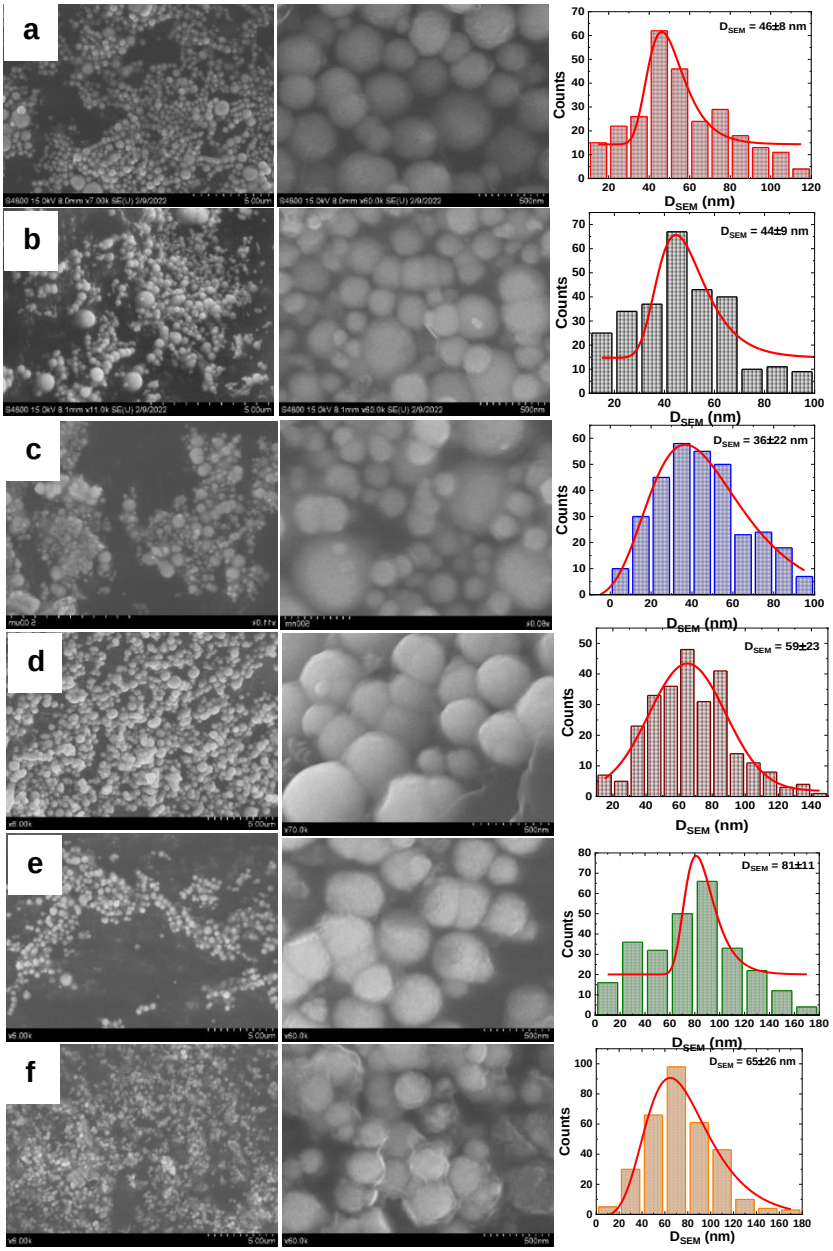

Figure 32: ZVI@CIT particles prepared at various reaction temperatures: 0, 10, 30, 40, 60, and 80^{o}C (a -f).

We also analyzed elemental composition of sample nanoparticles from SEM images using Energy Dispersive X-Ray. The EDS/X spectra for iron sulphate batch are shown in Figure 33 below and Figure SA9. Only four peaks for carbon from the citrate but majority from the carbon

tape and oxygen from contamination, also from the environment during sample storage and transportation and FeK and FeL for iron in the K and L shell are seen (Chang & Kang, 2009). Similar data is has been obtained for second third and fourth batch experiments (see Figure SA 9) but not included here to omit redundancy. As from the bar graphs, the amount of Fe is much higher than that of oxygen which is a clear indication of which almost majority of the sample is composed of zero-valent iron nanoparticles. Presence of significant amount of oxygen could be attributed to the normal reaction conditions.

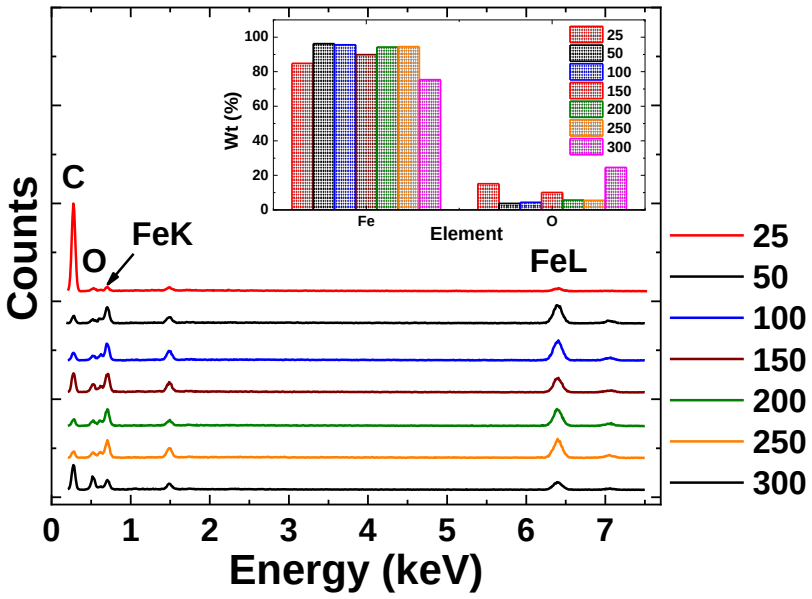

Figure 33: EDS/X spectra of particles synthesized at variable concentration of metal(core): 111.2, 55.6, 27.8, 18.5, 13.9, 11.12, and 9.27 mole/L (Inset bar graph is elemental compositions).

6.4. Magnetic Properties of cZVI Nanoparticles

Freshly prepared nanoparticles were investigated for magnetic behavior at a range of magnetic field and temperature with the help of vibrating sample magnetometer.

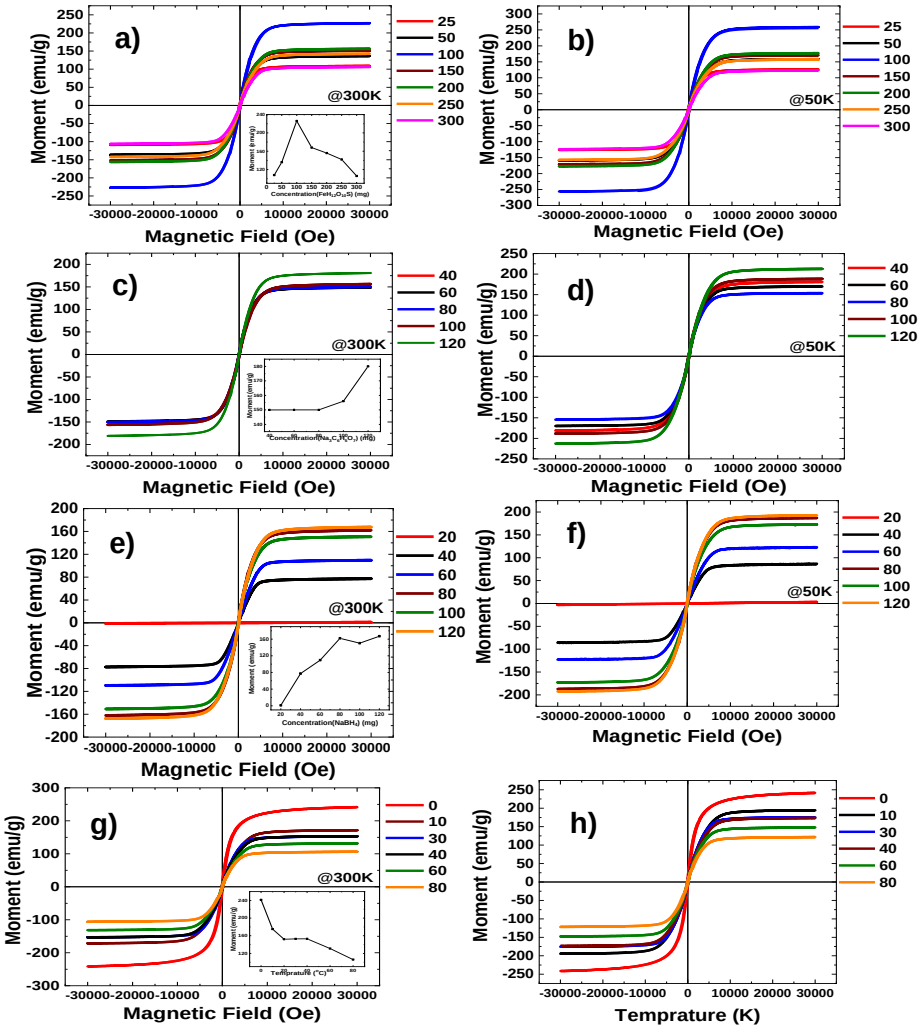

Figure 34: Hysteresis loops for sample core-shell nanoparticles. Those synthesized at variable concentrations of iron sulphate, a) at 300K and b) at 50K; at variable concentrations of sodium citrate, c) at 300K and d) at 50K; at variable concentrations of sodium borohydride, e) at 300K and f) at 50K and at variable reaction temperature, g) at 300K and h) at 50K. Inset in a), c), e) and g) are patterns in magnetic saturation with respect to concentration of the material understudy while h) is magnification of the hysteresis loop at 50K for the reaction batch at variable reaction temperature.

From the above hysteresis curves, it can be deduced that all sample core-shell nanoparticles have superparamagnetic behavior indicated in very low coercivity at 300K and 50K in Figure 36 (also

see Figure SA10). Assessment of the results in terms of stable and high Ms from first and second batch of the experiments, it is clear that iron concentration 27.8 mole/L and hydride concentration below 73.53 mole/L are appropriate for synthesis of the required core shell nanoparticles with favorable magnetic properties. This is also without the need for use of an inert gas as in many studies (Hauser et al., 2015).

Addition of sodium borohydride impacts hydrogen generation and nucleation of the nanoparticles by altering the basicity of the solution. In line with this, linear increase in Ms can be seen with increase in the concentration of sodium borohydride. Taking the results which show linear relationship, the concentration of the reducing agent affects nucleation of nanoparticles hence their magnetic behavior. We believe the nucleation process of the nanoparticles supports the order of ZVI core – iron oxide and citrate caping rapidly thus the role of an inert gas is compensated. Ultrahigh magnetic saturation (241emu/g) observed in response to low reaction temperatures. Furthermore, this particular sample was run in VSM for consecutive 14days (Figure SA11). Magnetization decreased over the 14-day time period and then started to increase after 14^{th} day. The reason for this change is beyond the scope of the researchers but we believe it occurred due to slow magnetic relaxation behavior.

6.5. Absorbance Band Gap Energy

Band gap energy (Eg) of ZVI nanoparticles was evaluated in V-770UV-Visible/NIR spectrophotometer (a single monochromators and dual detectors, 190 to 2700nm, Jasco). Eg is associated with reaction temperature and pressure, surface and interface, crystal structure and lattice strain thus, useful to assess application of nanoparticles in photocatalysis, antibacterial, magnetic storage and hyperthermia (Akbari et al., 2019; Fonseca-Cervantes et al., 2020; Getsoian et al., 2014). For example, increase in band gap has shown to relate with decrease in

grain size aka quantum size effect (Deotale & Nandedkar, 2016; Singh et al., 2018). The Eg of our nanoparticles is above 6eV in average and direct allowed transitions, see Figure 35 below and Figure SA13. It has net increase with increase in amount of core metal, the ligand and reducing agent as well as reaction temperature subsequent to decrease in sizes of nanoparticles in those conditions. However, due to higher band gap prevents them from harvesting light at visible region, these particles cannot be good candidates for photocatalytic reactions.

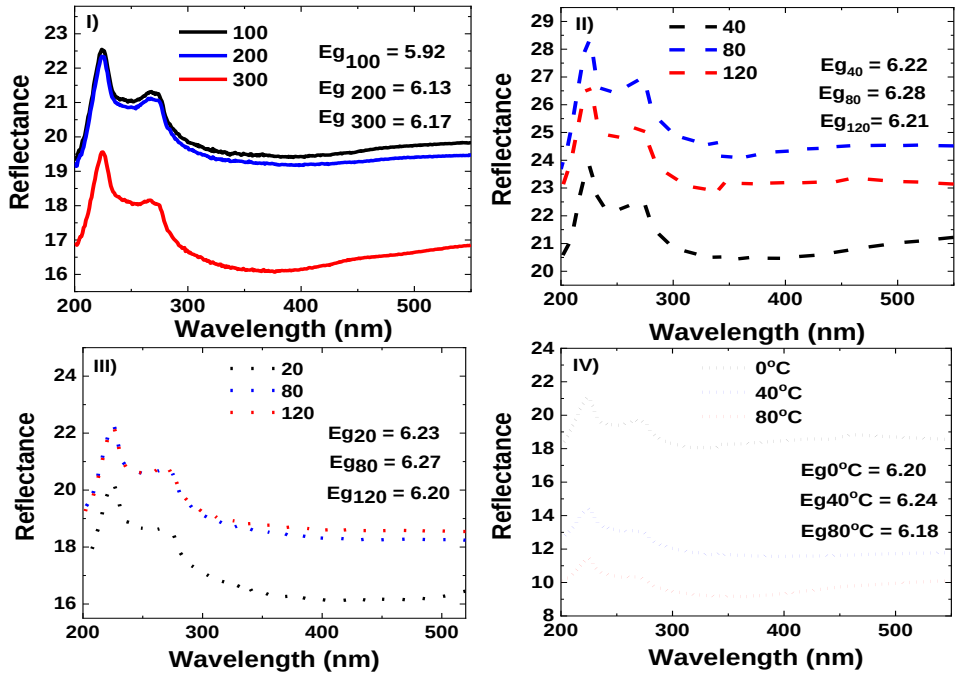

Figure 35: UV-Vis spectra and bandgap energy of selected nanoparticles for sample core-shell nanoparticles at increasing concentrations of iron sulphate, I), sodium citrate II), sodium borohydride, III) and at increasing reaction temperature, IV).

6.6. Relationship Between Magnetic and Textural Properties of Nanoparticles

It has been well established that magnetic behavior of magnetic nanoparticles is associated with their textural and optical properties. The goal of this work is also to investigate this relationship by tuning synthesis parameters in response to change in magnetic and textural properties of

nanoparticles. Related to magnetization, we extracted domain size (Dmag) and magnetic saturation (Ms) and coercivity (Hc) from hysteresis loops, and related to the structural properties, particle diameter (Dsem) and number of atoms was estimated from SEM images of nanoparticles at a specified resolution. Particles with small domain size showed high magnetic saturation (Ms) and this observance supports the presence of ZVI nanoparticles with single domain also due to their ultra-high superparamagnetic behavior corresponding to their domain size (Deotale & Nandedkar, 2016). Dmag is a more accurate description for size dependent magnetic saturation since the coating and additional impurities alter the trend in size consequently, Ms on per-gram unit basis. Apparently, in samples with less impurity or thin coating Dsem and Dmag are correlated. Moreover, number of atoms is correlated with high coercivity as in most of nanoparticles synthesized here regardless of change in composition of reactants. Nevertheless, in addition to reduced coercivity of nano spheres attributed to shape anisotropy, wide range and variable sizes tend to fluctuate the sequential increase or decrease of properties of the particles.

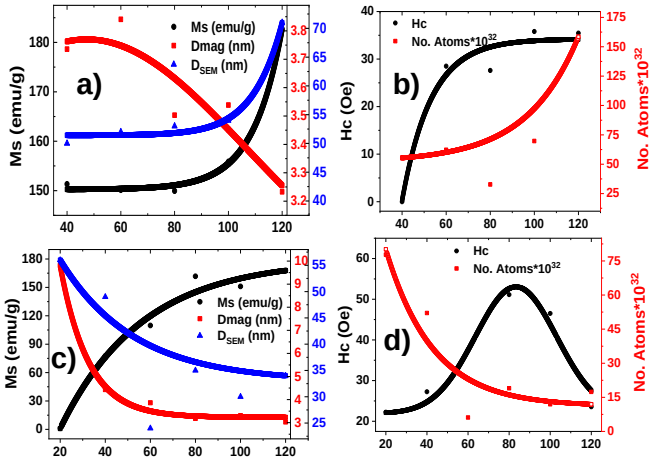

Figure 36: Relations ship between domain size and magnetic saturation; coercivity and number of atoms for second batch experiments (changing ligand concentration) a) and b) and third batch experiments (changing amount of reducing agent) c) and d).

5.7. Comparison with other studies and prospective applications

Compatibility for water treatment

Simple coprecipitation reaction liberates iron and covers it with thin iron oxide and many molecules of citrate. Citrate compounds not only stabilize the iron core nano particles but also modify the surfaces. Hence, two reaction sites i.e. a nucleophilic oxygen from the sodium oxide component and an electrophilic oxygen from the carbonyl carbon exists. This cites are one of the most common among adsorbents existed in many nano adsorbents including carbon nano tubes (CNT), graphene-based nanocomposites and metal oxides(Assis et al., 2019a; Awad et al., 2020). Additionally, the synthesis and functionalization of citrate on iron surface is a single step process. The resulting particles were very well dispersed in water due to hydrophilic nature of the ligand and efficient attachment to the nanometal (Qureashi et al.2021). Moreover, the synthesis procedures did not involve organic solvents, the materials have high salt tolerance which makes them cheap and biocompatible(Kotsmar et al., 2010).

Table 4: Findings from related studies in comparison with the present findings

No	Nanoparticles	Ms@300 K	Size (nm)	Shape	Hc	Purpose	Result	Active site	Mechanism	Ref
1	ZVI	-	20–30	Nanoflowers		Antimicrobial activity	100% inactivation for P. fluorescens; 80-100% for B. subtilis; no effects for Aspergillus versicolor in 5 min		Reaction with membrane, generation of reactive oxygen species; physical coating	(Diao & Yao, 2009)
2	ZVI	-	50	Spherical	-	Removal of Zn2+, Zn(II)–EDTA and Zn(II)–citrate	At pH of 7, 5 mg Zn^{2+} L^{-1} in 1hr	Iron oxide	adsorption	(Kržišnik et al., 2014)
	ZVI @ Silica fume									
	ZVI @ octa(cholinium)-polyhedral oligomeric silsesquioxane									
3	ZVI	-	3 and 30 mm	spiral coils	-	Removal of As and phosphates	~100% removal of Fe(II) and 85% of As	Iron oxide	Adsorption, ferrous ions co-precipitate As(III), Fe(II), $PO4^{2-}$	(Kowalski & Søgaard, 2014)
4	ZVI	-	(purity >98%, 400 mesh)	-	-	Swine wastewater treatment	COD Removal (89.2% a) and methane production (~128mL at $r_{ZVI/VSS}$ = 2.63)	Precipitation	Dissolved ferrous ions, flocculation, adsorption and precipitation, corrosion-induced H2	(D. Wu et al., 2015)
5	nZVI@ SiO_2 decorated with biotinylated peptide (Pe)	119.482	54 ± 10	Spherical	338.573	Magnetic resonance imaging	peptide was effectively conjugated with the superparamagnetic nZVI	Peptide	biomarker of neuroinflammation	(Gaona et al., 2021)
6	nZVI@ polydopamine	-	69	Amorphous	-	Dual-Modality Photothermal and Photodynamic Breast Cancer Therapy	- 26.3°C increase up on irradiation - ROS accumulation was increased by 3.3 fold compared to control cell induced -apoptosis in MCF-7 cells under NIR illumination	polydopamine	Heat and ROS generation	(Yu, Hsin Her et al., 2020)
7	Fe_3O_4@Citrate (500ºC)	58.8	276±129			Anode material for Li-ion batteries		Fe_2O_3@C	Oxidation of magnetite into hematite	(Jung et al., 2018)
	Fe_3O_4@Citrate (600ºC)	43.2	759±172							
	Fe_3O_4@Citrate (700ºC)	19.6	1158 ±122							
8	This study	241	65	Spherical	0-150	Synthesis and tuning		Citrate and Iron oxide	Adsorption , Reduction , Catalysis	This study

Adsorption/degradation of organic pollutants

Almost all organic pollutants bear hydrogen and carbon in their structure others possess heteroatoms such as oxygen, nitrogen, or sulfur in saturated and unsaturated bonds. Thus, the most common surface sorption mechanisms are hydrogen bonding, π-π interaction, electrostatic interaction, and van der Waals force Kotsmar et al., (2010); F. Wang et al., (2020) which both kinds of reactive oxygen cites, the pi bonds and hydrogen bonds on the methylene carbons are readily available for attracting organic pollutants in the capping citrate compounds. For example, citrate-coated magnetic iron oxide nanoparticles (IONPs) also with good dispersion in water adsorbed methylene blue (MB) between pH = 4−11) and Methylene orange (MO) at pH 4, 139 ± 4 mg/g and and 257 ± 16 mg/g respectively at 99% adsorption efficiency for nine consecutive cycles(Talbot et al., 2021). Additionally, citrate stabilized Ag nanoparticles showed efficient and superior catalytic ability on reduction of Rhodamine B compared to same nanoparticles coated by polyvinylpyrrolidone(Bastús et al., 2014). The major mechanism of removal of the pollutants dyes is through electrostatic interactions with the citrate ions. Adsorption of citrate-coated silver nanoparticles from aqueous dispersions of electrolytes (trisodium citrate ($Na_3C_6H_5O_7$), sodium chloride (NaCl) and sodium nitrate ($NaNO_3$) by using activated carbon demonstrate affinity of the citrate ion towards both organic pollutants and heavy metals(Gicheva & Yordanov, 2013).

Adsorption of inorganic pollutants

Surface interaction of citrate to nanomaterials and heavy metals is theoretically supported and practically proven(Assis et al., 2019b). Gold and silver coated with citrates showed efficiency towards adsorption of several heavy metals including (Pb^{2+}). In the similar study, gold nanoparticles (AuNPs) have been shown to be effective heavy metal sensors(Frost et al., 2017). In another study Au coated with citrate successfully reduced Hg(II) even in the presence of other

competitive ions(Ojea-Jiménez et al., 2012). Similar findings on Au, Ag are also reviewed elsewhere (Mensah et al., 2021).

Inhibition of waterborne pathogens

The well-known mechanism of antimicrobial action in nanoparticles are oxidative and non-oxidative stress induction and metal ion release that disrupt bacterial membranes by interfering in synthesis of bacterial proteins, hinder biofilm formation due to size and shape features penetrate the biofilm matrix and inhibit organism and other physicochemical properties (they are good carriers of antibiotics, prevent microbial resistance by increasing the serum, ease of transport is certain and controllable especially, if magnetic nanoparticles) (Hooper, 2001; Webster & Seil, 2012). In citrate functionalized Ag nanoparticles, size and shape was responsible for their efficiency against both gram – positive and gram – negative bacteria (Flores et al., 2013). Most of the particles synthesized here has size less than 100nm which is in the range of suitable size for such applications (Dey et al., 2015). The main source of antimicrobial efficacy of nanoparticles lies in the property of their surface. A single nanoparticle can be coated with several antibiotics with different mechanism of action which not only inhibit the microorganisms but also face little resistance (L. Wang et al., 2017; Webster & Seil, 2012).

cZVI nanoparticles have small proportion of iron oxide nanoparticles between the core and the shell. Thus, metal ions released from those oxides interact with the functional groups of proteins and nucleic acids, such as amino (–NH), mercapto (–SH), , and carboxyl (–COOH) groups in the cell membrane, and interfere in enzyme activity, inhibiting the microorganism or in the transfer of transmembrane electrons (L. Wang et al., 2017; Webster & Seil, 2012). Additionally, In citrate coated iron nanoparticles, surface functional groups are likely to interact with cell walls

and membranes of the pathogenic microorganisms since they are the first defensive mechanisms(Flores et al., 2013).

Catalytic efficiency

Citrate capped iron oxide nanoparticles efficiently catalyzed the condensation of barbituric acid and cinnamaldehyde to produce (E)-5-(3-phenylallylidene)pyrimidine2,4,6(1H,3H,5H)-trione with 83% yield with little amount (7.5% mole) of the particles (Cahyana et al., 2017)(46c). Their super paramagnetic property makes them recyclable catalysts but the surface chemistry, the carboxyl group in this case is the catalytic cite eventhough the present particles demonstrated band gap energy Eg = 6 which makes them inappropriate for photocatalytic reactions.

Compatibility for biomedical applications

The effectiveness of magnetic nanoparticles for magnetic hyperthermia and as contrast agents, biosensing and drug delivery has been extensively studied and specific feature of these particles which tend to estimate of their performance are identified. Some of these features are size, shape, composition, and shell-core structure on saturation magnetization, coercivity, blocking temperature, and relaxation time. Data collected from structural and magnetic properties of as synthesized nanoparticles have shown to satisfy most of those features. The discussion with respect to each application is elaborated below.

Application in magnetic hyperthermia

On application of alternating current magnetic field heating arises either from rotation of magnetic moments (Neal relaxation) or rotation of the magnetic particle itself (Brownian relaxation) or hysteresis loss. For superparamagnetic nanoparticles such as Fe@CIT the first factors are always prominent than the latter. As a result, the heating efficiency of nanoparticles

with coercivity greater than zero is usually calculated by the following formula (Kolhatkar et al., 2013).

SAR(W/g) = $C\frac{\Delta T}{\Delta t} = Av$ …….1

Where C is specific heat capacity of water, $\frac{\Delta T}{\Delta t}$ is the rate of change of temperature. A is area of hystresis loop and *v* is frequency.

If experimental data is used, the heating capacity that originate from the relaxation processes are associated with magnetic saturation (Ms) and magnetic anisotropy.

SAR(W/g) = $C\frac{\Delta T}{m\Delta t}$ =…….2

Previous studies on magnetic hyperthermia established certain size based on optimum heat generated in the experimental application. Most of the cZVI nanoparticles synthesized here has magnetic saturation between 106 and 241 emu/g and grain size 30 and 70 nm. The high magnetic property enables heat generation at minimum dose of nanoparticles because mass of the nanoparticles is inversely proportional to SAR and efficient transport across the biological medium. In many studies the SAR was observed to increases with domain size(Kolhatkar et al., 2013).

The value of blocking temperature (TB) is a starting point where ferromagnetic and ferrimagnetic nanoparticles show superparamagnetic property and is associated to slow relaxation of magnetization. In hyperthermia, blocking temperature is aids in determining the maximum heating capacities of nanoparticles. As determined from their zero-field cold and field cold curves, most nanoparticles have TB greater than 200K.

As contrast agents

In a study by Saraswathy et al., (2014), citrate coated iron nanoparticles synthesized by coprecipitation are studied as contrast agents at various concentrations of iron using longitudinal (T1) and transverse (T2) weighted MRI. On in vivo MR imaging of liver fibrosis model in rodents, sample nanoparticles showed nearly 79% increase in T2 and relaxivity ratio (r2) of 37.91compared to particles that lack citrate on their surface. This increment was proportional to concentration of samples. The cell viability and blood compatibility assay showed that particles have the right surface chemistry. Since size, magnetization, surface chemistry, stability, coating thickness and biocompatibility are parameters advantage for particles used in biomedical application in general and as contrast agents specifically, in line with these studies, the present particles are single domain and the citrate on the surface facilitates hydrogen bonding with aqueous solution hence improved dispersion compared to ferromagnetic materials and stable as confirmed by high zeta potential and 1200 ^{o}C decomposition temperature to remove citrate from the surface and storng Fe---O bond shown in IR spectra (Nimi N. et al., 2018; Saraswathy et al., 2014).

Compatibility for energy applications

Citrate capped Fe_3O_4 and related nanoparticles have significant use in lithium-ion batteries as anode material due to their light weight, resistance to change in volume while lithiation and enhanced electrical conductivity improve storage capacity and cyclic stability (J.-S. Xu & Zhu, 2012; Yu et al., 2022). Calcinating these nanoparticles at temperature above 500^{o}C transform into carbon coated Fe_2O_3 which is the active material in anode(M. Gao et al., 2013; Jung et al., 2018; Petnikota et al., 2015). At 700^{o}C, exfoliated graphene oxide caped FeO(EG/FeO) reduced from Fe_3O_4 is an active material in the anode, selected for its ability to prevent excess Li_2O

formation and hinder decaying compared to Fe_2O_3 and Fe_3O_4. Where, the GO coating serves as stabilizing agent and source of hydrogen and carbon dioxide that facilitate the reduction process at 650^oC reaction temperature. EG/FeO has shown 674 mAh/g reversible capacity at 400 mA/g, 78% capacity retention after 60h charge and 94% coulombic efficiencies(Jung et al., 2018). In a different study, three-dimensional composite (Fe_3O_4-C-rGO) used as anode for lithium ion batteries showed specific capacity of 842.7 mAh/g after 100 cycles. Theoretically, Fe_3O_4 has 925 mAh/g specific capacity and graphene oxide is known for high conductivity and surface area and excellent stability (B. Li et al., 2011).

Citrate coated iron nano particles are also suitable for enhanced oil recovery as nanoparticles, nanosensors, nanocomposites, coated nanoparticles, nanofluids due to several advantages with regard to adsorption capacity and affinity, nanoparticle adsorption of asphaltene, resistant to pH and salinity and interaction with precipitated asphaltenes at the interface between the two fluids and cost-effectiveness and reusability (Kotsmar et al., 2010; Sircar et al., 2022). Iron and other nanoparticles of different size aid into isolation and purification of polymers at certain temperature, pH and salinity conditions. In chemical flooding method of oil recovery, addition of nanoparticles increases viscosity, disjoining pressure, pore channel discharging, charging wettability and asphaltene precipitation. The resultant fluid is enhanced and stable with ease of mobility control(Amrouche et al., 2021; Betancur et al., 2020; Cheraghian et al., 2020; Franco et al., 2020; H. Zhang et al., 2014).

6.8. Conclusions

Simple and efficient synthesis platform lead to superparamagnetic crystalline iron nanoparticles stabilized in citrate compounds. We gained important knowledge of tuning magnetic and

structural properties of core shell nanoparticles by varying the composition of reactants. Our data revealed that at optimum concentration of the core metal and shell ligand magnetic saturation increased with increasing reducing agent and decreases with increasing reaction temperature. On average, particles with high Ms has small grain size and larger particles were less magnetic. Most importantly, most of the samples has magnetic saturation higher than all other similar stadies. And such tunable properties of magnetic nanoparticles have found advantage in water treatment and catalysis, magnetic hyperthermia, as contrast agents and in energy applications. In the second phase of this project we intend to study particles performance as efficient adsorbents to wards wide rang organic and in organic pollutants and inhibition of microorganisms. Invitro and In vivo hyperthermia bioassays are being studied and will be compiled and presented in our future report (research article).

CHAPTER 7

ROOM TEMPERATURE SUPERPARAMAGNETIC ORDER WITH COLOSSAL MAGNETOCRYSTALLINE ANISOTROPY IN AMINOFERROCENE-BASED GRAPHENE MOLECULAR MAGNETS

7.1. Introduction

Since the discovery of molecular magnets Coronado (2020); Luneau (2001) there has been growing interests to develop molecular materials that can exhibit cooperative magnetic interactions at room temperature. Molecular magnets (MMs) are a relatively new class of magnetic materials, in which molecular moieties bearing unpaired spin density interact electronically and magnetically (Coronado, 2020; Kahn, 1985). Because of their quantum size effects, lightweight, mechanical flexibility, tunable color or transparency, low-temperature processing, solubility, and compatibility with polymers and other classes of molecular materials, MMs have great advantages and unique properties compared to conventional magnets in high-density data storage. Furthermore, the use of MMs in the area of spintronic and qubits for quantum computing has the potential to become a disruptive technology, since organic materials can enhance preservation of electron spin orientation lifetime relative to inorganic conductors due to their inherently weak spin–orbit coupling.

However, producing room temperature molecular magnets was and still is a challenge. Only the work done by Manriquez et al. (Manriquez et al., 1991) regarding the reaction of bis (benzene) vanadium with tetra cyanoethylene, TCNE, affords an insoluble amorphous black solid that exhibits ferromagnetism at room temperature. The origin of the magnetic behavior was based on

three-dimensional antiferromagnetic exchange of the donor and acceptor spins resulting in ferromagnetic behavior. Then, this work has been continued to include other 3d metals such as Mn (Olson et al., 2015). Since then, the scientists have been focusing on development of new molecular magnets that operate near room temperature with the goal of enabling spintronic applications. Recently, a new MM system has been discovered by Guo et. al. (F.-S. Guo et al., 2022) that contains Dysprosium metallocene with magnetic hysteresis observed up to 70K. Such behavior is originated from spin-phonon coupling regimes. Since discovery of graphitic carbon on 1991 by Ijima (Lijima, 1991), there has been working on developing magnetic graphene or graphene based molecular magnets that might show a room temperature ferromagnetic behavior (Blundell & Pratt, 2004). Most of the graphene based molecular magnets (G-MMs); in particular those with near room temperature magnetic susceptibly are promising for the prospective applications in spintronics and quantum computing (Hong et al., 2013b; Sakurai et al., 2019). They exhibit long-range magnetic order more than other ligand based molecular magnets. Besides, ligand based molecular magnets suffer from tunneling at zero field, a major cause for their inefficiency for information storage (Wernsdorfer et al., 2002). Even though, graphene sheets lack magnetic property, structural change due to oxidation to graphene oxide and structural defects might introduce ferromagnetism (Diamantopoulou et al., 2017; Sarkar et al., 2014). In both graphene oxide and reduced graphene oxide, (Diamantopoulou et al., 2017; Sarkar et al., 2014) reported weak superparamagnetism at room temperature. Epoxide functional groups, composites are responsible for magnetic susceptibility of graphene oxide (Galpaya et al., 2014), creating unpaired spins on the carbon radicals (Lee et al., 2015b; M. Wang & Li, 2010). Surface N-doping also increases magnetization (M) in graphene oxide sheets to ca. 1.66 emu/g at 2 K (Y. Liu, Tang, et al., 2013) and by 64.1% when annealed at 500 °C(Y. Liu, Feng, et al.,

2013b). Hong et al., (2013a) have also published nitrophenyl functionalized graphene based molecular magnet with long-range magnetic order above 400K. The high surface area in graphene integrated with aryl radical on the surface created out-of-plane antiferromagnetic ordering. In a recent study, attachment of electron withdrawing substituted ligands to the graphene enhanced the charge transfer revealing magnetic and electronic properties (Zhu et al., 2020). Similar to this study, examined magnetic property of graphene oxide surface functionalized by aminoferrocene found out magnetization as collective effect of the sheets and the ferrocene moiety with critical temperature at 2 K(Sakurai et al., 2019).

In this study, we aimed to solve two major technical impediments for use and delivery of G-MMs. The first is the challenge to synthesize molecular magnets that can operate at room temperature. The second is to increase magnetic order stability by attempting to locate the ligand inside the layers and rely upon slight metallic behavior to increase the onsite magnetic anisotropy and strongly couple neighboring magnetic intercalants. For this reason, we select aminoferrocene for its efficacy to participate in electron transfer L. Guan et al. (2005) to be intercalated within the graphene oxide layers. The more favorable interaction of the graphene oxide layer and the aminoferrocene that does not alter their chemical properties is a noncovalent weak interaction that resulted from near proximity of delocalized $\pi -$ electrons (Lopes et al., 2010)

7.2. Structural Elucidation

The crystal structure was characterized using XRD as shown in Figure 37. A sharp peak at a range of 10^{o} is a good signifier of graphene oxide formation(Arthi G & Bd, 2015). Our calculation of the interlayer spacing using the Bragg law (Order of reflection (n) × Wavelength (λ) = 2 × Interplanar spacing (d) × Sinθ), Where, λ - wave length of incident X-ray, theta(θ)= peak position in radians) also indicated that GO layers have wider spacing (d_{001}= 1.0365 nm)

than the repeatedly reported d-spacing, which is less than 1 nm(Arthi G & Bd, 2015;Su et al., 2009). Some studies have also reported larger d-spacing claiming that d-spacing show an increase following the oxidation of graphite and effect of solvents (Blanton & Majumdar, 2012). This spacing will be filled with aminoferrocene sandwiched between the layers (Su et al., 2009). This also supports the ferrocene to stay trapped (e.g. intercalated) between the layers. In addition to the weak van der-waals interaction existed between the double conjugation of the graphene oxide and the diene in ferrocene (Avinash et al., 2010), the hydrogen bonding within the amino-group of ferrocene and oxygens of the GO-layer might have contributed to the stabilization of the interaction. The strongest interaction is expected to be columbic due to charge transfer between the aminoferrocene and the bilayer. In addition, as seen in Figure 37, the XRD peaks confirm the presence of the aminoferrocene and the GO-aminoferrocene molecular magnets and no presence for any related iron oxide phase structure.

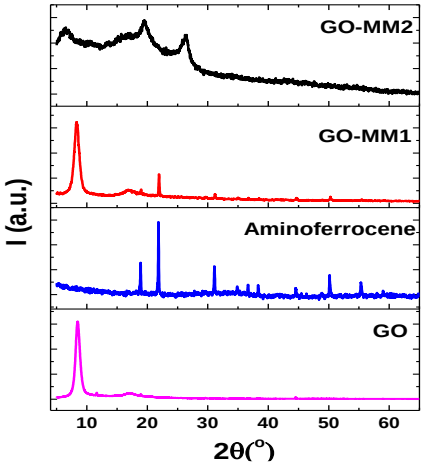

Figure 37: XRD spectra of GO-MM2, GO-MM1, aminoferrocene $[C10H12FeN]^+$ and Graphene oxide.

Fourier Transform Infrared Radiation Spectroscopy (FT-IR)

In order to verify the presence of the functional groups, FT-IR studies were performed under vacuum in transmission mode.

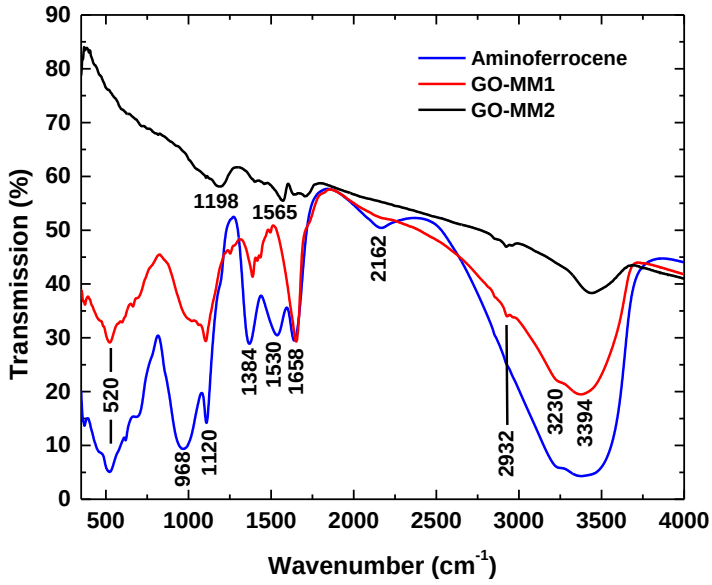

Figure 38. FT-IR spectra of amino ferrocene $[C_{10}H_{12}FeN]^+$(blue line), GO-MM1(red line) and GO-MM2 (black line).

For easier comparison and vibrational line assignments, in addition to the IR spectra of GO-MM1 and GO-MM2 samples, the aminoferrocene spectrum is also presented in Figure 38. The spectrum shows dominant vibrational lines at 520 cm^{-1} (ring-Fe-ring stretching), 968 cm^{-1} (CH bending), 1120 cm^{-1} (anti-symmetric cyclopentadienyl ring breathing mode), 1384 cm^{-1} (CC stretching), 1530 cm^{-1} (CC stretching), 1658 cm^{-1} (CO, CC, and the amino group stretching), 2162 cm^{-1} (CO and CC stretching), 3230 cm^{-1} (CH and OH stretching), and 3394 cm^{-1} (OH stretching) [41]. All these amino ferrocene vibrational lines exhibit shifts of ~ 35 cm^{-1} in average

from the vibrational frequencies characteristic to ferrocene(Lippincott & Nelson, 1958). A quick comparison between the IR spectra of GO-MM1 and GO-MM2 samples with the spectrum of amino ferrocene reveals a much stronger presence of aminoferrocene in the GO-MM1 sample, presence almost absent in the case of GO-MM2 sample. This remark is based on the similarity of vibrational lines observed in both, the GO-MM1 and the amino-ferrocene spectra. However, a closer look at these two spectra demonstrates that there are some vibrational differences, such as the decreases in the intensities of the 968 $cm^{-1}$and 1384 cm^{-1} bands and the disappearances of the 1530 cm^{-1} and 2162 cm^{-1} vibrations in the GO-MM1 spectrum. While these observations suggest a potential interaction between GO and aminoferrocene, it also masks the visualization of the characteristic GO vibrational modes, which can be depicted only by the weak vibrations at 2932 cm^{-1} (sp2 CH stretching) and 3230 cm^{-1} (OH stretching) (Avinash et al., 2010; L. Guan et al., 2005). Since the GO contains epoxide and hydroxyl functional on its basal plane, as well as carboxyl moieties at its edges, these two IR vibrations could be also associated with produced defects on the graphene network (Arthi G & Bd, 2015; Lee et al., 2015b). The IR spectrum of GO-MM2 shows absences of the amino-ferrocene absorptions at 520 cm^{-1}, 968 cm^{-1}, 1384 cm^{-1}, and 2162 cm^{-1}, upshifting of the amino-ferrocene lines at 1120 cm^{-1} and 1530 cm^{-1} to 1198 cm^{-1} and 1565 cm^{-1}, respectively, suggesting again a potential interaction between the GO and the amino-ferrocene. It also shows a slightly more visible presence of GO, with characteristics vibrations at 1630 cm^{-1} (CC stretching) and 1730 cm^{-1} (C=O stretching), besides those already observed in the GO-MM1 spectrum at 2932 cm^{-1} and 3230 cm^{-1}. The absence of 2162 cm^{-1} feature in both spectra of GO-MM samples, vibrational lines that could also be assigned to -N=C=O groups, implies a potential intercalation/absorption of aminoferrocene between GO layers or at its edges. It also could imply a complete reaction of the organic material with the

hydroxyl groups of GO. Moreover, since GO is highly hydrophilic, the strong, broad band at 3394 cm^{-1} is attributed to water absorption, as some water molecules might remain attached (Arthi G & Bd, 2015).

Raman Spectroscopy

To verify the presence of the aminoferrocene and graphene in the samples, Raman spectra of the GO-MM1 and GO-MM2 samples together with the aminoferrocene spectrum have been measured and are presented in Figure 39. It is conventional to investigate the quality of a carbon-based sample by employing the intensity and broadness of the characteristic GO Raman features, the D and G bands, with the D mode known to correspond to the disordered carbon line and the related symmetry lowering or finite-size effects in GO, and the G mode related to the graphitic sample properties (J. Gao et al., 2010; Kaniyoor & Ramaprabhu, 2012; Kudin et al., 2008; Yamada et al., 2013). The observed D and G peaks in Fig. 5 at 1336 cm^{-1} and at 1598 cm^{-1}, respectively, as well as the 2D bands at 2678 cm^{-1} and 2935 cm^{-1} are in good agreement with their reported literature values(J. Gao et al., 2010; Kaniyoor & Ramaprabhu, 2012; Kudin et al., 2008; Yamada et al., 2013). Comparison between the Raman spectra of the GO-MM1 and GO-MM2 samples reveals an enhancement of the G peak in the spectrum of the former sample. This increase in the ratio of the intensity of the D peak to that of the G peak, ID/IG, from a 1.1 to 1.4 value for the GO-MM1 and GO-MM2 samples, respectively, is an indicative of a recovery of sp2 domains in the GO and a reduction of its surface. This observation corroborates with the information obtained from other techniques used to analyze the samples, such as XRD and FT-IR. A slight increase is also observed in the intensities of 2D bands in the case of GO-MM2 sample, being attributed to the restoration of C-C interatomic distances and angles characteristic to GO. Also, the absence of the intense ferrocene vibrational lines at 307 cm^{-1} (ring-Fe-ring

stretching), 391 cm^{-1} (ring-Fe-ring stretching), 1108 cm^{-1} (symmetric ring breathing mode), 3100 cm^{-1} (symmetric CH stretching) in the spectra of the two GO-MM samples, again indicates a potential interaction between the organic material with the GO, in agreement with our previous FT-IR analysis.

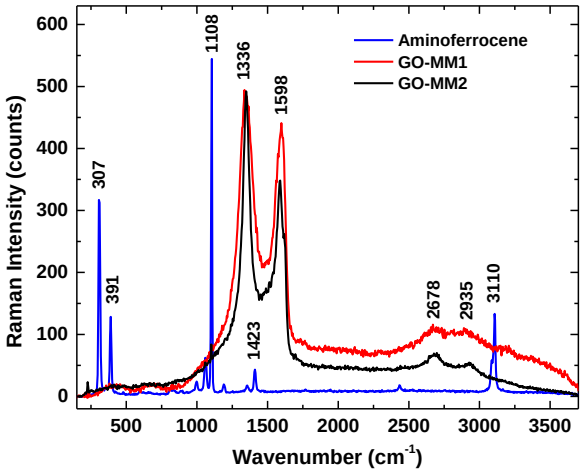

Figure 39. Raman spectra of amino-ferrocene (blue line), GO-MM1 (red line) and GO-MM2 (black line).

7.3. Magnetic Properties

In order to determine the magnetic range order of the prepared systems, magnetic measurements were carried out by using the vibrating sample magnetometer (VSM) in magnetic field range of -3T to 3T and temperature range from 50 to 400 K. The measurements include hysteresis loop at room temperature (300 K), 50 K and 350 K and the magnetization dependence on temperature at constant magnetic field of 200 Oe.

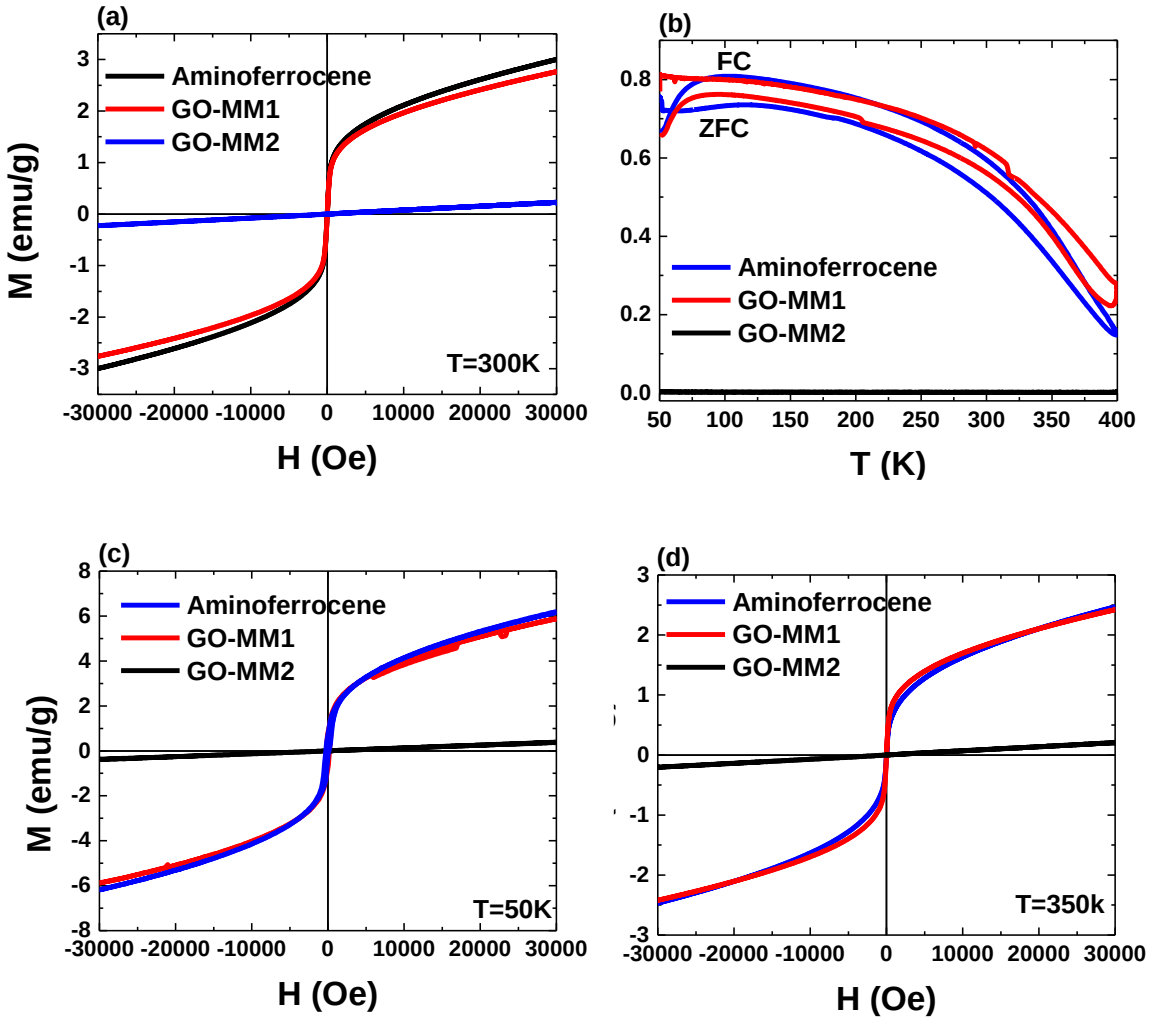

Figure 40. Hysteresis loop at room temperature (a)**,** Magnetization at zero-field-cooled (ZFC) and field-cooled (FC) at 200Oe (b) and Magnetization dependence of external magnetic field ((c) at 50K and (d) at 350k).

Aminoferrocene and GO-MM1 displayed closed hystersisis loops at room temperature with coercivity (H_C) close to zero of 0.34 and 12.82 Oe, respectively, revealing superparamagnetic behavior with magnetization (Ms) of 3.06 and 2.762 emu/g and GO-MM2 showed paramagnetic behavior (Figure 40 (a)). The MxT data were recorded by the ZFC/FC measurements at 200 Oe, which show the long-range magnetic order up to 400 K and confirm the superparamagnetic behavior of the amino-ferrocene and GO-MM1 samples with blocking temperature (T_B) of 75

and 95 K respectively (Figure 40 (b)). The GO-MM2 shows zero magnetization with no magnetic range order. The MxH data at 50 K and 350 K shows ferromagnetic behavior which confirm the long range ferromagnetic magnetic order of the amino-ferrocene and GO-MM1 samples and show paramagnetic behavior for the GO-MM2 sample (Figure 40 (c, d)). Since the samples have superparamagnetic behavior, the magnetocrystalline anisotropy was determined using Neel-Brown equation(El-Gendy et al., 2009a). The aminoferrocene and GO-MM1 samples show colossal magnetocrystalline anisotropy with 3 x 10^7 and 8 x 10^5 J/m^3 respectively. These values are comparable with pure iron metal for graphene based aminoferrocene (GO-MM1) and two order of magnitude larger than pure iron and one order of magnitude larger than CoFeC permanent magnet for aminoferrocene molecular magnets(El-Gendy et al., 2009b, 2015). The observed superparamagnetic behavior in amino-ferrocene might originate from the free electron that appear in iron caused by regenerated excess of sulfuric acid after elongated reaction time (Fig. 5). Or since the charged amino-ferrocene persists, the reason for magnetization is possibly due to electron withdrawing and deactivating effect of the charged nitrogen that is more electronegative than neighboring atoms. This decreases the $\pi-$ while increasing the $\sigma-$ electron density in ortho and para positions of the ring creating a paramagnetic coupling and de-shielding between the occupied σ with the unoccupied π orbitals and the unoccupied π* orbitals with the occupied σ orbitals(Viesser et al., 2017). While in GO-MM1, the magnetization is a collective action between the graphene oxide and the ligand-ferrocene (Sakurai et al., 2019). Interaction between π-orbitals in the sp2-bonded carbon atoms of graphene oxide sheets Enoki et al. (1996); Lopes et al. (2010) and ferrocene contribute to the magnetization of the graphene oxide assembly (Kaniyoor & Ramaprabhu, 2012). Furthermore, the magnetic de-shielding effect of charged amino-group facilitates magnetic field stream between each of these two agents

(Viesser et al., 2017). This interaction is further stabilized by hydrogen bond, more strong intermolecular interaction between the amino group and the nearby oxygen layers of the hydroxide or epoxide groups assuming that amino-ferrocene locates at the C-axis (center) of the layer. Some studies also reported that, the disorder in this intermolecular interaction is a cause for unmoved points by the symmetry operations (monocyclic symmetry and or space group) which are associated with induced ferromagnetism in that compound (W. Wang et al., 2013). If the amino ferrocene is at the edges, its interaction with OH of the carboxyl group will lead to different argument, which also make electron transfer very difficult. The low magnetization of similar structure reported in a study by (Sakurai et al., 2019) could be due to this reason. The results are even recorded at T=2K. In a separate experiment, when we changed the synthesis into a one-step mechanism where all the ingredients are added at once, including the separate procedure for preparation of amino-ferrocene, the product, (GO-MM2), was non-magnetic at room temperature. Clearly, amino-ferrocene should not be formed in this assembly because the nitration and reduction process should be done separately. Observing at FT-IR spectra of the structure, small peak for the graphene oxide with the carbonyl carbon and fewer hydroxyl groups support the above information. The purpose of sulfuric and nitric acid reaction is to produce an electrophile known as nitoronium ion (NO_2^+)(Olah et al., 1987). However, in the formation of GO-MM2 the acids are added collectively with other reagents including ferrocene. If ferrocene reacts with sulfuric acid or with nitric acid independently, the reaction distorts the link between cyclopentadiene anion with the metal leading to ferricinium ion, an inert compound which does not undergo electrophilic aromatic substitution reaction (Rausch, 1962; Woodward et al., 1951).

7.4. Theoretical Evidence (DFT Calculations)

In order to understand the reason for the observed magnetic properties in the aminoferrocene and GO-MM1, we have done theoretical studies using density of function theory (DFT) to verify the energy stability for the aminoferrocene to persist in between the layers. This interaction is exhibited constant energy with that bridge positions. In this case amino-ferrocene is situated perpendicular to both the layers. It was also found out that this bind energy is comparable to that of calculated benzene adsorption on graphene (Avinash et al., 2010).

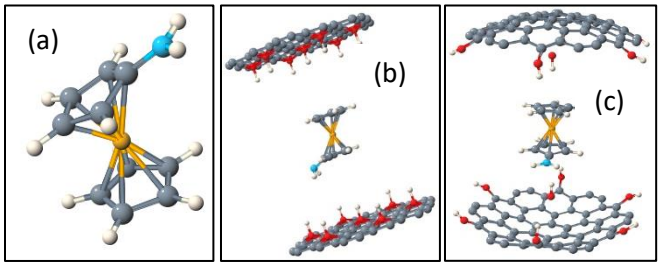

Figure 41. Pictured above are the gas-phase structure of aminoferrocene (a) and the unrelaxed (b) and relaxed (c) [C54(OH)7]2 @ Fe[C5H5 C5H4NH2] system. The initial graphene sheets were flat with chemisorbed OH on them. The final structure shows movement of the hydroxyl groups to the edge sites, chemisorbed, and, in two cases, into physisorbed phases. The graphene sheets are bent significantly at equilibrium.

Within the generalized-gradient approximation the aminoferrocene, C5H5FeC4H4NH2, neutral molecular resides in a singlet state and as expect from its iso-electronic counterpart, ferrocene, it has a large HOMO/LUMO gap. However, if two electrons are removed, the di-cation, converts to a S=1 state with two unpaired d-electrons on the Fe+2 center. The system has a HOMO/LUMO gap of 0.62 eV In the gas phase, the dication has a magnetic anisotropy of 9.1K and is primarily easy axis albeit with an appreciable transverse anisotropy due to the presence of the amine group. For the gas-phase dication, there is significant departure from parallel

pentacene planes in the gas phase as shown in Figure 41. To model the behavior of the amino ferrocene between two sheets of hydroxylated graphene, we have placed the molecule between two highly ordered hydroxylated sheets and allowed the structure to relax. For the overall neutral structures, several structural affects are observed. First, the OH radicals migrate away from the interior of the parallel sheets and bind to dangling bonds on the graphene sheets have been identified in previous work(Hooshmand et al., 2021; Pederson et al., 2000; Pederson & Jackson, 1990; Pederson & Khanna, 1999; Perdew et al., 1992; Porezag & Pederson, 1996, 1999). Second, there is a significant internal pressure induced by the presence of the aminoferrocene island, which leads the isolated graphene sheets taking on a spherical shape. Third, the OH radicals at the center of the parallel sheets steal some electrons from the aminoferrocene which causes a moment to form on the amino ferrocene. Based on numerical analyses of charge near the Fe ion, it appears that full charge transfer of two electrons to the two OH radicals does not appear (Table 5). The distortion of the aminoferrocene, found in the gas-phase dication, also does not occur as dramatically which is in accord with an incompletely ionized island. The strong bowing of the isolated graphene sheets suggests that the charge transfer and resulting magnetization could be strongly influenced by pressure effects.

Table 5: Magnetic anisotropy of the idealized intercalated structure as a function of constrained charge transfer. The physical structure considered here has two hydroxyl radicals in close proximity which are expected to steal two electrons from the aminoferrocene. The table below shows that the magnetic anisotropy of the system in close proximity to hydroxyl radicals increases which is consistent with the observation that the hydroxyl groups steal electrons from the metal center.

Island Charge	Island Spin	Charge State	Bond Descriptor		Magnetic Anisotrop

		Descriptor	(Fe-N)		y
Isolated					
0 (constrained)	0	0/0	3.25 Ang		0 K
1 (constrained)	1	1.01/29.2	3.28 Ang		3.3 K
2 (constrained)	2	1.94/28.2	3.49 Ang		9.1 K
Between Sheets					
(OH)2 (Target)	2	0.38/29.5	3.26 Ang		6.9K
F2					
F Cation					

We have calculated the vibrational spectra of the aminoferrocene in the neutral and +2 charge state (Figure 42). There is a qualitative difference in the Raman spectra at 1500 1/cm which should be a very clear indicator of the S=1 aminoferrocene.

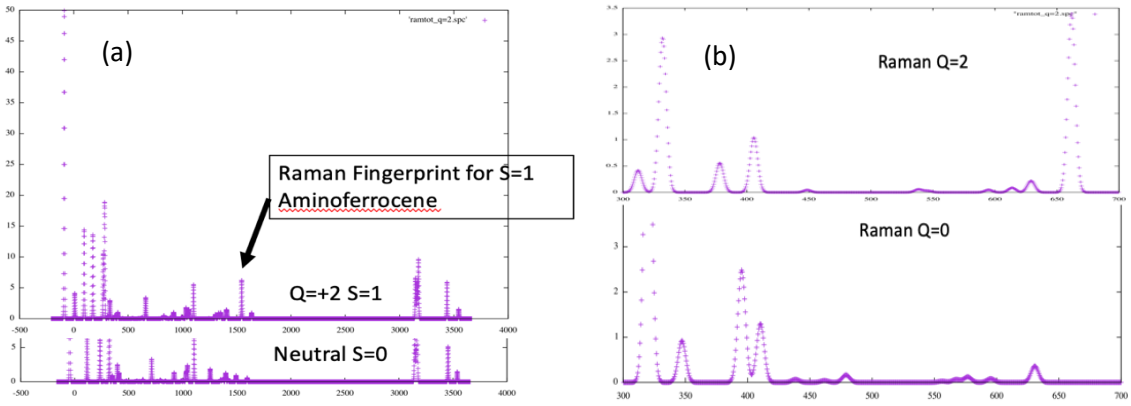

Figure 42: (a) Raman spectra of the +2 and neutral Fe[C5H5 C5H4NH2] molecule. Structure at 1500 1/cm is a clear indicator of a ionized aminoferrocene molecule. (b) Raman spectra of the +2 and neutral Fe[C5H5 C5H4NH2] molecule in the 300-700 1/cm range which show signatures that would help with identification of double cations of the aminoferrocene structure.

From the charge-Transfer Analysis (Table 6), the structural effects suggest that, at least within PBE-GGA, the capacity for electron withdrawing of the OH radicals from the aminoferrocene is

not, by itself, strong enough to create a dication with strong anisotropy between the two-graphene sheets. For the OH case, the calculated moment in charge suggest that a half of an electron is shared with the two OH radicals. These findings confirm the experimental observation of the magnetic order in both the aminoferrocene and GO-MM1 systems.

Table 6: Calculate charge-transfer energetics needed for predicting final charge state of the aminoferrocene. The resulting charge transfer (0.63 eV) is consistent with the slightly reduction of magnetic anisotropy calculated here. The distance between the Fe and OH is approximately 10.0 bohr. The distance between the two OH molecules is approximately 20.0 bohr. Therefore the coulomb energy gained when Q electrons equally transferred between the two OH radicals is given by (Q/2)2 /20- 2(Q)(Q/2)/10)*27.2116=-2.38Q2. The data indicates E(Q)= -3.69Q +2.85Q2 which predicts a metallization of the di-hydroxylated aminoferrocene system with a total Fe to OH charge transfer of 0.63 electrons.

Electron Transfer (Q) from Fe to (OH)2	2 Hydroxyls (eV)	1 Aminoferrocene	Coulomb Attraction	0
0	0	0	0	0
1	-4.52	6.13	-2.38	-0.77
2	-3.97	17.66	-9.52	4.17

7.5. Conclusions

Unlike graphene oxide, aminoferrocene in its ionic form (before deprotonated by a strong base) was successfully synthesized to appositely locate it between graphene oxide layers. The as-synthesized aminoferrocene molecular magnet shows unexpected colossal magnetocrystalline anisotropy with two order of magnitude larger than pure iron (Fe) and an order of magnitude larger than CoFe2C magnet. Such colossal anisotropy leads to thermal

stable long-range superparamagnetic order. The magnetic order originates from electron withdrawing capacity of the electron deficient nitrogen. Within the layers, this effect will transcend to the layers to enhance magnetization in addition to interaction of double bond electrons between each ring. The DFT data indicates E(Q)= -3.69Q +2.85Q2, which predicts a metallization of the di-hydroxylated amino-ferrocene system with a total Fe to OH charge transfer of 0.63 electrons. Furthermore, the results of the DFT calculations suggest that external effects such as pressure are likely to control the degree of charge transfer between the graphene sheets and the aminoferrocene. The DFT calculations confirm the experimental observation of the magnetic order in aminoferrocene and GO-MM1 systems. These outstanding observation open new routes for novel room temperature molecular magnets, which will have a great potential in spintronic and quantum computing devices.

CHAPTER 8

CONCLUSION, DISCUSSION, AND FUTURE DIRECTION

Because of their magnetic property (an advantage for recyclability (Guo et al., 2012)), less toxicity and effective recoverability, MNPs have great significance for many environmental and biomedical applications (Mahanty et al., 2019; Malhotra et al., 2020). Moreover, the surface chemistry of MNPs can be tuned to optimize recovery as well as improve adsorption affinity to specific metal and non-metal pollutants (J. Guo et al., 2012). We usefully demonstrated simultaneous reduction and coating of nanoparticles using phytochemicals extracted from plants. Functionalized crystalline iron oxide was formed, and results were confirmed using experimental and powerful instrumental techniques. Despite large number of phytochemicals believed to exist with all plant materials, high phenolic content is necessary for the plant extract to reduce nanoparticles. Otherwise, the reaction should be conducted under strong alkaline solutions using one of the strong basic solution. The reaction is also mediated by ionic and electrostatic interaction between phytochemicals such as phenols, alkaloids, terpenoids, flavonoids, reducing and sugars proteins, and metal precursors which some of them may not exist in some plants in abundance. In general, there needs to be acidic hydrogen that liberates from those compounds and reduces the metal in to lower oxidation states (Sahni et al., 2015). We recommend that future works to incorporate preliminary phytochemical test and identification and quantification of the major constituents prior to synthesis and applications. Additionally, a simple heat treatment improved magnetization of nanoparticles which is advantageous for ease manipulation of particles in actual water treatment with large amount of polluted water and need to be conducted

under supercritical condition of ethanol in the pressure reactor. It should be rational to assume some significant organic compound are lost during this process and the product should be regarded as bare nanoparticle. Growing nanoparticles on temperature and pH stable polymer is a novel approach as it helps to incorporate weak magnetic and non-magnetic particles that showed efficient capability for the purpose of reusing. Nevertheless, particles have more affinity to the aqueous medium that to the polymer PVA. As a result, reusability is determined by how stable phytochemicals are on the PVA surface. We suggest polishing the surface of PVA for example in polar organic solvent and increasing shaking time during growth of the nanoparticles to minimize the problem. The pressure on microfluidic device exacerbates the detachment of phytochemicals thus, the minimum possible pressure should be used, or the technique can be replaced by flash column chromatography at the expense of increased treatment time but efficient purification at larger scale. It is our believe that high removal efficiency for two organic pollutants under brackish water in a wide range temperature and pH conditions reported here will contribute to attract researchers and policy makers towards sustainable water treatment agents. Another asset of magnetic nanoparticles comes from their response towards alternating magnetic fields that produces heat sufficient to burst cancerous cells and this therapy called magnetic hyperthermia treatment. We attempt to solve two challenges associated with this technique. We introduced plant origin natural product as a coating material on the nanoparticles for the first time. These compounds were extracts using distilled water and are hydrophilic. This should solve the issue of dispersion of nanoparticles which is a limiting factor during transport and distribution around tumor cells at the target location. The natural products are antioxidants hence can savenge free radicals that would lead to a more serious cancer disorder. Studying this efficiency is worth of a separate project other researchers would like to pursue(Heyman et al.,

2017; Saleh Al-Hashemi & Hossain, 2016). Furthermore, particles with ultrahigh magnetic saturation and controllable size were developed. Since, high magnetic saturation produces large magnetothermal heating, it also means less dose and very short contact time. This will reduce duration of treatment for patients hence the pain that comes with it. Controlling particle size has been challenging research. The fact that many of the application of nanoparticles are sensitive to size, it became one area of research and technology interest(S. Sun & Zeng, 2002).

Magnetic materials have significant value in the history of modern data storage devices. Despite the introduction of advanced data storage devices, the next generation massive data storage devices still rely on magnetic materials. Thus, molecular magnets have been a center of scientific research and technological significance since long. However, before using molecular magnets for such applications, realization of stable molecular magnets that function at room temperature is still a challenge. With the help of our expertise with organic compounds and magnetic materials we prepared room temperature molecular magnet with long-range magnetic order that exhibits colossal magnetocrystalline anisotropy of two orders of magnitude higher than the pure iron metal. To prove this experimentally, a single layer graphene was oxidized to graphene oxide and further treated with amino ferrocene in similar procedure. The final product was nonmagnetic. To model the behavior of the aminoferrocene between two sheets of hydroxylated graphene we have used density functional theory by placing the aminoferrocene molecule between two highly ordered hydroxylated sheets and allowing the structure to relax. The strong bowing of the isolated graphene sheets suggests that the charge transfer and resulting magnetization could be strongly influenced by pressure effects. In contrast to strategies based on ligands surface attachment, our present work that uses interlayer intercalated amino ferrocene open new routes for the future molecular magnets as well as design of qubit arrays and quantum systems.

REFERENCES

Abenojar, E. C., Wickramasinghe, S., Bas-Concepcion, J., & Samia, A. C. S. (2016a). Structural effects on the magnetic hyperthermia properties of iron oxide nanoparticles. *Progress in Natural Science: Materials International*, *26*(5), 440–448. https://doi.org/10.1016/j.pnsc.2016.09.004

Abenojar, E. C., Wickramasinghe, S., Bas-Concepcion, J., & Samia, A. C. S. (2016b). Structural effects on the magnetic hyperthermia properties of iron oxide nanoparticles. *Progress in Natural Science: Materials International*, *26*(5), 440–448. https://doi.org/10.1016/j.pnsc.2016.09.004

Adamiano, A., Iafisco, M., & Tampieri, A. (2018). Magnetic core-shell nanoparticles. In *Core-Shell Nanostructures for Drug Delivery and Theranostics* (pp. 259–296). Elsevier. https://doi.org/10.1016/B978-0-08-102198-9.00009-0

Aghebati-Maleki, A., Dolati, S., Ahmadi, M., Baghbanzhadeh, A., Asadi, M., Fotouhi, A., Yousefi, M., & Aghebati-Maleki, L. (2020). Nanoparticles and cancer therapy: Perspectives for application of nanoparticles in the treatment of cancers. *Journal of Cellular Physiology*, *235*(3), 1962–1972. https://doi.org/10.1002/jcp.29126

Ahmed, S., Rajak, B. L., Gogoi, M., & Sarma, H. D. (2020). Magnetic nanoparticles mediated cancer hyperthermia. In *Smart Healthcare for Disease Diagnosis and Prevention* (pp. 153–173). Elsevier. https://doi.org/10.1016/B978-0-12-817913-0.00016-X

Akbari, A., Mehrabian, M., Salimi, Z., Dalir, S., & Akbarpour, M. (2019a). The comparison of antibacterial activities of CsPbBr3 and ZnO nanoparticles. *International Nano Letters*,

9(4), 349–353. https://doi.org/10.1007/s40089-019-0280-8

Akbari, A., Mehrabian, M., Salimi, Z., Dalir, S., & Akbarpour, M. (2019b). The comparison of antibacterial activities of CsPbBr3 and ZnO nanoparticles. *International Nano Letters*, *9*(4), 349–353. https://doi.org/10.1007/s40089-019-0280-8

Albarqi, H. A., Wong, L. H., Schumann, C., Sabei, F. Y., Korzun, T., Li, X., Hansen, M. N., Dhagat, P., Moses, A. S., Taratula, O., & Taratula, O. (2019). Biocompatible Nanoclusters with High Heating Efficiency for Systemically Delivered Magnetic Hyperthermia. *ACS Nano*, *13*(6), 6383–6395. https://doi.org/10.1021/acsnano.8b06542

Aleixandre-Tudó, J. L., Castelló-Cogollos, L., Aleixandre, J. L., & Aleixandre-Benavent, R. (2019). Renewable energies: Worldwide trends in research, funding and international collaboration. *Renewable Energy*, *139*, 268–278. https://doi.org/10.1016/j.renene.2019.02.079

Ali, A., Shah, T., Ullah, R., Zhou, P., Guo, M., Ovais, M., Tan, Z., & Rui, Y. (2021). Review on Recent Progress in Magnetic Nanoparticles: Synthesis, Characterization, and Diverse Applications. *Frontiers in Chemistry*, *9*, 629054. https://doi.org/10.3389/fchem.2021.629054

Ali Al-Timimi, B., & Yaakob, Z. (2022). Catalysts for the Simultaneous Production of Syngas and Carbon Nanofilaments Via Catalytic Decomposition of Biogas. In *Natural Gas—New Perspectives and Future Developments [Working Title]*. IntechOpen. https://doi.org/10.5772/intechopen.101320

Alola, A. A., Bekun, F. V., & Sarkodie, S. A. (2019). Dynamic impact of trade policy, economic growth, fertility rate, renewable and non-renewable energy consumption on ecological footprint in Europe. *Science of The Total Environment*, *685*, 702–709.

https://doi.org/10.1016/j.scitotenv.2019.05.139

Alonso-Cristobal, P., Laurenti, M., Lopez-Cabarcos, E., & Rubio-Retama, J. (2015). Efficient synthesis of core@shell Fe $_3$ O $_4$ @Au nanoparticles. *Materials Research Express*, *2*(7), 075002. https://doi.org/10.1088/2053-1591/2/7/075002

Alterary, S. S., & AlKhamees, A. (2021). Synthesis, surface modification, and characterization of Fe $_3$ O $_4$ @SiO $_2$ core@shell nanostructure. *Green Processing and Synthesis*, *10*(1), 384–391. https://doi.org/10.1515/gps-2021-0031

Amrouche, F., Gomari, S. R., Islam, M., & Xu, D. (2021). A novel hybrid technique to enhance oil production from oil-wet carbonate reservoirs by combining a magnetic field with alumina and iron oxide nanoparticles. *Journal of Cleaner Production*, *281*, 124891. https://doi.org/10.1016/j.jclepro.2020.124891

Ang, W. L., Hilal, N., & Leo, C. P. (2015). A review on the applicability of integrated/hybrid membrane processes in water treatment and desalination plants. *Desalination*, *363*, 2–18.

Ang, W. L., Mohammad, A. W., Hilal, N., & Leo, C. P. (2015). A review on the applicability of integrated/hybrid membrane processes in water treatment and desalination plants. *Desalination*, *363*, 2–18. https://doi.org/10.1016/j.desal.2014.03.008

Ansari, S. A., & Cho, M. H. (2016). Highly Visible Light Responsive, Narrow Band gap TiO2 Nanoparticles Modified by Elemental Red Phosphorus for Photocatalysis and Photoelectrochemical Applications. *Scientific Reports*, *6*(1), 25405. https://doi.org/10.1038/srep25405

Araújo, G. X., Rocha, R. D. C. da, & Rodrigues, M. B. (2019). Preparation and application of Zero Valent Iron immobilized in Activated Carbon for removal of hexavalent Chromium from synthetic effluent. *Ambiente e Agua - An Interdisciplinary Journal of Applied*

Science, *14*(5), 1. https://doi.org/10.4136/ambi-agua.2380

Archismita, M., Christian, Z., & Kloker, Gabriele. (2020). Water Purification and Microplastics Removal Using Magnetic Polyoxometalate-Supported Ionic Liquid Phases (magPOM-SILPs). *Angewandte Chemie International Edition*, *59*, 1601–1605.

Arthi G, P. B., & Bd, L. (2015). A Simple Approach to Stepwise Synthesis of Graphene Oxide Nanomaterial. *Journal of Nanomedicine & Nanotechnology*, *06*(01). https://doi.org/10.4172/2157-7439.1000253

Assis, M. B. da S., Werneck, I. H. S. R., de Moraes, G. N., Semaan, F. S., & Pacheco Pereira, R. (2019). Citrate-capped iron oxide nanoparticles: Ultrasound-assisted synthesis, structure and thermal properties. *Materials Research Express*, *6*(4), 045064. https://doi.org/10.1088/2053-1591/aaff2a

Avinash, M. B., Subrahmanyam, K. S., Sundarayya, Y., & Govindaraju, T. (2010). Covalent modification and exfolation of graphene oxide using ferrocene. *Nanoscale*, *2*, 1762–1766.

Awad, A. M., Jalab, R., Benamor, A., Nasser, M. S., Ba-Abbad, M. M., El-Naas, M., & Mohammad, A. W. (2020). Adsorption of organic pollutants by nanomaterial-based adsorbents: An overview. *Journal of Molecular Liquids*, *301*, 112335. https://doi.org/10.1016/j.molliq.2019.112335

Baig, N., Kammakakam, I., & Falath, W. (2021). Nanomaterials: A review of synthesis methods, properties, recent progress, and challenges. *Materials Advances*, *2*(6), 1821–1871. https://doi.org/10.1039/D0MA00807A

Barrera-Díaz, C. E., Balderas-Hernández, P., & Bilyeu, B. (2018a). Electrocoagulation: Fundamentals and Prospectives. In *Electrochemical Water and Wastewater Treatment* (pp. 61–76). Elsevier. https://doi.org/10.1016/B978-0-12-813160-2.00003-1

Barrera-Díaz, C. E., Balderas-Hernández, P., & Bilyeu, B. (2018b). Electrocoagulation: Fundamentals and Prospectives. In *Electrochemical Water and Wastewater Treatment* (pp. 61–76). Elsevier. https://doi.org/10.1016/B978-0-12-813160-2.00003-1

Bastús, N. G., Merkoçi, F., Piella, J., & Puntes, V. (2014). Synthesis of Highly Monodisperse Citrate-Stabilized Silver Nanoparticles of up to 200 nm: Kinetic Control and Catalytic Properties. *Chemistry of Materials*, *26*(9), 2836–2846. https://doi.org/10.1021/cm500316k

Bekun, F. V., Alola, A. A., & Sarkodie, S. A. (2019). Toward a sustainable environment: Nexus between CO2 emissions, resource rent, renewable and nonrenewable energy in 16-EU countries. *Science of The Total Environment*, *657*, 1023–1029. https://doi.org/10.1016/j.scitotenv.2018.12.104

Belli, T. J., Bassin, J. P., Costa, R. E., Akaboci, T. R. V., Battistelli, A. A., Lobo-Recio, M. A., & Lapolli, F. R. (2021). Evaluating the effect of air flow rate on hybrid and conventional membrane bioreactors: Implications on performance, microbial activity and membrane fouling. *Science of The Total Environment*, *755*, 142563. https://doi.org/10.1016/j.scitotenv.2020.142563

Betancur, S., Olmos, C. M., Pérez, M., Lerner, B., Franco, C. A., Riazi, M., Gallego, J., Carrasco-Marín, F., & Cortés, F. B. (2020). A microfluidic study to investigate the effect of magnetic iron core-carbon shell nanoparticles on displacement mechanisms of crude oil for chemical enhanced oil recovery. *Journal of Petroleum Science and Engineering*, *184*, 106589. https://doi.org/10.1016/j.petrol.2019.106589

Bhushan, B. (2018). Historical evolution of magnetic data storage devices and related conferences. *Microsystem Technologies*, *24*(11), 4423–4436.

https://doi.org/10.1007/s00542-018-4133-6

Bilgen, S. (2014). Structure and environmental impact of global energy consumption. *Renewable and Sustainable Energy Reviews*, *38*, 890–902. https://doi.org/10.1016/j.rser.2014.07.004

Blanton, T. N., & Majumdar, D. (2012). X-ray diffraction characterization of polymer intercalated graphite oxide. *Powder Diffraction*, *27*(2), 104–107. https://doi.org/10.1017/S0885715612000292

Blazar, D., Getahun, Y., & El Gendy, A. (2021). Magnetic Nanoparticles Hyperthermia, *Magnetic Nanoparticles in Human Health and Medicine: Current Medical Applications and Alternative Therapy of Cancer* (pp. 527–664-512). John Wiley & Sons.

Blundell, S. J., & Pratt, F. L. (2004a). Organic and molecular magnets. *Journal of Physics: Condensed Matter*, *16*(24), R771–R828. https://doi.org/10.1088/0953-8984/16/24/R03

Blundell, S. J., & Pratt, F. L. (2004b). Organic and molecular magnets. *Journal of Physics: Condensed Matter*, *16*(24), R771–R828. https://doi.org/10.1088/0953-8984/16/24/R03

Boretti, A., & Rosa, L. (2019). Reassessing the projections of the World Water Development Report. *Npj Clean Water*, *2*(1), 15. https://doi.org/10.1038/s41545-019-0039-9

C Reygaert, W. & Department of Biomedical Sciences, Oakland University William Beaumont School of Medicine, Rochester, MI, USA. (2018). An overview of the antimicrobial resistance mechanisms of bacteria. *AIMS Microbiology*, *4*(3), 482–501. https://doi.org/10.3934/microbiol.2018.3.482

Cahyana, A. H., Pratiwi, D., & Ardiansah, B. (2017). Citrate-capped superparamagnetic iron oxide (Fe_3O_4-CA) nanocatalyst for synthesis of pyrimidine derivative compound as antioxidative agent. *IOP Conference Series: Materials Science and Engineering*, *188*, 012008. https://doi.org/10.1088/1757-899X/188/1/012008

Chang, M. C., & Kang, H. Y. (2009). Remediation of pyrene-contaminated soil by synthesized nanoscale zero-valent iron particles. *Journal of Environmental Science and Health, Part A*, *44*(6), 576–582. https://doi.org/10.1080/10934520902784609

Chekalil, N., Tarhini, M., Elaissari, A., & Saïdi-Besbes, S. (2019). Multi-step synthesis of core–shell magnetic nanoparticles bearing acid-chelating functional moieties. *Research on Chemical Intermediates*, *45*(10), 4847–4861. https://doi.org/10.1007/s11164-019-03868-3

Chen, B., Wang, M., Duan, M., Ma, X., Hong, J., Xie, F., Zhang, R., & Li, X. (2019). In search of key: Protecting human health and the ecosystem from water pollution in China. *Journal of Cleaner Production*, *228*, 101–111. https://doi.org/10.1016/j.jclepro.2019.04.228

Cheraghian, G., Rostami, S., & Afrand, M. (2020). Nanotechnology in Enhanced Oil Recovery. *Processes*, *8*(9), 1073. https://doi.org/10.3390/pr8091073

Piramanayagam, S. N., & Chong, T. C. (2012). Introduction. In Developments in data storage: Materials perspective (pp. 1–9). essay, Wiley & Sons..

Clayton, G. E., Thorn, R. M. S., & Reynolds, D. M. (2019). Comparison of Trihalomethane Formation Using Chlorine-Based Disinfectants Within a Model System; Applications Within Point-of-Use Drinking Water Treatment. *Frontiers in Environmental Science*, *7*, 35. https://doi.org/10.3389/fenvs.2019.00035

Comstock, R. L. (2002). Review Modern magnetic materials in data storage. Journal of Materials Science: Materials in Electronics Volume, 13, 509–523. https://doi.org/https://doi.org/10.1023/A:1019642215245 Coronado, E. (2020). Molecular magnetism: From chemical design to spin control in molecules, materials and devices.

Nature Reviews Materials, *5*(2), 87–104. https://doi.org/10.1038/s41578-019-0146-8

Damyanov, C. A. (2018). *Conventional Treatment of Cancer Realities and Problems*. *1*(1), 9.

Dembski, S., Milde, M., Dyrba, M., Schweizer, S., Gellermann, C., & Klockenbring, T. (2011). Effect of pH on the Synthesis and Properties of Luminescent SiO_2 /Calcium Phosphate:Eu^{3+} Core–Shell Nanoparticles. *Langmuir*, *27*(23), 14025–14032. https://doi.org/10.1021/la2021116

Dembski, S., Schneider, C., Christ, B., & Retter, M. (2018). Core-shell nanoparticles and their use for in vitro and in vivo diagnostics. In *Core-Shell Nanostructures for Drug Delivery and Theranostics* (pp. 119–141). Elsevier. https://doi.org/10.1016/B978-0-08-102198-9.00005-3

Deotale, A. J., & Nandedkar, R. V. (2016). Correlation between Particle Size, Strain and Band Gap of Iron Oxide Nanoparticles. *Materials Today: Proceedings*, *3*(6), 2069–2076. https://doi.org/10.1016/j.matpr.2016.04.110

Deshpande, N. G., Ahn, C. H., Koli, R. R., Jamadar, A. S., Kim, D. S., Kim, Y. B., Jung, S. H., & Cho, H. K. (2020). Controlled nanostructured morphology of BiVO4 photoanodes for efficient on-demand catalysis in solar water-splitting and sustainable water-treatment. *Applied Surface Science*, *514*, 146075. https://doi.org/10.1016/j.apsusc.2020.146075

Dey, A., Dasgupta, A., Kumar, V., Tyagi, A., & Verma, A. K. (2015). Evaluation of the of antibacterial efficacy of polyvinylpyrrolidone (PVP) and tri-sodium citrate (TSC) silver nanoparticles. *International Nano Letters*, *5*(4), 223–230. https://doi.org/10.1007/s40089-015-0159-2

Diamantopoulou, A., Glenis, S., Zolnierkiwicz, G., Guskos, N., & Likodimos, V. (2017). Magnetism in pristine and chemically reduced graphene oxide. *Journal of Applied*

Physics, *121*(4), 043906. https://doi.org/10.1063/1.4974364

Diao, M., & Yao, M. (2009). Use of zero-valent iron nanoparticles in inactivating microbes. *Water Research*, *43*(20), 5243–5251. https://doi.org/10.1016/j.watres.2009.08.051

Dodd, A. C. (2009). A comparison of mechanochemical methods for the synthesis of nanoparticulate nickel oxide. *Powder Technology*, *196*(1), 30–35. https://doi.org/10.1016/j.powtec.2009.06.014

El-Gendy, A. A., Bertino, M., Clifford, D., Qian, M., Khanna, S. N., & Carpenter, E. E. (2015). Experimental evidence for the formation of $CoFe_2C$ phase with colossal magnetocrystalline-anisotropy. *Applied Physics Letters*, *106*(21), 213109. https://doi.org/10.1063/1.4921789

El-Gendy, A. A., Ibrahim, E. M. M., Khavrus, V. O., Krupskaya, Y., Hampel, S., Leonhardt, A., Büchner, B., & Klingeler, R. (2009a). The synthesis of carbon coated Fe, Co and Ni nanoparticles and an examination of their magnetic properties. *Carbon*, *47*(12), 2821–2828. https://doi.org/10.1016/j.carbon.2009.06.025

El-Gendy, A. A., Ibrahim, E. M. M., Khavrus, V. O., Krupskaya, Y., Hampel, S., Leonhardt, A., Büchner, B., & Klingeler, R. (2009b). The synthesis of carbon coated Fe, Co and Ni nanoparticles and an examination of their magnetic properties. *Carbon*, *47*(12), 2821–2828. https://doi.org/10.1016/j.carbon.2009.06.025

El-Gendy, A. A., Khavrus, V. O., Hampel, S., Leonhardt, A., Büchner, B., & Klingeler, R. (2010). Morphology, Structural Control, and Magnetic Properties of Carbon-Coated Nanoscaled NiRu Alloys. *The Journal of Physical Chemistry C*, *114*(24), 10745–10749. https://doi.org/10.1021/jp101965x

Elsa, Oliveti, & Jonathan Cullen. (2018). Toward a sustainable materials system An

unprecedented effort is needed to achieve sustainable materials production and use. *Science*, *360*(6396), 1397–1398.

Enoki, T., Enomoto, M., Enomoto, M., Yamaguchi, K., Yoneyama, N., Yamaura, J., Miyazaki, A., & Saito, G. (1996). Molecular Magnets Based on Charge Transfer Complexes. *Molecular Crystals and Liquid Crystals Science and Technology. Section A. Molecular Crystals and Liquid Crystals*, *285*(1), 19–26. https://doi.org/10.1080/10587259608030773

Enriquez-Navas, P. M., & Garcia-Martin, M. L. (2012). Application of Inorganic Nanoparticles for Diagnosis Based on MRI. In *Frontiers of Nanoscience* (Vol. 4, pp. 233–245). Elsevier. https://doi.org/10.1016/B978-0-12-415769-9.00009-1

Fatima, H., Charinpanitkul, T., & Kim, K.-S. (2021). Fundamentals to Apply Magnetic Nanoparticles for Hyperthermia Therapy. *Nanomaterials*, *11*(5), 1203. https://doi.org/10.3390/nano11051203

Flores, C. Y., Miñán, A. G., Grillo, C. A., Salvarezza, R. C., Vericat, C., & Schilardi, P. L. (2013). Citrate-Capped Silver Nanoparticles Showing Good Bactericidal Effect against Both Planktonic and Sessile Bacteria and a Low Cytotoxicity to Osteoblastic Cells. *ACS Applied Materials & Interfaces*, *5*(8), 3149–3159. https://doi.org/10.1021/am400044e

Fonseca-Cervantes, O. R., Pérez-Larios, A., Romero Arellano, V. H., Sulbaran-Rangel, B., & Guzmán González, C. A. (2020). Effects in Band Gap for Photocatalysis in TiO2 Support by Adding Gold and Ruthenium. *Processes*, *8*(9), 1032. https://doi.org/10.3390/pr8091032

Franco, C. A., Giraldo, L. J., Candela, C. H., Bernal, K. M., Villamil, F., Montes, D., Lopera, S. H., Franco, C. A., & Cortés, F. B. (2020). Design and Tuning of Nanofluids Applied to

Chemical Enhanced Oil Recovery Based on the Surfactant–Nanoparticle–Brine Interaction: From Laboratory Experiments to Oil Field Application. *Nanomaterials*, *10*(8), 1579. https://doi.org/10.3390/nano10081579

Frey, N. A., Peng, S., Cheng, K., & Sun, S. (2009). Magnetic nanoparticles: Synthesis, functionalization, and applications in bioimaging and magnetic energy storage. *Chemical Society Reviews*, *38*(9), 2532. https://doi.org/10.1039/b815548h

Frost, M. S., Dempsey, M. J., & Whitehead, D. E. (2017). The response of citrate functionalised gold and silver nanoparticles to the addition of heavy metal ions. *Colloids and Surfaces A: Physicochemical and Engineering Aspects*, *518*, 15–24. https://doi.org/10.1016/j.colsurfa.2016.12.036

Galdames, A., Ruiz-Rubio, L., Orueta, M., Sánchez-Arzalluz, M., & Vilas-Vilela, J. L. (2020). Zero-Valent Iron Nanoparticles for Soil and Groundwater Remediation. *International Journal of Environmental Research and Public Health*, *17*(16), 5817. https://doi.org/10.3390/ijerph17165817

Galpaya, D., Wang, M., George, G., Motta, N., Waclawik, E., & Yan, C. (2014). Preparation of graphene oxide/epoxy nanocomposites with significantly improved mechanical properties. *Journal of Applied Physics*, *116*(5), 053518. https://doi.org/10.1063/1.4892089

Gao, J., Liu, F., Liu, Y., Ma, N., Wang, Z., & Zhang, X. (2010). Environment-Friendly Method To Produce Graphene That Employs Vitamin C and Amino Acid. *Chemistry of Materials*, *22*(7), 2213–2218. https://doi.org/10.1021/cm902635j

Gao, M., Zhou, P., Wang, P., Wang, J., Liang, C., Zhang, J., & Liu, Y. (2013). FeO/C anode materials of high capacity and cycle stability for lithium-ion batteries synthesized by

carbothermal reduction. *Journal of Alloys and Compounds*, *565*, 97–103. https://doi.org/10.1016/j.jallcom.2013.03.012

Gaona, I. M. S., Castillo, Y. M., Losada-Barragán, M., Sanchez, K. V., Rincón, J., Vargas, C. A. P., & Pérez, D. L. (2021). Characterization of Zero-Valent Iron Nanoparticles Functionalized with a Biomarker Peptide. *Materials Research*, *24*(5), e20200599. https://doi.org/10.1590/1980-5373-mr-2020-0599

Garcia-Ordiales, E., Loredo, J., Covelli, S., Esbrí, J. M., Millán, R., & Higueras, P. (2017). Trace metal pollution in freshwater sediments of the world's largest mercury mining district: Sources, spatial distribution, and environmental implications. *Journal of Soils and Sediments*, *17*(7), 1893–1904. https://doi.org/10.1007/s11368-016-1503-5

Gehrke, I., Geiser, A., & Somborn-Schulz, A. (2015). Innovations in nanotechnology for water treatment. *Nanotechnology, Science and Applications*, 1. https://doi.org/10.2147/NSA.S43773

Getsoian, A. "Bean," Zhai, Z., & Bell, A. T. (2014). Band-Gap Energy as a Descriptor of Catalytic Activity for Propene Oxidation over Mixed Metal Oxide Catalysts. *Journal of the American Chemical Society*, *136*(39), 13684–13697. https://doi.org/10.1021/ja5051555

Ghosh Chaudhuri, R., & Paria, S. (2012). Core/Shell Nanoparticles: Classes, Properties, Synthesis Mechanisms, Characterization, and Applications. *Chemical Reviews*, *112*(4), 2373–2433. https://doi.org/10.1021/cr100449n

Gicheva, G., & Yordanov, G. (2013). Removal of citrate-coated silver nanoparticles from aqueous dispersions by using activated carbon. *Colloids and Surfaces A: Physicochemical and Engineering Aspects*, *431*, 51–59.

https://doi.org/10.1016/j.colsurfa.2013.04.039

Gitis, V., & Hankins, N. (2018). Water treatment chemicals: Trends and challenges. *Journal of Water Process Engineering*, *25*, 34–38. https://doi.org/10.1016/j.jwpe.2018.06.003

Glaspell, G., Abdelsayed, V., Saoud, K. M., & El-Shall, M. S. (2006). Vapor-phase synthesis of metallic and intermetallic nanoparticles and nanowires: Magnetic and catalytic properties. *Pure and Applied Chemistry*, *78*(9), 1667–1689. https://doi.org/10.1351/pac200678091667

Guan, L., Shi, Z., Li, M., & Gu, Z. (2005). Ferrocene-filled single-walled carbon nanotubes. *Carbon*, *43*(13), 2780–2785. https://doi.org/10.1016/j.carbon.2005.05.025

Guan, W.-J., Zheng, X.-Y., Chung, K. F., & Zhong, N.-S. (2016). Impact of air pollution on the burden of chronic respiratory diseases in China: Time for urgent action. *The Lancet*, *388*(10054), 1939–1951. https://doi.org/10.1016/S0140-6736(16)31597-5

Guibert, C., Dupuis, V., Peyre, V., & Fresnais, J. (2015). Hyperthermia of Magnetic Nanoparticles: Experimental Study of the Role of Aggregation. *The Journal of Physical Chemistry C*, *119*(50), 28148–28154. https://doi.org/10.1021/acs.jpcc.5b07796

Gul, S., Khan, S. B., Rehman, I. U., Khan, M. A., & Khan, M. I. (2019). A Comprehensive Review of Magnetic Nanomaterials Modern Day Theranostics. *Frontiers in Materials*, *6*, 179. https://doi.org/10.3389/fmats.2019.00179

Guo, F.-S., He, M., Huang, G.-Z., Giblin, S. R., Billington, D., Heinemann, F. W., Tong, M.-L., Mansikkamäki, A., & Layfield, R. A. (2022). Discovery of a Dysprosium Metallocene Single-Molecule Magnet with Two High-Temperature Orbach Processes. *Inorganic Chemistry*, *61*(16), 6017–6025. https://doi.org/10.1021/acs.inorgchem.1c03980

Gupta, J., Hassan, P. A., & Barick, K. C. (2021). Core-shell Fe_3O_4@ZnO nanoparticles for

magnetic hyperthermia and bio-imaging applications. *AIP Advances*, *11*(2), 025207. https://doi.org/10.1063/9.0000135

Hadi, M., Mesdaghinia, A., Yunesian, M., Nasseri, S., Nodehi, R. N., Smeets, P. W. M. H., Schijven, J., Tashauoei, H., & Jalilzadeh, E. (2019). Optimizing the performance of conventional water treatment system using quantitative microbial risk assessment, Tehran, Iran. *Water Research*, *162*, 394–408. https://doi.org/10.1016/j.watres.2019.06.076

Hanh, N. T., Xuyen, N. T., & Thuy, T. T. T. (2018). Synthesis and characterization of Fe_3O_4/GO nanocomposite for drug carrier. *Vietnam Journal of Chemistry*, *56*(5), 642–646. https://doi.org/10.1002/vjch.201800063

Hanjra, M. A., & Qureshi, M. E. (2010). Global water crisis and future food security in an era of climate change. *Food Policy*, *35*(5), 365–377. https://doi.org/10.1016/j.foodpol.2010.05.006

Haseena, M., Malik, M. F., Malik, M. F., Javed, A., Arshad, S., Asif, N., Zulfiqar, S., & Hanif, J. (2017). Water pollution and human health. Environmental Risk Assessment and Remediation, 1(3), 16–19. Hashim, N., Abdullah, S., Hassan, L. S., Ghazali, S. R., & Jalil, R. (2021). A study of neem leaves: Identification of method and solvent in extraction. *Materials Today: Proceedings*, *42*, 217–221. https://doi.org/10.1016/j.matpr.2020.11.726

Haumann, J., Joosten, E. (Bert) A., & Everdingen, M. H. J. van den B. (2017). Pain prevalence in cancer patients: Status quo or opportunities for improvement? *Current Opinion in Supportive & Palliative Care*, *11*(2), 99–104. https://doi.org/10.1097/SPC.0000000000000261

Hauser, A. K., Mathias, R., Anderson, K. W., & Zach Hilt, J. (2015). The effects of synthesis method on the physical and chemical properties of dextran coated iron oxide nanoparticles. *Materials Chemistry and Physics*, *160*, 177–186. https://doi.org/10.1016/j.matchemphys.2015.04.022

Hergt, R., & Dutz, S. (2007). Magnetic particle hyperthermia—Biophysical limitations of a visionary tumour therapy. *Journal of Magnetism and Magnetic Materials*, *311*(1), 187–192. https://doi.org/10.1016/j.jmmm.2006.10.1156

Heyman, L., Houri-Haddad, Y., Heyman, S. N., Ginsburg, I., Gleitman, Y., & Feuerstein, O. (2017). Combined antioxidant effects of Neem extract, bacteria, red blood cells and Lysozyme: Possible relation to periodontal disease. *BMC Complementary and Alternative Medicine*, *17*(1), 399. https://doi.org/10.1186/s12906-017-1900-3

Hong, J., Bekyarova, E., de Heer, W. A., Haddon, R. C., & Khizroev, S. (2013). Chemically Engineered Graphene-Based 2D Organic Molecular Magnet. *ACS Nano*, *7*(11), 10011–10022. https://doi.org/10.1021/nn403939r

Hooper, D. C. (2001). Mechanisms of Action of Antimicrobials: Focus on Fluoroquinolones. *Clinical Infectious Diseases*, *32*(Supplement_1), S9–S15. https://doi.org/10.1086/319370

Hooshmand, Z., Yu, J.-X., Cheng, H.-P., & Pederson, M. R. (2021). Electronic control of strong magnetic anisotropy in Co-based single-molecule magnets. *Physical Review B*, *104*(13), 134411. https://doi.org/10.1103/PhysRevB.104.134411

How, Z. T., Kristiana, I., Busetti, F., Linge, K. L., & Joll, C. A. (2017). Organic chloramines in chlorine-based disinfected water systems: A critical review. *Journal of Environmental Sciences*, *58*, 2–18. https://doi.org/10.1016/j.jes.2017.05.025

Ibrahim, R. L., & Ajide, K. B. (2021). Disaggregated environmental impacts of non-renewable

energy and trade openness in selected G-20 countries: The conditioning role of technological innovation. *Environmental Science and Pollution Research*, *28*(47), 67496–67510. https://doi.org/10.1007/s11356-021-15322-2

Jang, B., Chae, O. B., Park, S.-K., Ha, J., Oh, S. M., Na, H. B., & Piao, Y. (2013). Solventless synthesis of an iron-oxide/graphene nanocomposite and its application as an anode in high-rate Li-ion batteries. *Journal of Materials Chemistry A*, *1*(48), 15442. https://doi.org/10.1039/c3ta13717a

Jayaswal, K., Sahu, V., & Gurjar, B. R. (2018). Water Pollution, Human Health and Remediation. In S. Bhattacharya, A. B. Gupta, A. Gupta, & A. Pandey (Eds.), *Water Remediation* (pp. 11–27). Springer Singapore. https://doi.org/10.1007/978-981-10-7551-3_2

Joudeh, N., & Linke, D. (2022). Nanoparticle classification, physicochemical properties, characterization, and applications: A comprehensive review for biologists. *Journal of Nanobiotechnology*, *20*(1), 262. https://doi.org/10.1186/s12951-022-01477-8

Jung, W. S., Oh, H.-D., Kadam, A. N., & Lee, S.-W. (2018). Calcination Temperature Effect on Citrate-Capped Iron Oxide Nanoparticles as Lithium-Storage Anode Materials. *Physica Status Solidi (a)*, *215*(20), 1701004. https://doi.org/10.1002/pssa.201701004

Kandasamy, G., Sudame, A., Luthra, T., Saini, K., & Maity, D. (2018). Functionalized Hydrophilic Superparamagnetic Iron Oxide Nanoparticles for Magnetic Fluid Hyperthermia Application in Liver Cancer Treatment. *ACS Omega*, *3*(4), 3991–4005. https://doi.org/10.1021/acsomega.8b00207

Kaniyoor, A., & Ramaprabhu, S. (2012). A Raman spectroscopic investigation of graphite oxide derived graphene. *AIP Advances*, *2*(3), 032183. https://doi.org/10.1063/1.4756995

Kantarjian, H., & Rajkumar, S. V. (2015). Why Are Cancer Drugs So Expensive in the United States, and What Are the Solutions? *Mayo Clinic Proceedings*, *90*(4), 500–504. https://doi.org/10.1016/j.mayocp.2015.01.014

Khan, I., Saeed, K., & Khan, I. (2019). Nanoparticles: Properties, applications and toxicities. *Arabian Journal of Chemistry*, *12*(7), 908–931. https://doi.org/10.1016/j.arabjc.2017.05.011

Khan, S., Siddique, R., Sajjad, W., Nabi, G., Hayat, K. M., Duan, P., & Yao, L. (2017). Biodiesel Production From Algae to Overcome the Energy Crisis. *HAYATI Journal of Biosciences*, *24*(4), 163–167. https://doi.org/10.1016/j.hjb.2017.10.003

Khatami, M., Alijani, H., Nejad, M., & Varma, R. (2018). Core@shell Nanoparticles: Greener Synthesis Using Natural Plant Products. *Applied Sciences*, *8*(3), 411. https://doi.org/10.3390/app8030411

kianfar, E. (2021). Magnetic Nanoparticles in Targeted Drug Delivery: A Review. *Journal of Superconductivity and Novel Magnetism*, *34*(7), 1709–1735. https://doi.org/10.1007/s10948-021-05932-9

Kolhatkar, A., Jamison, A., Litvinov, D., Willson, R., & Lee, T. (2013). Tuning the Magnetic Properties of Nanoparticles. *International Journal of Molecular Sciences*, *14*(8), 15977–16009. https://doi.org/10.3390/ijms140815977

Kahn, O. (1985). Dinuclear Complexes with Predictable Magnetic Properties. *Angewandte Chemie International Edition in English*, 24(10), 834–850. https://doi.org/10.1002/anie.198508341

Koo, B., Xiong, H., Slater, M. D., Prakapenka, V. B., Balasubramanian, M., Podsiadlo, P., Johnson, C. S., Rajh, T., & Shevchenko, E. V. (2012). Hollow Iron Oxide Nanoparticles

for Application in Lithium Ion Batteries. *Nano Letters*, *12*(5), 2429–2435. https://doi.org/10.1021/nl3004286

Kotsmar, C., Yoon, K. Y., Yu, H., Ryoo, S. Y., Barth, J., Shao, S., Prodanović, M., Milner, T. E., Bryant, S. L., Huh, C., & Johnston, K. P. (2010a). Stable Citrate-Coated Iron Oxide Superparamagnetic Nanoclusters at High Salinity. *Industrial & Engineering Chemistry Research*, *49*(24), 12435–12443. https://doi.org/10.1021/ie1010965

Kotsmar, C., Yoon, K. Y., Yu, H., Ryoo, S. Y., Barth, J., Shao, S., Prodanović, M., Milner, T. E., Bryant, S. L., Huh, C., & Johnston, K. P. (2010b). Stable Citrate-Coated Iron Oxide Superparamagnetic Nanoclusters at High Salinity. *Industrial & Engineering Chemistry Research*, *49*(24), 12435–12443. https://doi.org/10.1021/ie1010965

Kowalski, K. P., & Søgaard, E. G. (2014). Implementation of zero-valent iron (ZVI) into drinking water supply – Role of the ZVI and biological processes. *Chemosphere*, *117*, 108–114. https://doi.org/10.1016/j.chemosphere.2014.05.088

Kržišnik, N., Mladenovič, A., Škapin, A. S., Škrlep, L., Ščančar, J., & Milačič, R. (2014). Nanoscale zero-valent iron for the removal of Zn2+, Zn(II)–EDTA and Zn(II)–citrate from aqueous solutions. *Science of The Total Environment*, *476–477*, 20–28. https://doi.org/10.1016/j.scitotenv.2013.12.113

Kudin, K. N., Ozbas, B., Schniepp, H. C., Prud'homme, R. K., Aksay, I. A., & Car, R. (2008). Raman Spectra of Graphite Oxide and Functionalized Graphene Sheets. *Nano Letters*, *8*(1), 36–41. https://doi.org/10.1021/nl071822y

Kumar, K. S., Kumar, V. B., & Paik, P. (2013). Recent Advancement in Functional Core-Shell Nanoparticles of Polymers: Synthesis, Physical Properties, and Applications in Medical Biotechnology. *Journal of Nanoparticles*, *2013*, 1–24.

https://doi.org/10.1155/2013/672059

Kwizera, E. A., Chaffin, E., Shen, X., Chen, J., Zou, Q., Wu, Z., Gai, Z., Bhana, S., O'Connor, R., Wang, L., Adhikari, H., Mishra, S. R., Wang, Y., & Huang, X. (2016). Size- and Shape-Controlled Synthesis and Properties of Magnetic–Plasmonic Core–Shell Nanoparticles. *The Journal of Physical Chemistry C*, *120*(19), 10530–10546. https://doi.org/10.1021/acs.jpcc.6b00875

Kwizera, E. A., Chaffin, E., Wang, Y., & Huang, X. (2017). Synthesis and properties of magnetic-optical core–shell nanoparticles. *RSC Advances*, *7*(28), 17137–17153. https://doi.org/10.1039/C7RA01224A

Lapo, Bogani, & Wolfgang, Wernsdorfer. (2008). Molecular spintronics using single-molecule magnets. *Nature Materials*, *7*, 179–186.

Lee, D., Seo, J., Zhu, X., Cole, J. M., & Su, H. (2015). Magnetism in graphene oxide induced by epoxy groups. *Applied Physics Letters*, *106*(17), 172402. https://doi.org/10.1063/1.4919529

Lettieri-Barbato, D., & Aquilano, K. (2018). Pushing the Limits of Cancer Therapy: The Nutrient Game. *Frontiers in Oncology*, *8*, 148. https://doi.org/10.3389/fonc.2018.00148

Li, B., Cao, H., Shao, J., & Qu, M. (2011). Enhanced anode performances of the Fe3O4–Carbon–rGO three dimensional composite in lithium ion batteries. *Chemical Communications*, *47*(37), 10374. https://doi.org/10.1039/c1cc13462k

Li, M. (2007). Peak oil, the rise of China and India, and the global energy crisis. *Journal of Contemporary Asia*, *37*(4), 449–471. https://doi.org/10.1080/00472330701654451

Li, Q., Kartikowati, C. W., Horie, S., Ogi, T., Iwaki, T., & Okuyama, K. (2017). Correlation between particle size/domain structure and magnetic properties of highly crystalline

Fe3O4 nanoparticles. *Scientific Reports*, *7*(1), 9894. https://doi.org/10.1038/s41598-017-09897-5

Li, S., Li, X., & Ho, S.-H. (2022). Microalgae as a solution of third world energy crisis for biofuels production from wastewater toward carbon neutrality: An updated review. *Chemosphere*, *291*, 132863. https://doi.org/10.1016/j.chemosphere.2021.132863

Li, Shengnan, Li, Xue, & Ho, Shih-Hsin. (2022). Microalgae as a solution of third world energy crisis for biofuels production from wastewater toward carbon neutrality: An updated review. *Chemosphere*, *291*(132863), 1–13.

Li, X., Elliott, D. W., & Zhang, W. (2006). Zero-Valent Iron Nanoparticles for Abatement of Environmental Pollutants: Materials and Engineering Aspects. *Critical Reviews in Solid State and Materials Sciences*, *31*(4), 111–122. https://doi.org/10.1080/10408430601057611

Lijima, S. (1991). Helical Microtubules. *Nature*, *354*, 56–58.

Lin, W.-C., Li, Z., & Burns, M. A. (2017). A Drinking Water Sensor for Lead and Other Heavy Metals. *Analytical Chemistry*, *89*(17), 8748–8756. https://doi.org/10.1021/acs.analchem.7b00843

Lippincott, E. R., & Nelson, R. D. (1958). The vibrational spectra and structure of ferrocene and ruthenocene. Spectrochimica Acta, 10(3), 307–329. https://doi.org/10.1016/0371-1951(58)80097-1

Liu, X., Zhang, Y., Wang, Y., Zhu, W., Li, G., Ma, X., Zhang, Y., Chen, S., Tiwari, S., Shi, K., Zhang, S., Fan, H. M., Zhao, Y. X., & Liang, X.-J. (2020). Comprehensive understanding of magnetic hyperthermia for improving antitumor therapeutic efficacy. *Theranostics*, *10*(8), 3793–3815. https://doi.org/10.7150/thno.40805

Liu, Y., Feng, Q., Tang, N., Wan, X., Liu, F., Lv, L., & Du, Y. (2013). Increased magnetization of reduced graphene oxide by nitrogen-doping. *Carbon*, *60*, 549–551. https://doi.org/10.1016/j.carbon.2013.03.060

Liu, Y., Tang, N., Wan, X., Feng, Q., Li, M., Xu, Q., Liu, F., & Du, Y. (2013). Realization of ferromagnetic graphene oxide with high magnetization by doping graphene oxide with nitrogen. *Scientific Reports*, *3*(1), 2566. https://doi.org/10.1038/srep02566

Lopes, M., Candini, A., Urdampilleta, M., Reserbat-Plantey, A., Bellini, V., Klyatskaya, S., Marty, L., Ruben, M., Affronte, M., Wernsdorfer, W., & Bendiab, N. (2010). Surface-Enhanced Raman Signal for Terbium Single-Molecule Magnets Grafted on Graphene. *ACS Nano*, *4*(12), 7531–7537. https://doi.org/10.1021/nn1018363

Lyon, J. L., Fleming, D. A., Stone, M. B., Schiffer, P., & Williams, M. E. (2004). Synthesis of Fe Oxide Core/Au Shell Nanoparticles by Iterative Hydroxylamine Seeding. *Nano Letters*, *4*(4), 719–723. https://doi.org/10.1021/nl035253

Luneau, D. (2001). Molecular magnets. *Current Opinion in Solid State and Materials Science*, *5*(2), 123–129. https://doi.org/10.1016/S1359-0286(00)00043-7

Mahmoudi, K., Bouras, A., Bozec, D., Ivkov, R., & Hadjipanayis, C. (2018). Magnetic hyperthermia therapy for the treatment of glioblastoma: A review of the therapy's history, efficacy and application in humans. *International Journal of Hyperthermia*, *34*(8), 1316–1328. https://doi.org/10.1080/02656736.2018.1430867

Majidi, S., Zeinali Sehrig, F., Farkhani, S. M., Soleymani Goloujeh, M., & Akbarzadeh, A. (2016). Current methods for synthesis of magnetic nanoparticles. *Artificial Cells, Nanomedicine, and Biotechnology*, *44*(2), 722–734. https://doi.org/10.3109/21691401.2014.982802

Manriquez, J. M., Yee, G. T., McLean, R. S., Epstein, A. J., & Miller, J. S. (1991). A Room-Temperature Molecular/Organic-Based Magnet. *Science*, *252*(5011), 1415–1417. https://doi.org/10.1126/science.252.5011.1415

Mariotto, A. B., Robin Yabroff, K., Shao, Y., Feuer, E. J., & Brown, M. L. (2011). Projections of the Cost of Cancer Care in the United States: 2010-2020. *JNCI Journal of the National Cancer Institute*, *103*(2), 117–128. https://doi.org/10.1093/jnci/djq495

Martinez-Boubeta, C., Simeonidis, K., Oró, J., Makridis, A., Serantes, D., & Balcells, L. (2021). Finding the Limits of Magnetic Hyperthermia on Core-Shell Nanoparticles Fabricated by Physical Vapor Methods. *Magnetochemistry*, *7*(4), 49. https://doi.org/10.3390/magnetochemistry7040049

Masanet, E., Shehabi, A., Lei, N., Smith, S., & Koomey, J. (2020). Recalibrating global data center energy-use estimates. *Science*, *367*(6481), 984–986. https://doi.org/10.1126/science.aba3758

Masunga, N., Mamba, B. B., Getahun, Y. W., El-Gendy, A. A., & Kefeni, K. K. (2021). Synthesis of single-phase superparamagnetic copper ferrite nanoparticles using an optimized coprecipitation method. *Materials Science and Engineering: B*, *272*, 115368. https://doi.org/10.1016/j.mseb.2021.115368

Meng, X., & Li, X. (2018). Size Limit and Energy Analysis of Nanoparticles during Wrapping Process by Membrane. *Nanomaterials*, *8*(11), 899. https://doi.org/10.3390/nano8110899

Mensah, M. B., Lewis, D. J., Boadi, N. O., & Awudza, J. A. M. (2021). Heavy metal pollution and the role of inorganic nanomaterials in environmental remediation. *Royal Society Open Science*, *8*(10), 201485. https://doi.org/10.1098/rsos.201485

Mühl, T., Elefant, D., Graff, A., Kozhuharova, R., Leonhardt, A., Mönch, I., Ritschel, M.,

Simon, P., Groudeva-Zotova, S., & Schneider, C. M. (2003). Magnetic properties of aligned Fe-filled carbon nanotubes. *Journal of Applied Physics, 93*(10), 7894–7896. https://doi.org/10.1063/1.1557824

Nam, N. H., & Luong, N. H. (2019). Nanoparticles: Synthesis and applications. In *Materials for Biomedical Engineering* (pp. 211–240). Elsevier. https://doi.org/10.1016/B978-0-08-102814-8.00008-1

Naz, H., Aisha Akram, N., Ashraf, M., Ingo Hefft, D., & Latief Jan, B. (2022). Leaf extract of neem (Azadirachta indica) alleviates adverse effects of drought in quinoa (Chenopodium quinoa Willd.) plants through alterations in biochemical attributes and antioxidants. *Saudi Journal of Biological Sciences, 29*(3), 1367–1374. https://doi.org/10.1016/j.sjbs.2022.01.038

Neoh, C. H., Noor, Z. Z., Mutamim, N. S. A., & Lim, C. K. (2016). Green technology in wastewater treatment technologies: Integration of membrane bioreactor with various wastewater treatment systems. *Chemical Engineering Journal, 283*, 582–594. https://doi.org/10.1016/j.cej.2015.07.060

Nimi N., Saraswathy, A., Nazeer, S. S., Francis, N., Shenoy, S. J., & Jayasree, R. S. (2018). Biosafety of citrate coated zerovalent iron nanoparticles for Magnetic Resonance Angiography. *Data in Brief, 20*, 1829–1835. https://doi.org/10.1016/j.dib.2018.08.157

Njuguna, D. W., Mahrouseh, N., Onisoyonivosekume, D., & Varga, O. (2020). National Policies to Prevent and Manage Cervical Cancer in East African Countries: A Policy Mapping Analysis. *Cancers, 12*(6), 1520. https://doi.org/10.3390/cancers12061520

Nomoev, A. V., Bardakhanov, S. P., Schreiber, M., Bazarova, D. G., Romanov, N. A., Baldanov, B. B., Radnaev, B. R., & Syzrantsev, V. V. (2015). Structure and mechanism of the

formation of core–shell nanoparticles obtained through a one-step gas-phase synthesis by electron beam evaporation. *Beilstein Journal of Nanotechnology*, *6*, 874–880. https://doi.org/10.3762/bjnano.6.89

Obaidat, I., Issa, B., & Haik, Y. (2015). Magnetic Properties of Magnetic Nanoparticles for Efficient Hyperthermia. *Nanomaterials*, *5*(1), 63–89. https://doi.org/10.3390/nano5010063

Ojea-Jiménez, I., López, X., Arbiol, J., & Puntes, V. (2012). Citrate-Coated Gold Nanoparticles As Smart Scavengers for Mercury(II) Removal from Polluted Waters. *ACS Nano*, *6*(3), 2253–2260. https://doi.org/10.1021/nn204313a

Olah, G. A., Yamato, T., Hashimoto, T., Shih, J. G., Trivedi, N., Singh, B. P., Piteau, M., & Olah, J. A. (1987). Aromatic substitution. 53. Electrophilic nitration, halogenation, acylation, and alkylation of (.alpha.,.alpha.,.alpha.-trifluoromethoxy)benzene. *Journal of the American Chemical Society*, *109*(12), 3708–3713. https://doi.org/10.1021/ja00246a030

Olivetti, E. A., & Cullen, J. M. (2018). Toward a sustainable materials system. *Science*, *360*(6396), 1396–1398. https://doi.org/10.1126/science.aat6821

Olson, C. S., Gangopadhyay, S., Hoang, K., Alema, F., Kilina, S., & Pokhodnya, K. (2015). Magnetic Exchange in Mn^{II} [TCNE] (TCNE = Tetracyanoethylene) Molecule-Based Magnets with Two- and Three-Dimensional Magnetic Networks. *The Journal of Physical Chemistry C*, *119*(44), 25036–25046. https://doi.org/10.1021/acs.jpcc.5b06313

Pai, C.-W., Leong, D., Chen, C.-Y., & Wang, G.-S. (2020). Occurrences of pharmaceuticals and personal care products in the drinking water of Taiwan and their removal in conventional water treatment processes. *Chemosphere*, *256*, 127002.

https://doi.org/10.1016/j.chemosphere.2020.127002

Pandey, P. K., Kass, P. H., Soupir, M. L., Biswas, S., & Singh, V. P. (2014). Contamination of water resources by pathogenic bacteria. *AMB Express*, *4*(1), 51. https://doi.org/10.1186/s13568-014-0051-x

Pasinszki, T., & Krebsz, M. (2020). Synthesis and Application of Zero-Valent Iron Nanoparticles in Water Treatment, Environmental Remediation, Catalysis, and Their Biological Effects. *Nanomaterials*, *10*(5), 917. https://doi.org/10.3390/nano10050917

Patil-Sen, Y., Torino, E., De Sarno, F., Ponsiglione, A. M., Chhabria, V., Ahmed, W., & Mercer, T. (2020a). Core-Shell Nanoparticles for Potential Use in Hyperthermia-Enabled Drug Release and as an Enhanced Contrast Agent. *Nanotechnology*, *31*(37), 375102.

Patil-Sen, Y., Torino, E., De Sarno, F., Ponsiglione, A. M., Chhabria, V., Ahmed, W., & Mercer, T. (2020b). Biocompatible superparamagnetic core-shell nanoparticles for potential use in hyperthermia-enabled drug release and as an enhanced contrast agent. *Nanotechnology*, *31*(37), 375102. https://doi.org/10.1088/1361-6528/ab91f6

Pederson, M. R., & Jackson, K. A. (1990). Variational mesh for quantum-mechanical simulations. *Physical Review B*, *41*(11), 7453–7461. https://doi.org/10.1103/PhysRevB.41.7453

Pederson, M. R., & Khanna, S. N. (1999). Magnetic anisotropy barrier for spin tunneling in Mn 12 O 12 molecules. *Physical Review B*, *60*(13), 9566–9572. https://doi.org/10.1103/PhysRevB.60.9566

Pederson, M. R., Porezag, D. V., Kortus, J., & Patton, D. C. (2000). Strategies for Massively Parallel Local-Orbital-Based Electronic Structure Methods. *Physica Status Solidi (b)*, *217*(1), 197–218. https://doi.org/10.1002/(SICI)1521-3951(200001)217:1<197::AID-

PSSB197>3.0.CO;2-B

Peiravi, M., Eslami, H., Ansari, M., & Zare-Zardini, H. (2022). Magnetic hyperthermia: Potentials and limitations. *Journal of the Indian Chemical Society*, *99*(1), 100269. https://doi.org/10.1016/j.jics.2021.100269

Perdew, J. P., Chevary, J. A., Vosko, S. H., Jackson, K. A., Pederson, M. R., Singh, D. J., & Fiolhais, C. (1992). Atoms, molecules, solids, and surfaces: Applications of the generalized gradient approximation for exchange and correlation. *Physical Review B*, *46*(11), 6671–6687. https://doi.org/10.1103/PhysRevB.46.6671

Petnikota, S., Marka, S. K., Banerjee, A., Reddy, M. V., Srikanth, V. V. S. S., & Chowdari, B. V. R. (2015). Graphenothermal reduction synthesis of 'exfoliated graphene oxide/iron (II) oxide' composite for anode application in lithium ion batteries. *Journal of Power Sources*, *293*, 253–263. https://doi.org/10.1016/j.jpowsour.2015.05.075

Piazza, R. D., Viali, W. R., dos Santos, C. C., Nunes, E. S., Marques, R. F. C., Morais, P. C., da Silva, S. W., Coaquira, J. A. H., & Jafelicci, M. (2020). PEGlatyon-SPION surface functionalization with folic acid for magnetic hyperthermia applications. *Materials Research Express*, *7*(1), 015078. https://doi.org/10.1088/2053-1591/ab6700

Pimentel, B., Caraballo-Vivas, R. J., Checca, N. R., Zverev, V. I., Salakhova, R. T., Makarova, L. A., Pyatakov, A. P., Perov, N. S., Tishin, A. M., Shtil, A. A., Rossi, A. L., & Reis, M. S. (2018). Threshold heating temperature for magnetic hyperthermia: Controlling the heat exchange with the blocking temperature of magnetic nanoparticles. *Journal of Solid State Chemistry*, *260*, 34–38. https://doi.org/10.1016/j.jssc.2018.01.001

Piñeros, M., Laversanne, M., Barrios, E., Cancela, M. de C., de Vries, E., Pardo, C., & Bray, F. (2022). An updated profile of the cancer burden, patterns and trends in Latin America and

the Caribbean. *The Lancet Regional Health - Americas*, *13*, 100294. https://doi.org/10.1016/j.lana.2022.100294

Pinto, M., Ramalho, P. S. F., Moreira, N. F. F., Gonçalves, A. G., Nunes, O. C., Pereira, M. F. R., & Soares, O. S. G. P. (2020). Application of magnetic nanoparticles for water purification. *Environmental Advances*, *2*, 100010. https://doi.org/10.1016/j.envadv.2020.100010

Podolska, M. J., Barras, A., Alexiou, C., Frey, B., Gaipl, U., Boukherroub, R., Szunerits, S., Janko, C., & Muñoz, L. E. (2020). Graphene Oxide Nanosheets for Localized Hyperthermia—Physicochemical Characterization, Biocompatibility, and Induction of Tumor Cell Death. *Cells*, *9*(3), 776. https://doi.org/10.3390/cells9030776

Porezag, D., & Pederson, M. R. (1996). Infrared intensities and Raman-scattering activities within density-functional theory. *Physical Review B*, *54*(11), 7830–7836. https://doi.org/10.1103/PhysRevB.54.7830

Porezag, D., & Pederson, M. R. (1999). Optimization of Gaussian basis sets for density-functional calculations. *Physical Review A*, *60*(4), 2840–2847. https://doi.org/10.1103/PhysRevA.60.2840

Pourreza, N., Parham, H., & Pourbati, M. A. (2016). Magnetic iron oxide nanoparticles modified by methyl trioctyl ammonium chloride as an adsorbent for the removal of erythrosine from aqueous solutions. *Desalination and Water Treatment*, *57*(37), 17454–17462. https://doi.org/10.1080/19443994.2015.1086892

Primc, D., Belec, B., & Makovec, D. (2016). Synthesis of composite nanoparticles using co-precipitation of a magnetic iron-oxide shell onto core nanoparticles. *Journal of Nanoparticle Research*, *18*(3), 64. https://doi.org/10.1007/s11051-016-3374-5

Qa, M., & Ms, K. (2016). Effect on Human Health due to Drinking Water Contaminated with Heavy Metals. *Journal of Pollution Effects & Control*, *05*(01). https://doi.org/10.4172/2375-4397.1000179

Qi, W., Shapter, J. G., Wu, Q., Yin, T., Gao, G., & Cui, D. (2017). Nanostructured anode materials for lithium-ion batteries: Principle, recent progress and future perspectives. *Journal of Materials Chemistry A*, *5*(37), 19521–19540. https://doi.org/10.1039/C7TA05283A

Qian, F., Dixon, D. R., Newcombe, G., Ho, L., Dreyfus, J., & Scales, P. J. (2014). The effect of pH on the release of metabolites by cyanobacteria in conventional water treatment processes. *Harmful Algae*, *39*, 253–258. https://doi.org/10.1016/j.hal.2014.08.006

Qureashi, A., Pandith, A. H., Bashir, A., Manzoor, T., Malik, L. A., & Sheikh, F. A. (2021). Citrate coated magnetite: A complete Magneto Dielectric, Electrochemical and DFT study for detection and removal of heavy metal ions. *Surfaces and Interfaces*, *23*, 101004.

Rajan, A., Sharma, M., & Sahu, N. K. (2020). Assessing magnetic and inductive thermal properties of various surfactants functionalised Fe3O4 nanoparticles for hyperthermia. *Scientific Reports*, *10*(1), 15045. https://doi.org/10.1038/s41598-020-71703-6

Rane, A. V., Kanny, K., Abitha, V. K., & Thomas, S. (2018). Methods for Synthesis of Nanoparticles and Fabrication of Nanocomposites. In *Synthesis of Inorganic Nanomaterials* (pp. 121–139). Elsevier. https://doi.org/10.1016/B978-0-08-101975-7.00005-1

Rausch, M. D. (1963). Metallocene Chemistry—a decade of progress. Canadian Journal of Chemistry, 41(5), 1289–1314. https://doi.org/10.1139/v63-182

Rehwold, R. (1982). Water chemicals codex. *Environmental Science and Technology*, *16*(11), A616–A618.

Rytov, R. A., Bautin, V. A., & Usov, N. A. (2022). Towards optimal thermal distribution in magnetic hyperthermia. *Scientific Reports*, *12*(1), 3023. https://doi.org/10.1038/s41598-022-07062-1

Sahni, G., Panwar, A., & Kaur, B. (2015). Controlled green synthesis of silver nanoparticles by Allium cepa and Musa acuminata with strong antimicrobial activity. *International Nano Letters*, *5*(2), 93–100. https://doi.org/10.1007/s40089-015-0142-y

Sakurai, M., Koley, P., & Aono, M. (2019). Tunable Magnetism of Organometallic Nanoclusters by Graphene Oxide On-Surface Chemistry. *Scientific Reports*, *9*(1), 14509. https://doi.org/10.1038/s41598-019-50433-4

Saleh Al-Hashemi, Z. S., & Hossain, M. A. (2016). Biological activities of different neem leaf crude extracts used locally in Ayurvedic medicine. *Pacific Science Review A: Natural Science and Engineering*, *18*(2), 128–131. https://doi.org/10.1016/j.psra.2016.09.013

Salehizadeh, H., Hekmatian, E., Sadeghi, M., & Kennedy, K. (2012). Synthesis and characterization of core-shell Fe3O4-gold-chitosan nanostructure. *Journal of Nanobiotechnology*, *10*(1), 3. https://doi.org/10.1186/1477-3155-10-3

Sanad, M. F., Meneses-Brassea, B. P., Blazer, D. S., Pourmiri, S., Hadjipanayis, G. C., & El-Gendy, A. A. (2021). Superparamagnetic Fe/Au Nanoparticles and Their Feasibility for Magnetic Hyperthermia. *Applied Sciences*, *11*(14), 6637. https://doi.org/10.3390/app11146637

Saraswathy, A., Nazeer, S. S., Jeevan, M., Nimi, N., Arumugam, S., Harikrishnan, V. S., Varma, P. R. H., & Jayasree, R. S. (2014). Citrate coated iron oxide nanoparticles with enhanced

relaxivity for in vivo magnetic resonance imaging of liver fibrosis. *Colloids and Surfaces B: Biointerfaces*, *117*, 216–224. https://doi.org/10.1016/j.colsurfb.2014.02.034

Sarkar, S. K., Raul, K. K., Pradhan, S. S., Basu, S., & Nayak, A. (2014). Magnetic properties of graphite oxide and reduced graphene oxide. *Physica E: Low-Dimensional Systems and Nanostructures*, *64*, 78–82. https://doi.org/10.1016/j.physe.2014.07.014

Sekoai, P. T., Ouma, C. N. M., du Preez, S. P., Modisha, P., Engelbrecht, N., Bessarabov, D. G., & Ghimire, A. (2019). Application of nanoparticles in biofuels: An overview. *Fuel*, *237*, 380–397. https://doi.org/10.1016/j.fuel.2018.10.030

Shakoor, M. B., Nawaz, R., Hussain, F., Raza, M., Ali, S., Rizwan, M., Oh, S.-E., & Ahmad, S. (2017). Human health implications, risk assessment and remediation of As-contaminated water: A critical review. *Science of The Total Environment*, *601–602*, 756–769. https://doi.org/10.1016/j.scitotenv.2017.05.223

Sharma, M., Kalita, P., Senapati, K. K., & Garg, A. (2018). Study on Magnetic Materials for Removal of Water Pollutants. In S. Soloneski & M. L. Larramendy (Eds.), *Emerging Pollutants—Some Strategies for the Quality Preservation of Our Environment*. InTech. https://doi.org/10.5772/intechopen.75700

Singh, M., Goyal, M., & Devlal, K. (2018). Size and shape effects on the band gap of semiconductor compound nanomaterials. *Journal of Taibah University for Science*, *12*(4), 470–475. https://doi.org/10.1080/16583655.2018.1473946

Sircar, A., Rayavarapu, K., Bist, N., Yadav, K., & Singh, S. (2022). Applications of nanoparticles in enhanced oil recovery. *Petroleum Research*, *7*(1), 77–90. https://doi.org/10.1016/j.ptlrs.2021.08.004

Soloveva, A. Yu., Eremenko, N. K., Obraztsova, I. I., Eremenko, A. N., & Gubin, S. P. (2018).

Synthesis and Optical Properties of Fe@Au, Ni@Au Bimetallic Core–Shell Nanoparticles. *Russian Journal of Inorganic Chemistry*, *63*(4), 444–448. https://doi.org/10.1134/S0036023618040204

Su, Q., Pang, S., Alijani, V., Li, C., Feng, X., & Müllen, K. (2009). Composites of graphene with large aromatic molecules. *Advanced Materials*, *21*(31), 3191–3195. https://doi.org/10.1002/adma.200803808

Sugumaran, P. J., Liu, X.-L., Herng, T. S., Peng, E., & Ding, J. (2019). GO-Functionalized Large Magnetic Iron Oxide Nanoparticles with Enhanced Colloidal Stability and Hyperthermia Performance. *ACS Applied Materials & Interfaces*, *11*(25), 22703–22713. https://doi.org/10.1021/acsami.9b04261

Sun, S., & Zeng, H. (2002). Size-Controlled Synthesis of Magnetite Nanoparticles. *Journal of the American Chemical Society*, *124*(28), 8204–8205. https://doi.org/10.1021/ja026501x

Sun, X., Zhang, Y., Chen, G., & Gai, Z. (2017). Application of Nanoparticles in Enhanced Oil Recovery: A Critical Review of Recent Progress. *Energies*, *10*(3), 345. https://doi.org/10.3390/en10030345

Sung, H., Ferlay, J., Siegel, R. L., Laversanne, M., Soerjomataram, I., Jemal, A., & Bray, F. (2021). Global Cancer Statistics 2020: GLOBOCAN Estimates of Incidence and Mortality Worldwide for 36 Cancers in 185 Countries. *CA: A Cancer Journal for Clinicians*, *71*(3), 209–249. https://doi.org/10.3322/caac.21660

Suriyanto, Ng, E. Y. K., & Kumar, S. D. (2017). Physical mechanism and modeling of heat generation and transfer in magnetic fluid hyperthermia through Néelian and Brownian relaxation: A review. *BioMedical Engineering OnLine*, *16*(1), 36.

https://doi.org/10.1186/s12938-017-0327-x

Talbot, D., Queiros Campos, J., Checa-Fernandez, B. L., Marins, J. A., Lomenech, C., Hurel, C., Godeau, G. D., Raboisson-Michel, M., Verger-Dubois, G., Obeid, L., Kuzhir, P., & Bee, A. (2021). Adsorption of Organic Dyes on Magnetic Iron Oxide Nanoparticles. Part I: Mechanisms and Adsorption-Induced Nanoparticle Agglomeration. *ACS Omega*, *6*(29), 19086–19098. https://doi.org/10.1021/acsomega.1c02401

Thiesen, B., & Jordan, A. (2008). Clinical applications of magnetic nanoparticles for hyperthermia. *International Journal of Hyperthermia*, *24*(6), 467–474. https://doi.org/10.1080/02656730802104757

Tipantuna, C., & Hesselbach, X. (2020). NFV/SDN Enabled Architecture for Efficient Adaptive Management of Renewable and Non-Renewable Energy. *IEEE Open Journal of the Communications Society*, *1*, 357–380. https://doi.org/10.1109/OJCOMS.2020.2984982

Tiwari, A., Tripathi, A. K., & Khare, P. (2021). A comprehensive study of synthesis and applications of core/shell nanoparticles. *International Journal of Engineering, Science and Technology*, *13*(1), 153–157. https://doi.org/10.4314/ijest.v13i1.23S

Tom, A. P. (2021). Nanotechnology for sustainable water treatment – A review. *Materials Today: Proceedings*, S2214785321042565. https://doi.org/10.1016/j.matpr.2021.05.629

Vasilakaki, M., Binns, C., & Trohidou, K. N. (2015). Susceptibility losses in heating of magnetic core/shell nanoparticles for hyperthermia: A Monte Carlo study of shape and size effects. *Nanoscale*, *7*(17), 7753–7762. https://doi.org/10.1039/C4NR07576E

Viesser, R. V., Ducati, L. C., Tormena, C. F., & Autschbach, J. (2017). The unexpected roles of sigma and pi orbitals in electron donor and acceptor group effects on the C-13 NMR chemical shifts in substituted benzenest. *Chemical Science*, *8*(9), 6570–6576.

Vineis, P., & Wild, C. P. (2014). Global cancer patterns: Causes and prevention. *The Lancet*, *383*(9916), 549–557. https://doi.org/10.1016/S0140-6736(13)62224-2

Wang, F., Zhang, M., Sha, W., Wang, Y., Hao, H., Dou, Y., & Li, Y. (2020). Sorption Behavior and Mechanisms of Organic Contaminants to Nano and Microplastics. *Molecules*, *25*(8), 1827. https://doi.org/10.3390/molecules25081827

Wang, L., Hu, C., & Shao, L. (2017). The antimicrobial activity of nanoparticles: Present situation and prospects for the future. *International Journal of Nanomedicine*, *Volume 12*, 1227–1249. https://doi.org/10.2147/IJN.S121956

Wang, M., & Li, C. M. (2010). Magnetism in graphene oxide. *New Journal of Physics*, *12*(12), 129801. https://doi.org/10.1088/1367-2630/12/12/129801

Wang, W., Yan, L.-Q., Cong, J.-Z., Zhao, Y.-L., Wang, F., Shen, S.-P., Zou, T., Zhang, D., Wang, S.-G., Han, X.-F., & Sun, Y. (2013). Magnetoelectric coupling in the paramagnetic state of a metal-organic framework. *Scientific Reports*, *3*(1), 2024. https://doi.org/10.1038/srep02024

Webster, T. J., & Seil, I. (2012). Antimicrobial applications of nanotechnology: Methods and literature. *International Journal of Nanomedicine*, 2767. https://doi.org/10.2147/IJN.S24805

Werber, J. R., Osuji, C. O., & Elimelech, M. (2016). Materials for next-generation desalination and water purification membranes. *Nature Reviews Materials*, *1*(5), 16018. https://doi.org/10.1038/natrevmats.2016.18

Wernsdorfer, W., Aliaga-Alcalde, N., Hendrickson, D. N., & Christou, G. (2002). Exchange-biased quantum tunnelling in a supramolecular dimer of single-molecule magnets. *Nature*, *416*(6879), 406–409. https://doi.org/10.1038/416406a

Williams, H. M. (2017). The application of magnetic nanoparticles in the treatment and monitoring of cancer and infectious diseases. *Bioscience Horizons: The International Journal of Student Research, 10*. https://doi.org/10.1093/biohorizons/hzx009

Włodarczyk, A., Gorgoń, S., Radoń, A., & Bajdak-Rusinek, K. (2022). Magnetite Nanoparticles in Magnetic Hyperthermia and Cancer Therapies: Challenges and Perspectives. *Nanomaterials*, *12*(11), 1807. https://doi.org/10.3390/nano12111807

Wolf-Baca, M., & Piekarska, K. (2020). Biodiversity of organisms inhabiting the water supply network of Wroclaw. Detection of pathogenic organisms constituting a threat for drinking water recipients. *Science of The Total Environment*, *715*, 136732. https://doi.org/10.1016/j.scitotenv.2020.136732

Woodward, R. B., Rosenblum, M., & Whiting, M. C. (1952). A NEW AROMATIC SYSTEM. American Chemical Society , 74(13), 3458–3459. https://doi.org/https://doi.org/10.1021/ja01133a543

Wu, D., Zheng, S., Ding, A., Sun, G., & Yang, M. (2015). Performance of a zero valent iron-based anaerobic system in swine wastewater treatment. *Journal of Hazardous Materials*, *286*, 1–6. https://doi.org/10.1016/j.jhazmat.2014.12.029

Wu, K., Liao, S.-H., Liu, C.-H., Bastakoti, B. P., Chang, Y., Yamauchi, Y., Lin, F.-H., & Suzuki, N. (2015). Functionalized magnetic iron oxide/alginate core-shell nanoparticles for targeting hyperthermia. *International Journal of Nanomedicine*, 3315. https://doi.org/10.2147/IJN.S68719

Wuana, R., & Okieimen, F. (2014). Heavy Metals in Contaminated Soils: A Review of Sources, Chemistry, Risks and Best Available Strategies for Remediation. In E. Asrari (Ed.), *Heavy Metal Contamination of Water and Soil* (pp. 1–50). Apple Academic Press.

https://doi.org/10.1201/b16566-3

Xiong, R., Wang, Y., Zhang, X., & Lu, C. (2014). Facile synthesis of magnetic nanocomposites of cellulose@ultrasmall iron oxide nanoparticles for water treatment. *RSC Adv.*, *4*(43), 22632–22641. https://doi.org/10.1039/C4RA01397B

Xu, J.-S., & Zhu, Y.-J. (2012). Monodisperse Fe_3O_4 and γ-Fe_2O_3 Magnetic Mesoporous Microspheres as Anode Materials for Lithium-Ion Batteries. *ACS Applied Materials & Interfaces*, *4*(9), 4752–4757. https://doi.org/10.1021/am301123f

Xu, W., Yang, T., Liu, S., Du, L., Chen, Q., Li, X., Dong, J., Zhang, Z., Lu, S., Gong, Y., Zhou, L., Liu, Y., & Tan, X. (2022). Insights into the Synthesis, types and application of iron Nanoparticles: The overlooked significance of environmental effects. *Environment International*, *158*, 106980. https://doi.org/10.1016/j.envint.2021.106980

Yamada, Y., Yasuda, H., Murota, K., Nakamura, M., Sodesawa, T., & Sato, S. (2013). Analysis of heat-treated graphite oxide by X-ray photoelectron spectroscopy. *Journal of Materials Science*, *48*(23), 8171–8198. https://doi.org/10.1007/s10853-013-7630-0

Yang, M., Li, J., Gu, P., & Fan, X. (2021). The application of nanoparticles in cancer immunotherapy: Targeting tumor microenvironment. *Bioactive Materials*, *6*(7), 1973–1987. https://doi.org/10.1016/j.bioactmat.2020.12.010

Yaqoob, A. A., Parveen, T., Umar, K., & Mohamad Ibrahim, M. N. (2020). Role of Nanomaterials in the Treatment of Wastewater: A Review. *Water*, *12*(2), 495. https://doi.org/10.3390/w12020495

Yelenich, O. V., Solopan, S. O., Greneche, J. M., & Belous, A. G. (2015). Synthesis and properties MFe2O4 (M = Fe, Co) nanoparticles and core–shell structures. *Solid State Sciences*, *46*, 19–26. https://doi.org/10.1016/j.solidstatesciences.2015.05.011

Yew, Y. P., Shameli, K., Miyake, M., Kuwano, N., Bt Ahmad Khairudin, N. B., Bt Mohamad, S. E., & Lee, K. X. (2016). Green Synthesis of Magnetite (Fe3O4) Nanoparticles Using Seaweed (Kappaphycus alvarezii) Extract. *Nanoscale Research Letters*, *11*(1), 276. https://doi.org/10.1186/s11671-016-1498-2

Yu, Hsin Her, Lin, Chia-Hua, Chen, Yi-Chun, Chen, Hung-Hsiang, Lin, Yu-Jing, & Lin, Kun-Yi Andrew. (2020). Dopamine-Modified Zero-Valent Iron Nanoparticles for Dual-Modality Photothermal and Photodynamic Breast Cancer Therapy. *ChemMedChem*, *15*, 1645–1651.

Yu, S., Guo, B., Zeng, T., Qu, H., Yang, J., & Bai, J. (2022). Graphene-based lithium-ion battery anode materials manufactured by mechanochemical ball milling process: A review and perspective. *Composites Part B: Engineering*, *246*, 110232. https://doi.org/10.1016/j.compositesb.2022.110232

Yuan, H., & He, Z. (2015). Integrating membrane filtration into bioelectrochemical systems as next generation energy-efficient wastewater treatment technologies for water reclamation: A review. *Bioresource Technology*, *195*, 202–209. https://doi.org/10.1016/j.biortech.2015.05.058

Zaaba, N. I., Foo, K. L., Hashim, U., Tan, S. J., Liu, W.-W., & Voon, C. H. (2017). Synthesis of Graphene Oxide using Modified Hummers Method: Solvent Influence. *Procedia Engineering*, *184*, 469–477. https://doi.org/10.1016/j.proeng.2017.04.118

Zambrzycki, C., Shao, R., Misra, A., Streb, C., Herr, U., & Güttel, R. (2021). Iron Based Core-Shell Structures as Versatile Materials: Magnetic Support and Solid Catalyst. *Catalysts*, *11*(1), 72. https://doi.org/10.3390/catal11010072

Zhang, G., Liao, Y., & Baker, I. (2010). Surface engineering of core/shell iron/iron oxide

nanoparticles from microemulsions for hyperthermia. *Materials Science and Engineering: C*, *30*(1), 92–97. https://doi.org/10.1016/j.msec.2009.09.003

Zhang, H., Nikolov, A., & Wasan, D. (2014). Enhanced Oil Recovery (EOR) Using Nanoparticle Dispersions: Underlying Mechanism and Imbibition Experiments. *Energy & Fuels*, *28*(5), 3002–3009. https://doi.org/10.1021/ef500272r

Zhang, W., Yadav, R., Tian, Y.-C., Tyagi, S. K. S., Elgendy, I. A., & Kaiwartya, O. (2022). Two-Phase Industrial Manufacturing Service Management for Energy Efficiency of Data Centers. *IEEE Transactions on Industrial Informatics*, *18*(11), 7525–7536. https://doi.org/10.1109/TII.2022.3153508

Zhou, Q., Yang, N., Li, Y., Ren, B., Ding, X., Bian, H., & Yao, X. (2020). Total concentrations and sources of heavy metal pollution in global river and lake water bodies from 1972 to 2017. *Global Ecology and Conservation*, *22*, e00925. https://doi.org/10.1016/j.gecco.2020.e00925

Zhu, X., Hale, A., Christou, G., & Hebard, A. F. (2020). Electronegative ligands enhance charge transfer to Mn_{12} single-molecule magnets deposited on graphene. *Journal of Applied Physics*, *127*(6), 064303. https://doi.org/10.1063/1.5128329

Zhuang, L., Zhang, W., Zhao, Y., Shen, H., Lin, H., & Liang, J. (2015). Preparation and Characterization of Fe3O4 Particles with Novel Nanosheets Morphology and Magnetochromatic Property by a Modified Solvothermal Method. *Scientific Reports*, *5*(1), 9320. https://doi.org/10.1038/srep09320

SUPPLEMENTARY DATA AND APPENDIX

Table SA1: concentration ions added during the study of the effect of ions in methylene blue absorption towards nanoparticles.

Ions	**Concentration(mg/L)**	**Concentration(mmol/L)**
NaCl	1295	37
Na2SO4	249	3
NaNO3	50	0.5
NaHCO3	242	4
MgSO4.7H2O	63	3
CaSO4	159	4
KCl	50	0.67

Table SA2: Ratio of reactants, experimental yield, of core shell nanoparticles

No	Concentrations			$FeSO_{11}H_2$: $Na_3C_6H_5O_7$: $NaBH_4$	Yield(mg)
	Analyte	mg/ml	mole/L		
1	Iron sulfate heptahydrate ($FeSO_{11}H_{2)}$	2.5	111.2	1.25:1:5	2.89
2		5.0	55.6	2.5:1:5	6.4
3		10.0	27.8	5:1:5	16.4
4		15.0	18.5	7.5:1:5	27.3
5		20.0	13.9	10:1:5	43.7
6		25.0	11.12	12.5:1:5	49.1
7		30.0	9.27	15:1:5	52.2
8	Sodium citrate dihydrate ($Na_3C_6H_5O_7$)	4.0	73.53	10:1:5	31.1
9		6.0	49.01	10:2:5	8.7
10		8.0	36.76	10:3:5	7
11		10.0	29.41	10:4:5	9.5
12		12.0	24.50	10:5:5	1.4
13	Sodium borohydride ($NaBH_4$)	2.0	18.92	10:1:1	33.4
14		4.0	9.45	10:1:2	8.4
15		6.0	6.30	10:1:3	16.4
16		8.0	4.72	10:1:4	36.3
17		10.0	3.78	10:1:5	33
18		12.0	3.15	10:1:6	37.6
19	Temperature	0^oC		10:1:5	32.8
20		$10\ ^oC$			32.8
21		$30\ ^oC$			37.2

22		40 °C		37.2
23		60 °C		24.2
24		80 °C		32.6

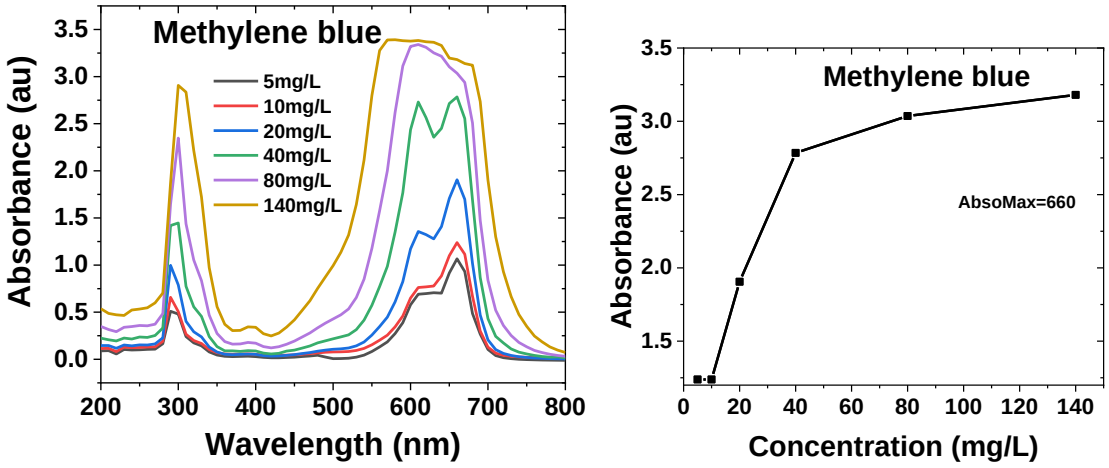

Figure SA1**:** Methylene blue at different concentrations

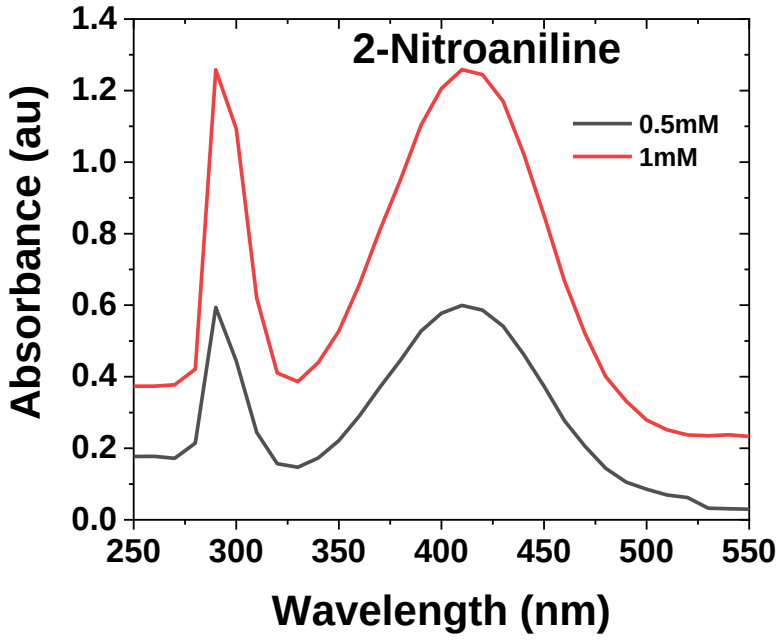

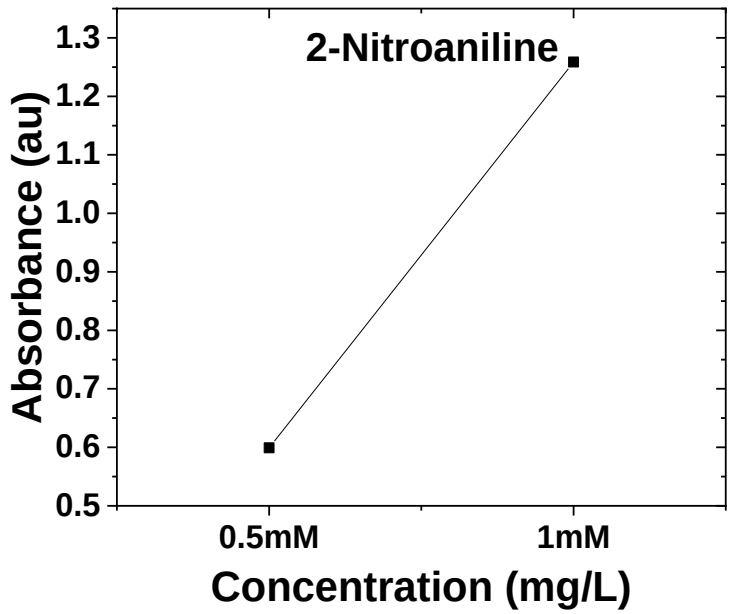

Figure SA2: 2-Nitro aniline at different concentrations

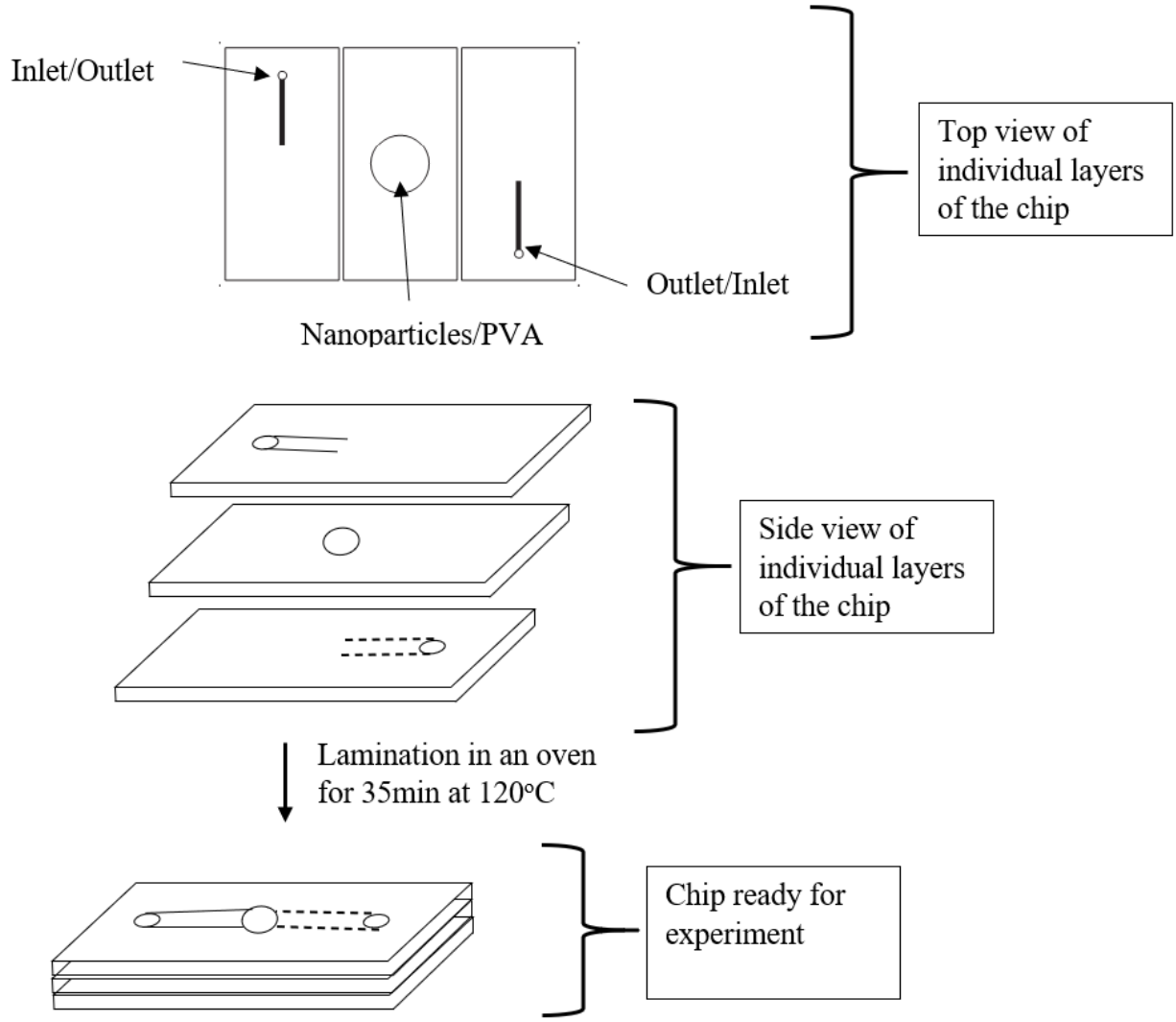

Figure SA3: Continuous single adsorbent Microfluidic chip design

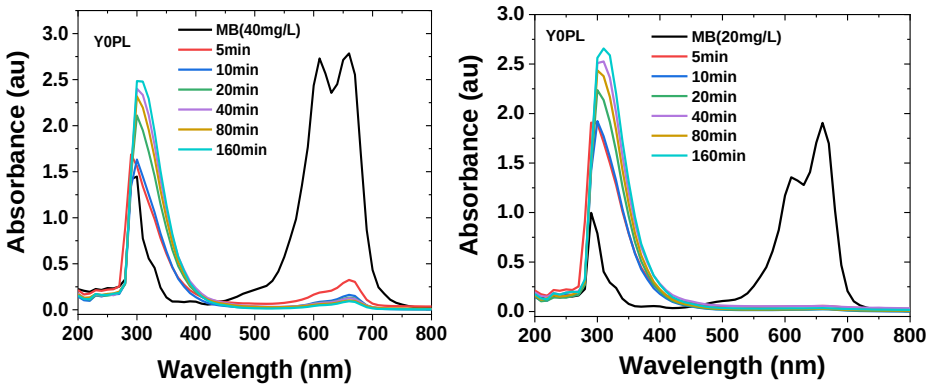

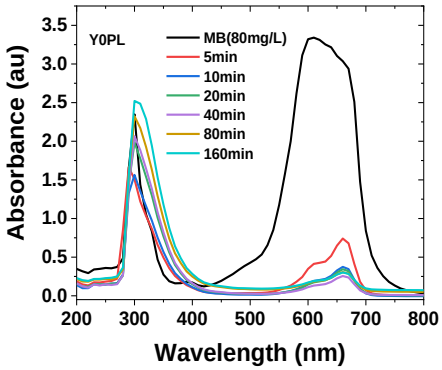

Figure SA4: Absorption performance of Y0PL at 20, 40 and 80mg/L

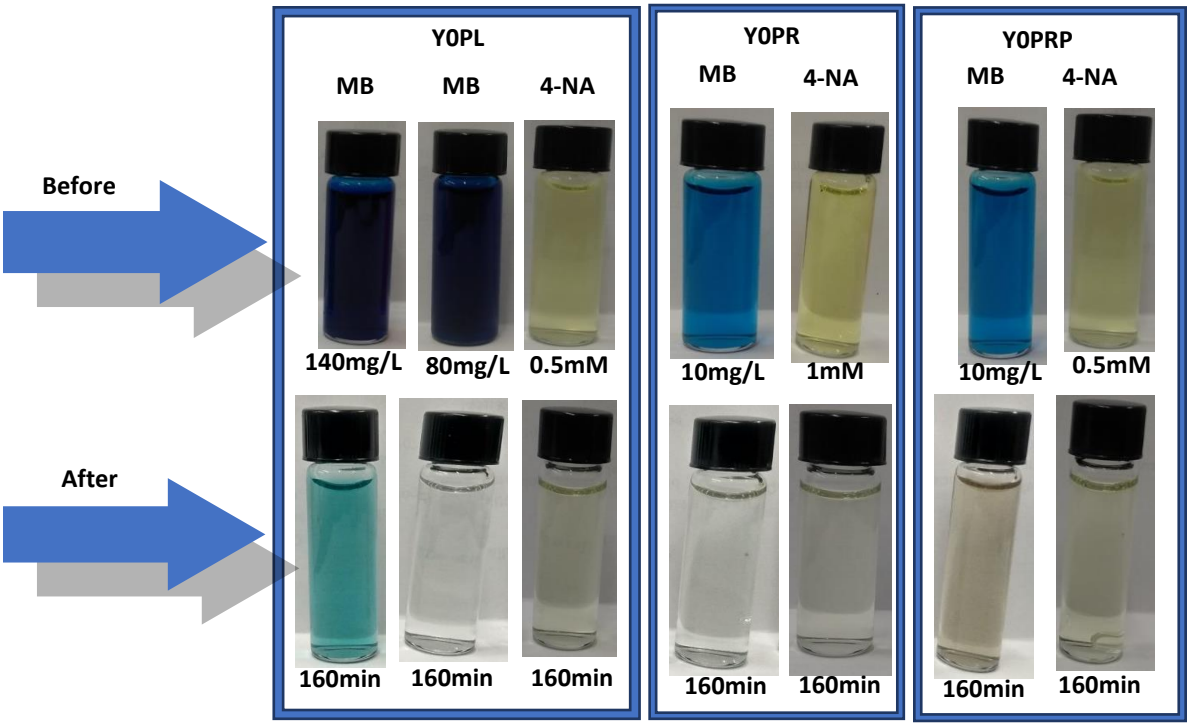

Figure SA5: Photograph images of MB and 4-NA of before and after treatment by the sample nanoparticles at 160minutes.

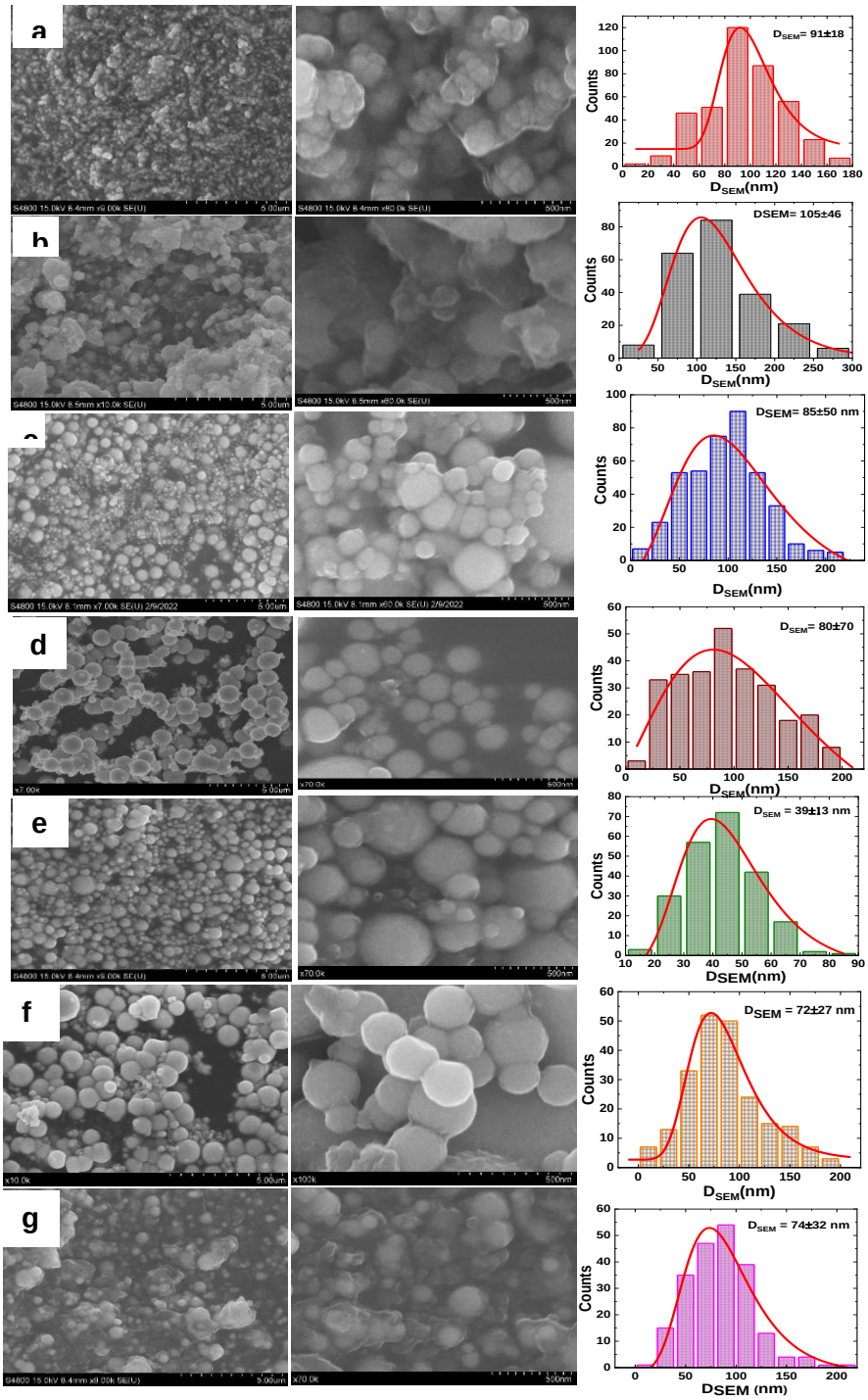

Figure SA6: SEM images of particles synthesized at variable concentration of metal(core): 111.2, 55.6, 27.8, 18.5, 13.9, 11.12, and 9.27 mole/L (a-g).

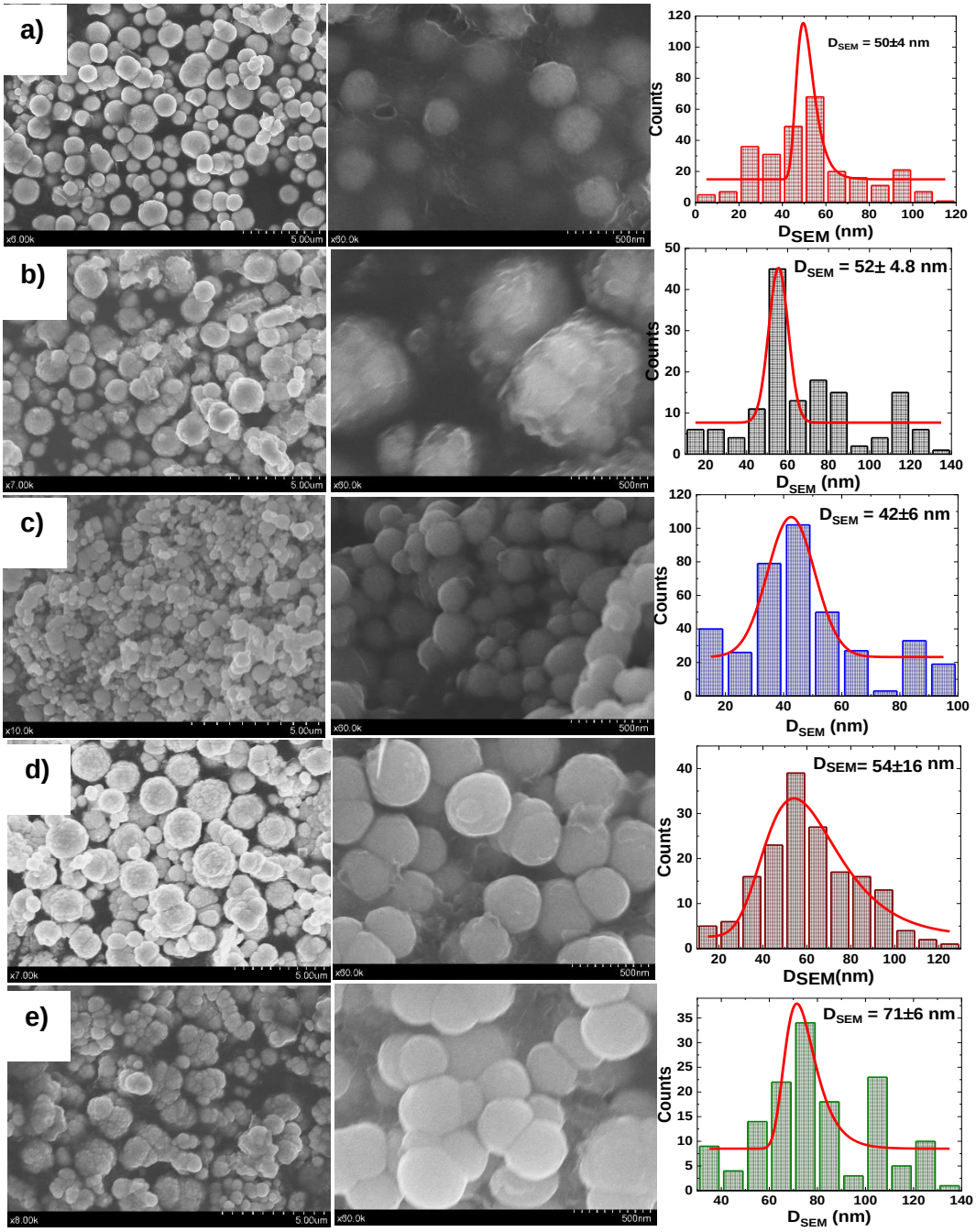

Figure SA7: SEM images of particles synthesized at variable concentration of ligand (Citrate shell): 73.53, 49.01, 36.76, 29.41 and 24.50 mole/L (a-e).

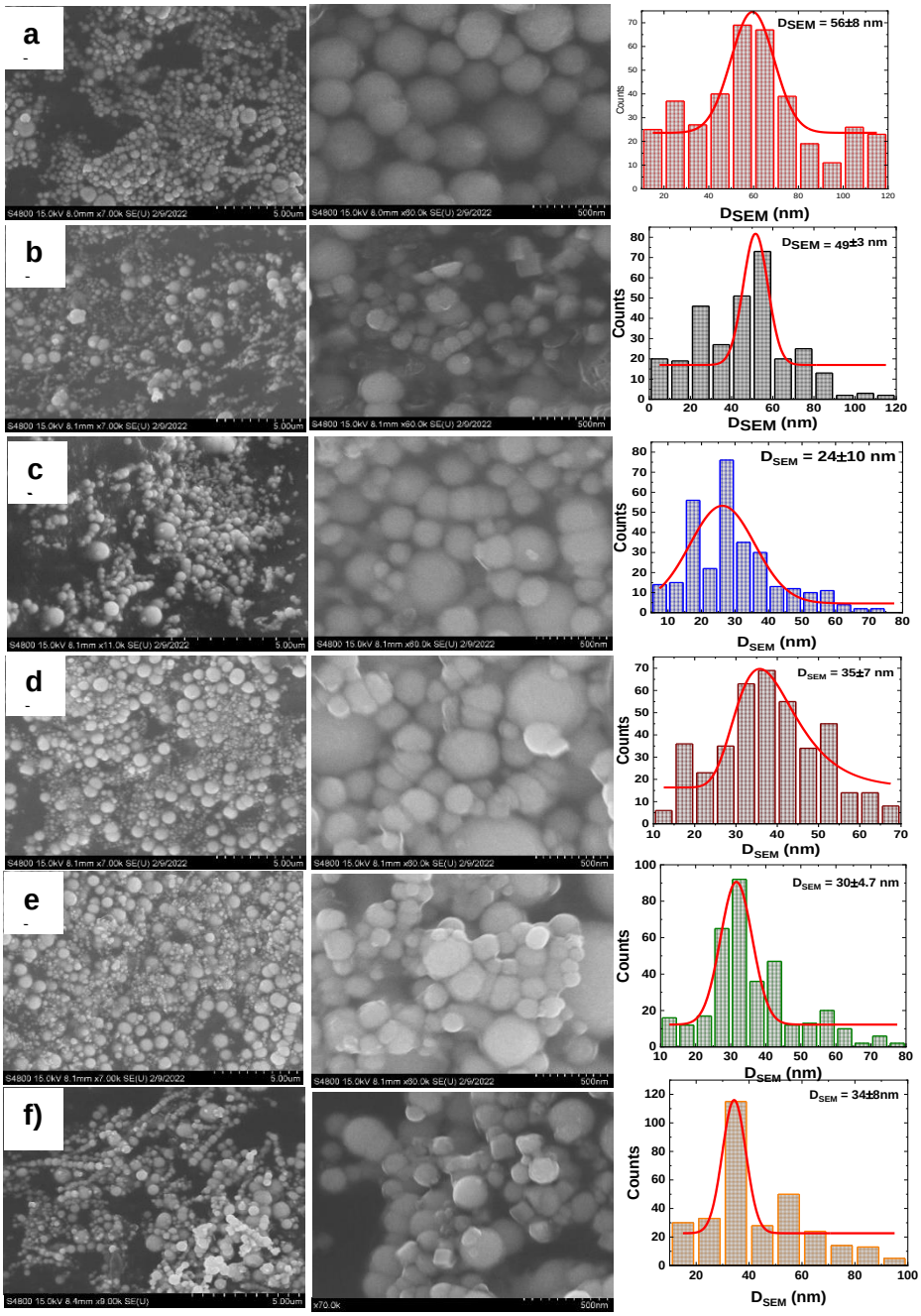

Figure SA8: SEM images of particles synthesized at variable concentration of reducing agent ($NaBH_4$): 18.92, 9.45, 6.30, 4.72, 3.78, 3.15mole/L (a-f)

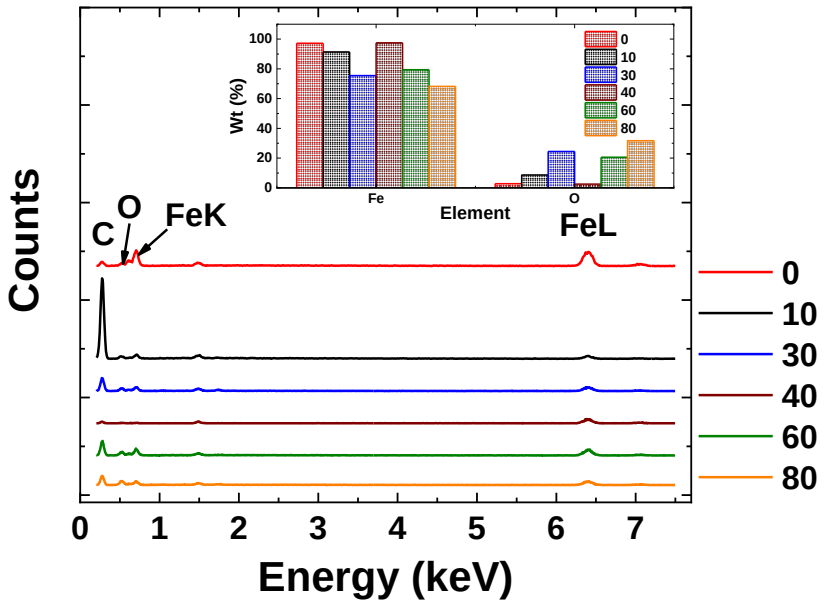

Figure SA9: EDX spectra of particles synthesized at variable reaction temperature: 0 to 80 ^{o}C (Inset bar graph is elemental compositions).

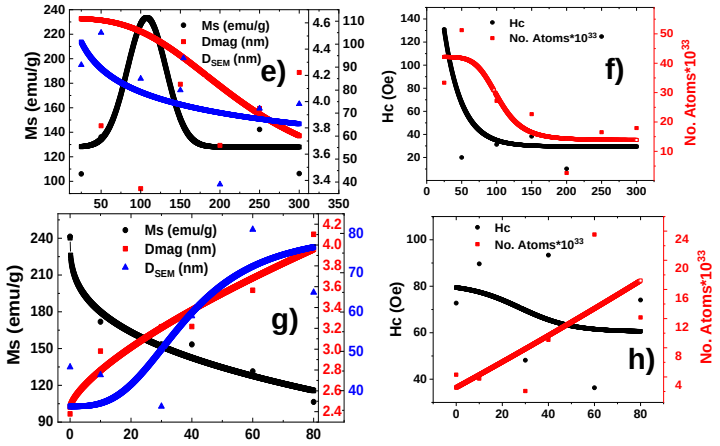

Figure SA10: Relations ship between domain size, magnetic saturation e) and coercivity and number of atoms f) for the first batch experiments (changing metal concentration) e) and f) and fourth batch experiments (changing reaction temperature) g) and h).

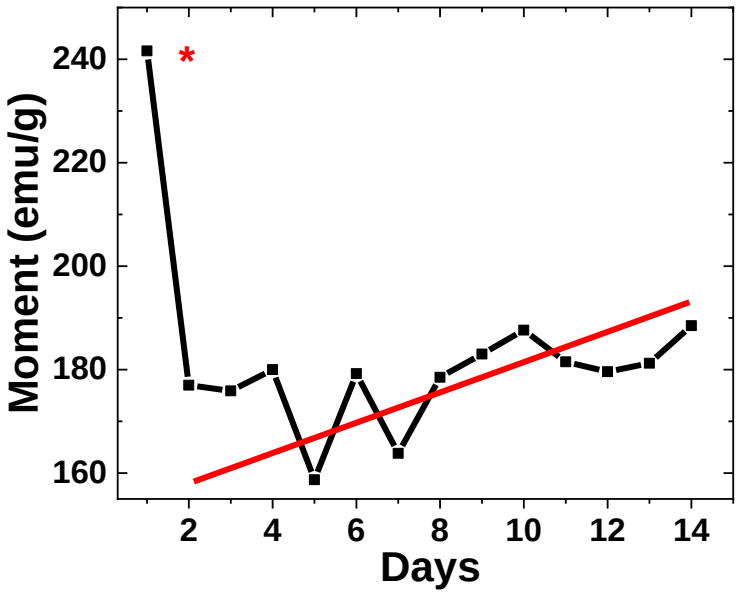

Figure SA11: Change in magnetic saturation over time of nanoparticles with the highest magnetic saturation (10:1:5 at 0^{o}C).

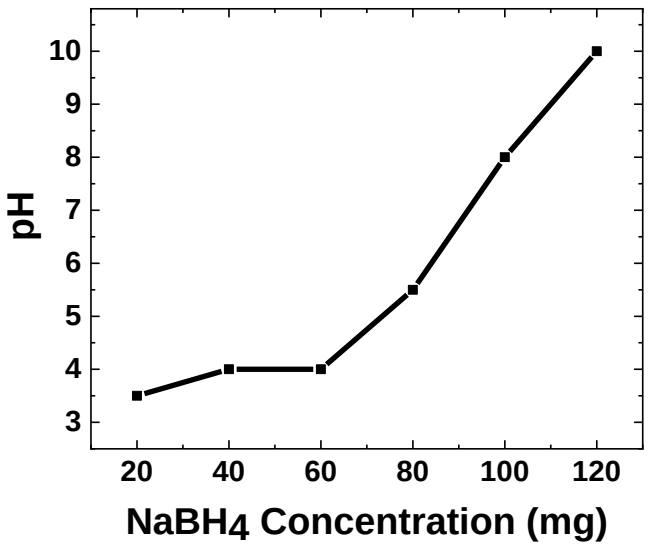

Figure SA12: Change in pH at a reaction chamber as influenced by change in concentration sodium borohydride at 22- 24 0^{o}C).

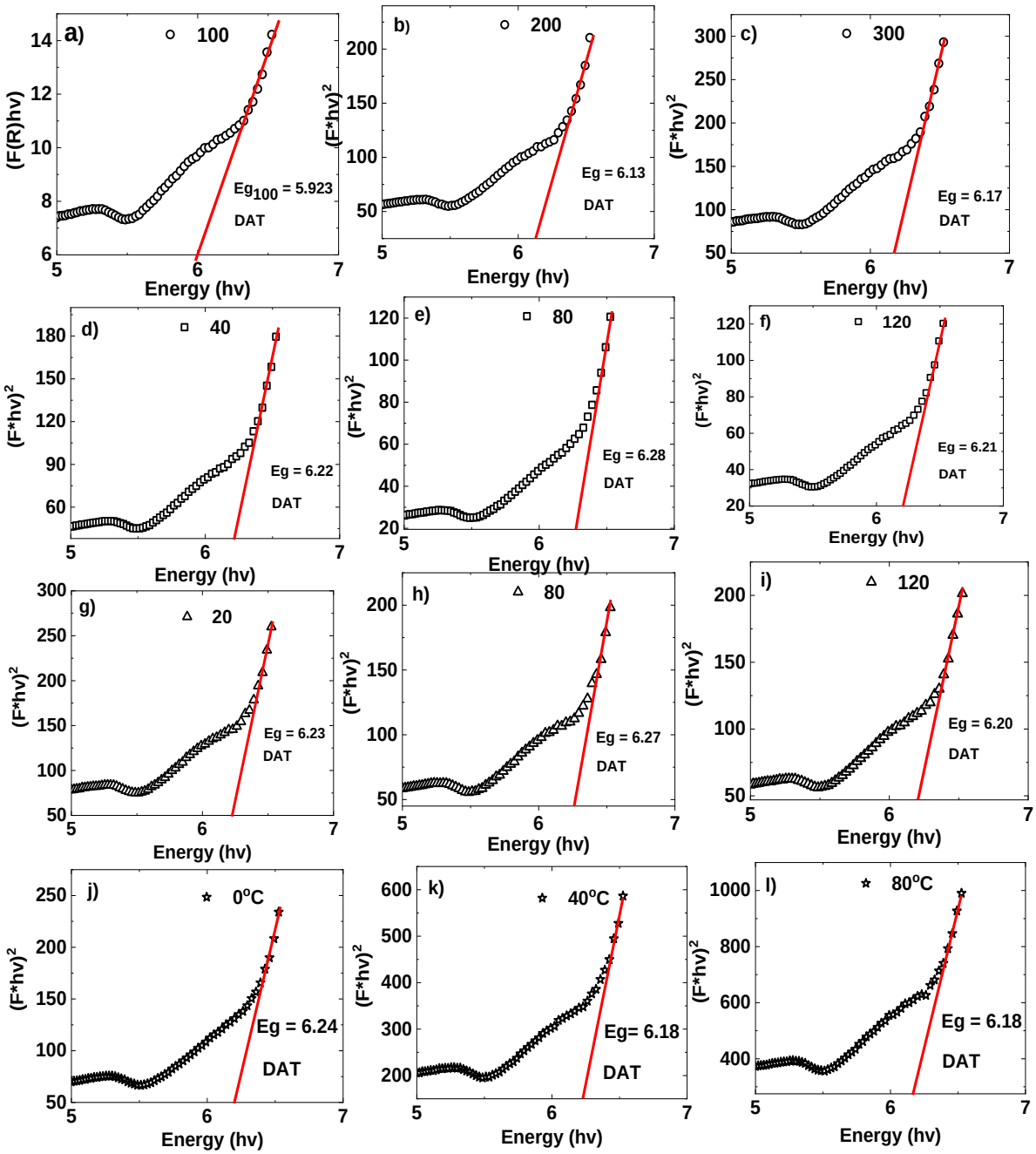

Figure SA13: Band gap energies of some selected nanoparticles; at variable metal concentrations, a) to c), variable ligand concentrations d) to f), variable concentrations of reducing agent, g) to i), and increasing reaction temperature, j) to l).

Author(s) year	Organisms	Results	Study remarks
Groundwater			
Bitton et al. (1983)	*Salmonella, E. coli, S. faecalis, enteroviruses*	*S. faecalis* decay rate was similar to viruses	Survival of pathogens in groundwater
Schijven and Hassanizadeh (2000)	Viruses	Viruses attachment with soil was influenced by pH, and favorable sites	Soil passage impacts on virus removal at field-scale
Pang et al. (2004)	*E. coli* and F-RNA phages	Pathogens were sorbed in aquifer material	Transport of *E. coli* and F-RNA phages
Nevecherya et al. (2005)	*Salmonella*, viruses, *E. coli*, shigellos	Mathematical model was derived for temperature depends inactivation rate	Pathogenic bacteria and viruses survival in groundwater
Filip and Demnerova (2009)	*Bacillus megaterium* and *Staphylococcus*	Pathogens survived 10 to 100 days	Pathogens survival in groundwater; FT-IR characterization
Grisey et al. (2010)	Total coliforms, *E. coli, Enterococci, Pseudomonas aeruginosa, Salmonella and Staphylococcus aureus*	Bacterial density monitoring coupled with artificial trace experiments proved useful in locating pathogens sources	Pathogens survival in groundwater and landfill leachate
Rivers			
Chin (2010)	Fecal coliform	Summer and rainfall raises pathogens	Urban areas impacts on stream pathogens
Smith et al. (1973)	*Salmonella*, fecal coliforms, streptococci	*Salmonella* decline was close to fecal coliform	Usefulness of indicators organisms
Burton et al. (1987)	*Pseudomonas aeruginosa, Salmonella newport, E. coli*	Clay in sediments improves *E. coli* survival	Survival of pathogens in fresh water sediments
Smith et al. (1987)	*E. coli*, Fecal bacteria	U.S. rivers shows decline in fecal indicator	Water quality assessment from 1974 to 1981
Terzieva and McFeters (1991)	*E. coli, Campylobacter jejuni, Yersinia enterocolitica*	Temperate zone surface water serve as a rersisitent verhicle in transimsision of bacteria between animals and humans	Survival and injury study of bacteria in agricultural surface water
Terzieva and McFeters (1991)	*Yersinia enterocolitica* and *E. coli*	Experimental design and environmental play major role in pathogens survival	Survival in stream water, comparison between field and lab studies
Fraser et al. (1998)	Fecal coliform	Model predicted pathogens	Modelling non-point source pollution
Lakes and reservoirs			
Beaver and Crisman (1989)	Ciliates	Grazing habits of ciliates are discussed	Predators roles in fresh water
Rubentschik et al. (1936)	*Serratia marcescens*	Adsorption of bacteria could be questionable	Adsorption of bacteria in salt lakes
Mac Kenzie et al. (1994)	*Cryptosporidium*	*C. oocysts* study passes through the filtration system of water supply	Contaminated water from Milwaukee lake caused outbreak
Wcislo and Chrost (2000)	*E. coli*	Predators controlled pathogen levels	Survival of pathogens in man-made reservoir
Kistemann et al. (2002)	*E. coli*, coliform, fecal streptococcal, and *Clostridium perfringens*	Most of the pathogens increases during extreme runoff events	Microbial load in drinking water reservoir during rainfall events
Howe et al. (2002)	*Cryptosporidium oocysts*	Animal feces was a major source of pathogens	Water supply's oocysts caused outbreak in northern England
Ishii et al. (2006)	*E. coli*	*E. coli* survived longer in soil	Presence and growth of *E. coli* in Lake superior watershed

Figure SA 14: Pathogen contamination in freshwater environment (ground water, rivers and lakes and reservoirs) Reproduced from (Pandey et al., 2014)

VITA

Yohannes Getahun is a researcher in Environmental/Material Science and Engineering Program at The University of Texas at El Paso. He earned his bachelor's degree in chemistry from Arbaminch University in 2009 and master's degree in organic chemistry from Mekelle University in 2012. Yohannes worked as researcher and assistant professor in two different universities from 2012 to 2020. He engaged in teaching and leadership positions where, as assistant professor he delivered various chemistry and biochemistry courses to undergraduate and graduate students as well as advised undergraduate students in their final research projects. He was Head of Career Center at Adigrat University where he did notable work on industry and university relations and trained graduating students on job readiness. He also worked as vice chair for the Department of Chemistry and chair to different committees at the department at the same university. He won four university funded research grants (Award Number VPRCS/540/2009 (2016)| VPRCS/548/2008 (2015)| VPRCS/015/2007 (2014)| VPRCS/514/2006 (2013). He is also a recipient of scholarships from Indian Government (2018). He joined Environmental Science and Engineering PhD program in 2020 under his mentor Ahmed El Gendy. His research focus on interdisciplinary approach towards solving environmental problems. Specifically, he develops nanoparticles and organic (molecular) compounds for water treatment, biomedical and energy applications. He accentuates developing efficient and affordable materials and technology for water treatment for use in developing countries. His expertise in water treatment: adsorption, degradation, catalysis, recyclability; natural products extraction, separation, and characterization; synthesis and modification of organic compounds; synthesis, functionalization and preparation of magnetic and nonmagnetic nanoparticles has allowed him to participate in various environmental projects as well as publish several scientific works in peer reviewed journals. He worked as research associate in chemistry and physics laboratories. He is affiliated ASPIRE WTRC Future Faculty Fellow (May 2021). He was a participant in an international conference (APS March Meeting 2021), Grad Expo (2022), and Finalist in 3MT thesis event(2022).